Effect of Drugs on the Cardiac Transport, Metabolism and Action of Idarubicin:
Pharmacokinetic and Pharmacodynamic Modeling

Dissertation

Zur Erlangung des akademischen Grades
doctor rerum naturalium (Dr. rer. nat)

vorgelegt der

Mathematisch-Naturwissenschaftlich-Technischen Fakultät
der Martin-Luther-Universität Halle-Wittenberg

von Wonku Kang, MS.
geb. 03. 11. 1969 in Taejon, Südkorea

Gutachter:
1. Prof. Dr. Michael Weiss
2. Prof. Dr. Reinhard Neubert
3. Prof. Dr. Peter Langguth
Halle (Saale), den 06. Nov. 2002

„The fear of the Lord is the beginning of knowledge.“
(The Proverbs 1:7)

„A Man's heart plans his way, but the Lord directs his steps.“
(The Proverbs 16:9)

Table of Contents

Results and Discussion

Abbreviations

ABC	ATP-binding cassette
AIC	Akaike information criterion
ANOVA	Analysis of variance
AUC	Area under the concentration-time curve
AUE	Area under the effect-time curve
CVR	Coronary vascular resistance
CYP 450	Cytochrome P-450
DOX	Doxorubicin
EDHF	Endothelium-derived hyperpolarizing factor
FSD	Fractional standard deviations
IDA	Idarubicin
IDOL	Idarubicinol
LVDP	Left ventricular developed pressure
$LVdP/dt_{max}$	Maximum value of rate of left ventricular pressure development
$LVdP/dt_{min}$	Minimum value of rate of left ventricular pressure development
LVEDP	Left ventricular enddiastolic pressure
LVSP	Left ventricular systolic pressure
MDR	Multidrug resistance
MRP	Multidrug resistance-related protein
NO	Nitric oxide
NOS	Nitric oxide synthase
One-way RM ANOVAs	One-way repearted measurement analysis of variances
PBPK	Physiologically based pharmacokinetics
PGI_2	Prostacycline
P-gp	P-glycoprotein
PK/PD	Pharmacokinetic and pharmacodynamic
SNLR	Simultaneous nonlinear regression
SR	Sarcoplasmic reticulum

Introduction

Chapter 1. Idarubicin and Idarubicinol

Idarubicin (IDA, 4-demethoxydaunorubicin) is one of potent anthracycline antibiotic derivatives which has a broad spectrum against a wide range of human neoplasms, especially for the treatment of acute leukemias and breast cancer (Robert et al., 1987; Elbaek et al., 1989). IDA has been developed in an effort to achieve a more effective and less toxic anthracyline. Its chemical structure (Figure 1) is derived from daunorubicin, i.e., the C-4 methoxy group in the D ring of daunorubicin is substituted with a hydrogen atom (Arcamone, 1985). Due to the molecular modification, IDA has a higher lipophilicity compared with doxorubicin (DOX) and daunorubicin. The high lipophilic property exerts that IDA is the first anthracycline which can be administered via the oral route.

	R_1	R_2
Idarubicin	- H	- CH_3
Daunorubicin	- OCH_3	- CH_3
Doxorubicin	- OCH_3	- CH_2OH
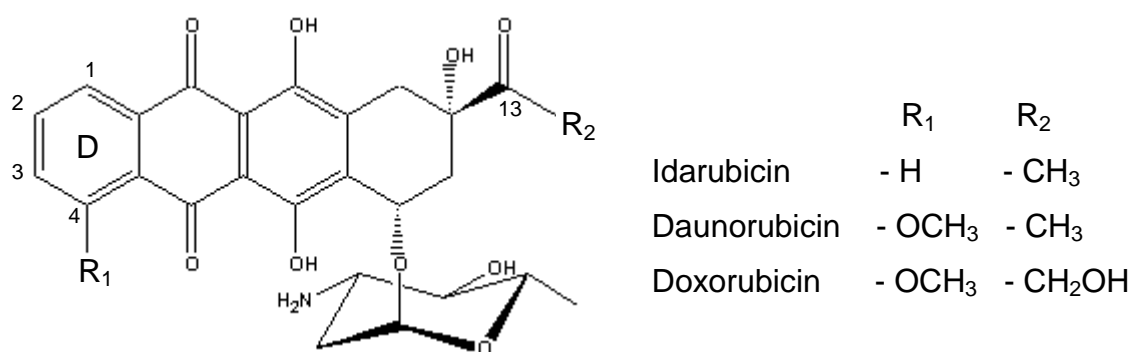
Figure 1. Structures of idarubicin, daunorubicin and doxorubicin.

Like daunorubicin, IDA is extensively metabolized to a 13-hydroxy derivative, idarubicinol (IDOL) as shown in Figure 2. The reduction at C-13 in anthracyclines is usually characterized by aldoketoreductase with a high stereoselectivity (Gewirtz and Yanovich, 1987). This enzyme has a much better affinity for substrates which have C-14 methyl group (daunorubicin and IDA) rather than C-14 hydroxymethyl group (doxorubicin and epirubicin). Therefore, IDOL is present at high concentrations in plasma after administration of IDA. Most 13-dihydrometabolites of anthracyclines are

devoid of significant cytotoxic activity, mainly because they have a low degree of uptake into the cell. However, IDOL is much more potent than the other anthracycline alcoholic metabolites such as doxorubicinol and daunorubicinol probably because of its lipophilicity, and is equipotent with the parent drug (Kuffel et al., 1992; Schott and Robert, 1989). IDOL has been reported to possess significant growth inhibitory activity when incubated with tumor cell lines. Following administration of IDA to adult and pediatric cancer patients, high plasma concentrations and prolonged elimination of IDOL are observed, resulting in systemic exposure much greater than that to IDA (Ames and Spreafico, 1992). Furthermore, the fact that IDOL can be detected in the cerebrospinal fluid has been particular interest for clinical use (Reid et al., 1990).
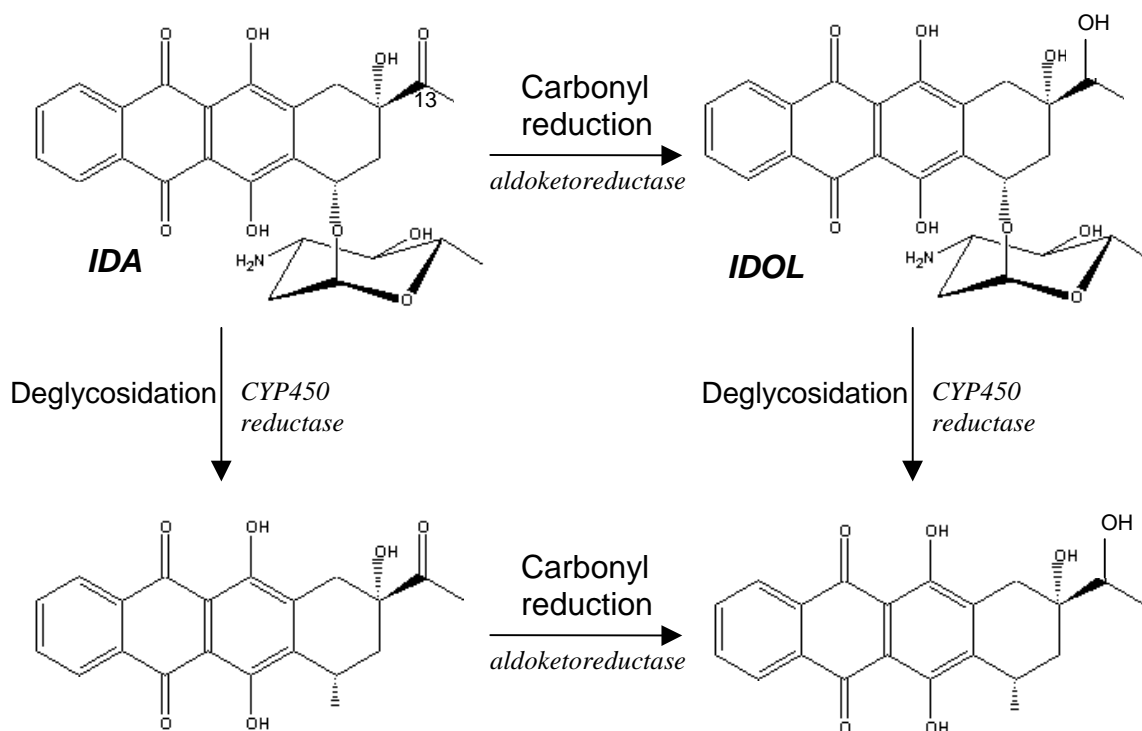
Figure 2. Metabolism of idarubicin.

Unfortunately, the clinical usefulness of IDA as described above is limited by a well-described but incompletely understood cardiac toxicity (Anderlini et al., 1995).

1 - 1. Cardiotoxicity of Anthracyclines

Acute (e.g., nonspecific electrocardiogram changes, hypotensive effects) and subacute (myocarditis) anthracycline cardiotoxicity usually are reversible within several days, whereas chronic administration of anthracyclines can cause a cumulative, dose-dependent cardiomyopathy, and produce significant morbidity and mortality. It has been hypothesized that the mechanism of cardiac toxicity may involve free radical generation with resultant lipid peroxidation, intracellular calcium overload and decrease in energy-carrier production, toxic effect of alcohol metabolite, and influence on the cell membranes, etc.

1-1-1. Free Radical Generation

Anthracyclines and other quinone-containing drugs are able to form free radical by either an oxidative or a non-oxidative inhibition of the electron transport chain. The proposed mechanism of anthracycline cardiotoxicity involves lipid peroxidation initiated by hydroxyl radical formed from the combination of superoxide and hydrogen peroxide (Goodman and Hochstein, 1977; Myers et al., 1977). Anthracyclines can catalytically increase active peroxide levels at the expense of cellular reductants. It has been believed that NADPH-cytochrome P450 reductase and mitochondrial NADH dehydrogenase present in cardiac sarcoplasmic reticulum and mitochondria are responsible for the reduction of anthracyclines in cardiac tissues (Kalyanaraman and Baker, 1990; Thornalley et al., 1986). Lipid peroxidation due to free radical formed by anthracyclines may cause changes in membrane structure, fluidity and permeability.

1-1-2. Nitric Oxide Synthase Inhibition

The role of nitric oxide synthase (NOS) in anthracycline-induced cardiotoxicity has also been considered. Anthracycline derivatives inhibit endothelium-dependent relaxation in rat aorta (Wakabayashi et al., 1991), and NOS induction in vascular smooth muscle (Wakabayashi et al., 2000). Luo and Vincent (1994) demonstrated that doxorubicin inhibits the brain isoform of NOS by a noncompetitive manner. They speculated that the combination of doxorubicin and NOS could lead to superoxide generation. Vasquez-Vivar et al. (1997) reported that doxorubicin binds to the reductase domain of

endothelial NOS, so that superoxide formation is dramatically increased and nitric oxide formation is decreased. The imbalance between nitric oxide and superoxide levels may play a key role in the cardiotoxicity of doxorubicin.

1-1-3. Ca^{2+} Homeostasis Pertubation

Sarcoplasmic reticulum (SR) releases, sequesters, and stores the calcium which determines both systolic and diastolic cardiac function. SR has two primary sites of function, longitudinal tubules and terminal cisternae. Longitudinal tubules sequester and transport calcium to terminal cisternae where calcium is stored for subsequent release to the contractile apparatus. Terminal cisternae have calcium release sites activated by calcium (calcium activated Ca^{2+} channel). Although it has been suggested that the cardiac effects of anthracyclines are due to impaired myocardial Ca^{2+} handling, the mechanism appears still unclear (Matsushita et al. 2000). Several studies indicated that anthracyclines activate the cardiac SR Ca^{2+} release channel (ryanodine receptor) leading to an intracellular Ca^{2+} overload associated with an impairment of Ca^{2+} transients and a decrease in myocardial contractility (Holmberg and Williams, 1990; Earm et al., 1994; Temma et al, 1994; Temma et al, 1996; Maeda et al., 1999). Anthracyclines may also increase cytoplasmic calcium by inhibiting Na^+/Ca^{2+} exchange and/or Ca-ATPase of sarcolemma (Caroni et al., 1981; Harada et al., 1990).

1-1-4. Active metabolite

It has been hypothesized that anthracycline metabolites may also mediate the cardiac toxicity (Olson and Mushlin, 1990). Doxorubicinol is not only more potent than doxorubicin at inhibiting the force contraction (Olson et al., 2000), but also prevents complete relaxation between contractions of isolated cardiac muscle (Mushlin et al., 1985). Boucek and his colleagues (1987) reported that doxorubicinol is a potent inhibitor of three ion pumps: 1) the calcium pump from heart muscle SR, 2) the Na^+/K^+ pump of cardiac sarcolemma and 3) the cationic pumps that regulate the resting levels of myoplasmic calcium which plays a major role in regulating the extent of myofibrillar relaxation. Daunorubicinol, but not daunorubicin, also inhibits Ca^{2+} uptake by SR from canine cardiac muscle at concentrations similar to those observed in vivo (Cusack et al., 1993). Therefore anthracycline alcoholic metabolites are likely candidates to mediate

the pertubation in Ca^{2+} homeostasis.

The treatment of cancer with anthracyclines is further complicated by the phenomenon of multidrug resistance (MDR) which is caused by the (over)expression of the *MDR1* gene, which encodes the P-glycoprotein (P-gp).

1-2. P-glycoprotein (P-gp)

1-2-1. Physiological role of P-gp

P-glycoprotein (P-gp) is a member of the ATP-binding cassette (ABC) superfamily of proteins that is highly conserved in distantly related species from eukaryotes to vertebrates (Gros et al., 1986). P-gp produced by multidrug resistance (MDR) genes consists of two homologous domains containing 12 transmembrane segments and two nucleotide binding domains. ABC transporters are responsible for the translocation of nutrients, peptides, organic ions and toxins (Gottesman and Pastan, 1993). P-glycoprotein is not restricted to tumor cells but is normally localized in mainly in tissues with excretory function, e.g., brush border membrane of enterocytes in intestine (van Asperen et al., 1998), canalicular membrane of hepatocytes, and capillary endothelial cells of the brain (van Asperen et al., 1997). The adrenal glands possess high levels of P-gp distributed on the surface of cells in both the cortex and medulla (Gottesman and Pastan, 1993). It is also found in heart (Rodriguez et al., 1999; Abernethy et al., 2000), placenta, testis (Thiebaut et al., 1987) and normal leukocytes (Klimecki et al., 1994).

The physiological role of P-gp is not completely understood, but it could protect against environmental toxins and promote excretion of steroid hormones, drugs, and electrodes. This membrane transporter most likely plays an important part in drug disposition, e.g., it has been suggested that normal P-gp function could influence many key steps in drug kinetics, such as reducing gastrointestinal absorption, enhancing bile and urine excretion, and preventing entry of drugs to the central nervous system (Fromm et al., 1999).

Most P-gp substrates are hydrophobic and amphipathic and usually contain electron donor groups arranged in distinct spatial patterns (Rodriguez et al., 1999). The function of P-gp at the molecular level has been extensively characterized; it is known to be

saturable for drugs, as well as osmotically sensitive and ATP dependent (Sharom, 1997).

1-2-2. Multidrug Resistance (MDR)

Cancer chemotheraphy has a limited potential for cancer cure due to acquired or intrinsic resistance of cancer cell to anticancer agents. Resistance to one drug often implies to a series of different drugs, so called multidrug resistance (MDR). There have been known two P-gp encoding genes, MDR1 and MDR2, both localized in human chromosome 7. The typical MDR phenotype is mainly due to the overexpression of membrane glycoproteins such as P-glycoprotein (P-gp, ca 170 kDa, the most important molecule) and MDR-related protein (MRP, ca 190 kDa) (Baggetto, 1997). Drug resistance to anthracyclines may be partly attributed to the action of P-gp, an active plasma membrane drug influx and/or efflux pump, which decreases the intracellular accumulation of cytotoxic drugs. The initial and major emphasis of P-gp research was to explain the occurrence of MDR in tumors, but a new focus on of interest has been the study of the role of P-gp in transport of many other drugs.

1-3. Strategies to Overcome Cardiotoxicity and MDR in Anthracycline Chemotherapy

1-3-1. Strategies against Cardiotoxicity

Attempts to diminish anthracycline cardiotoxicity have been directly toward: 1) decreasing myocardial concentrations of anthracyclines and their metabolites, 2) developing less cardiotoxic analogues, and 3) concurrently administering other drugs which block or overcome the harmful effects of anthracyclines on the myocardium.

Since it has been generally accepted that cardiotoxicity seems to be related to peak plasma level of anthracyclines, clinicians have changed the dose regimen to decrease anthracycline exposure of myocardium by slowly infusion of those drugs to keep the plasma concentration low (Eichholtz-Wirth, 1980). Many complexes of anthracyclines using liposome, dextran and albumin microspheres have also been investigated. These complexes decrease peak concentration and function as slow-release formulations

(Mayer et al., 1997).

Lots of efforts in the search for anthacycline analogues which have a higher therapeutic-to-toxic ratio have been paid. Experimental studies have identified numerous potentially less cardiotoxic analogues, however, few of these agents showed sufficient advantage over doxorubicin to warrant clinical evaluation (Casazza et al., 1980). In the third category, various cardioprotective substances have been examined, e.g., free radical scavengers (Mcginness et al., 1986; Fujita et al., 1982), calcium channel blockers, histamine and catecholamine blockers (Bristow et al., 1980), and carnitine and EDTA derivatives (McFalls et al., 1986).

1-3-2. Strategies against P-gp mediated MDR

In strategies to overcome P-gp-mediated multidrug resistance, firstly, one could possibly avoid the problem using cytotoxic drugs that are not substrates of P-gp and thus retain activity in cells with high P-gp expression levels, or develop non-cross-resistant analogues of MDR drugs (Roovers et al., 1999). It would be attractive to chemically modify MDR drugs in order to delete their affinity for P-gp. The ability of anthracyclines to circumvent MDR is shown to improve with increasing lipophilicity (Lampidis et al., 1997). Thus, the highly lipophilic anthracyclines, IDA has been an attractive substitute for conventional anthracyclines in MDR cancer. IDA has been shown to preserve substantial cytotoxicity in various selected MDR cell lines (Ross et al., 1995), in cells transfected with the MDR1 gene (Kuffel and Ames, 1995), and in P-gp-positive blasts retrieved from leukemia patients treated with the drug (Nussler et al., 1997).

Secondly, the use of chemosensitizers like P-gp modulators (Rodriguez et al., 1999) that interfere with the drug efflux driven by P-gp may restore drug sensitivity in MDR cells. P-gp has a broad specificity for substrates, and nontoxic drugs may competitively inhibit the efflux of cytotoxic drugs by P-gp and thereby downregulate MDR (Ford and Hait, 1990). Several classes of inhibitors have been identified among drugs that were developed for other therapeutic indications, including calcium channel blockers, calmodulin antagonists, steroid hormonal agents and immunosupressive agents (Ferry et al., 1996).

In these trials of MDR circumvention an increase of cardiotoxicity has to be considered

due to cardiac uptake enhancement of anticancer agents. To date, the effect of MDR inhibition remains unclear on the heart as a main target organ for anthracycline toxicity. Furthermore, although the determination of optimal therapeutic range of anthracyclines is dependent on the peak concentration and the change of area under the time concentration curve, the uptake amount of the drugs into the heart is unlikely proportional to the plasma concentration. Therefore, cardiac uptake transport mechanism of anthracyclines should be clarified and must be the first step to figure out and to regulate the anthracycline induced cardiomyopathy.

Chapter 2. Purposes

The clinical utility of IDA is limited by severe cardiotoxicity; however, the transport mechanism of IDA into the heart is still unclear. Therefore, this study is designed to investigate the uptake mechanism of IDA into the intact heart. To verify the uptake mechanism of IDA in the myocardial transport process doxorubicin and hypothermic condition are examined. It has been generally assumed that IDA diffuses passively into the cell because of its high lipophylicity. However, it is controversial whether cellular uptake transport of anthracyclines occurs via saturable mechanism or passive diffusion. Since most research has been accomplished at the cellular level using steady state experiments, it is doubtful whether these results reflect the processes at the level of the whole organs. Furthermore, the quantification of cardiac uptake process of IDA using a mathematical modeling approach would provide essential information to optimize dosage regimens in anthracycline chemotherapy.

The anthracycline chemotherapy is further complicated by the phenomenon of MDR, caused by the (over)expression of the MDR1 gene, which encodes P-gp. However, the current strategy to reverse MDR by P-gp inhibitors might be accompanied by an increase in anthracycline cardiotoxicity. Therefore, the effect of P-gp inhibitors (verapamil, amiodarone, PSC 833) are tested to elucidate what the role of P-gp in the transport of IDA, a well-known P-gp substrate is, and how the kinetic change influences IDA-induced myocardial impairment. Xanthine derivatives (caffeine, theophylline) are also investigated to check their effects on the IDA induced cardiac performance.

The formation of IDOL in the heart tissue is of special interest because it has been speculated that the cardiotoxicity of anthracyclines could be related to its myocardial metabolism. Therefore, metabolism inhibitors (phenobarbital, rutin) are examined to elucidate how they influence the generation of IDOL from IDA in the heart, and whether the change of metabolism affects dynamic response of IDA. The effect of drugs which mentioned above on the generation and disposition kinetics of IDOL after IDA administration is also simultaneously investigated in the series of experiments.

Chapter 3. Pharmacokinetic and Pharmacodynamic (PK/PD) Modeling

3-1. Physiologically based Pharmacokinetic Modeling

A physiologically based pharmacokinetic (PBPK) model depicts the body as a number of well-mixed compartments representing individual organs such as the heart, brain, lung, muscle, liver, skin and adipose tissue (Figure 3). The model assumes that intercompartmental transport occurs by blood flow only and that instantaneous equilibrium is achieved between tissue and the blood. Differential mass balance equations have been written for each compartment to describe the input, output, metabolism and sequestration of the drug. The conventional method in PBPK is destructive sampling where the concentration in various tissue phases of the organs can be measured. The main advantage of the destructive sampling method is the
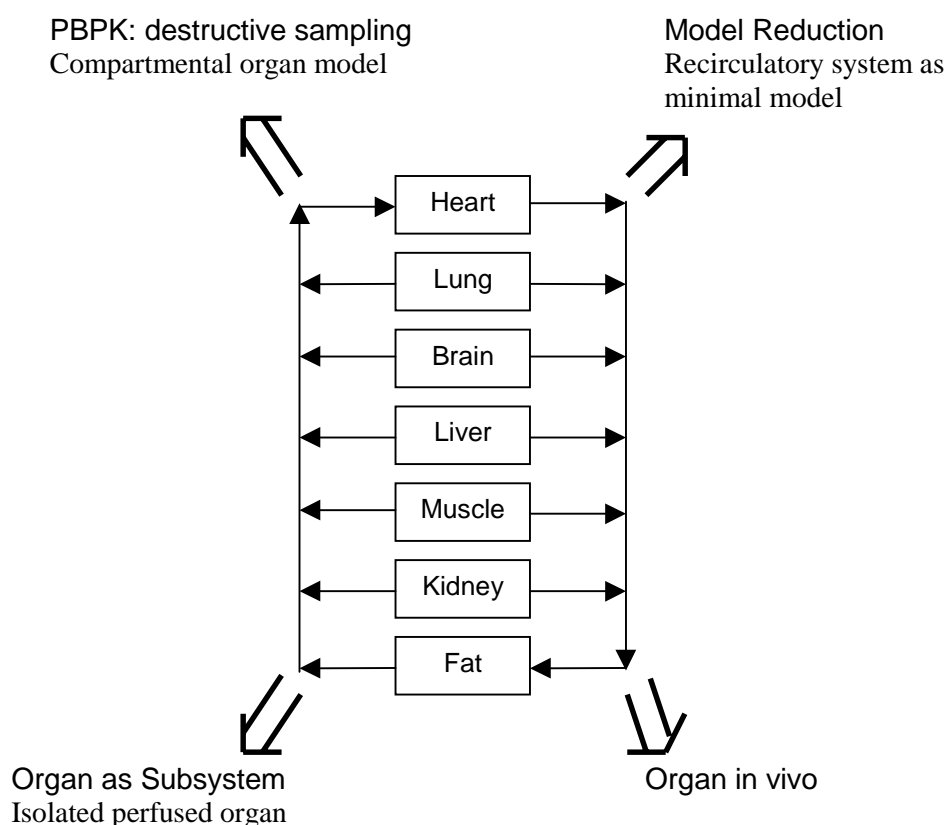

Figure 3. Identification of physiological multi-organ models.

simultaneous collection of kinetic information in the various organs allowing scaling-up of pharmacokinetics from animal to human, whereas the important drawback of the method is the limited number of measurements disturbed by interindividual variability and the necessity of an independent determination of organ flows (Figure 3; Weiss, 1998).

As a first approximation whole body physiological models are based on organ models in its simplest form, i.g., well-mixed compartments. The model utilizes a basic anatomic (organ volume), physiological (blood flow rates and membrane permeability) and biochemical (enzyme reactions, transporters) information. The conventional homogeneous model implies that the distribution kinetics within the organs is flow limited. However, on the basis of physiological irrelevance of the well-stirred assumption in organs the more physiologically correct representations have been introduced to figure out a heterogeneous system, for example, "parallel tube" model, "distributed parallel" model, "tanks-in-series" model, "dispersion" model, etc. A crucial point in mechanistic pharmacokinetic modeling is the appropriate description of mixing and distribution of drugs in a heterogeneous system. The development of multiple indicator dilution techniques differentiates the anatomic subcompartments within an organ system. Furthermore, the theory of organ transit time density of drug molecules provides a better understanding of drug behavior in organ model as a pharmacokinetic subsystem (Weiss, 1992).

A physiologically based model permits the prediction of drug amount in any target tissue at any time and may provide considerable insight into drug dynamics (Harrison and Gibaldi, 1977). In addition, changes in absorption, distribution, metabolism and excretion of drug in certain pathophysiological or artificial conditions could be predicted by altering estimates.

3-2. Pharmacodynamics

Pharmacodynamics assesses "what the drug does to the body", whereas pharmacokinetics characterizes "what the body does to the drug", namely, concentration-time course of drugs in different body fluids. Pharmacodynamics was used to describe either concentration-effect relationships or the time course of

pharmacological effect after a drug administration (Holford and Sheiner, 1981). Pharmacodynamic studies measure the magnitude of a pharmacodynamic effect as a function of dosing regimen and time. Pharmacodynamic studies may be incorporated into the design of pharmacokinetic studies and clinical trials that are also intended to provide evidence of efficacy and safety.

3-3. Pharmacokinetic and Pharmacodynamic (PK/PD) Modeling

The modeling of pharmacokinetic and pharmacodynamic (PK/PD) relationship builds a bridge between these two classical disciplines (Figure 4). The model links the concentration-time profile as assessed by pharmacokinetics to the intensity of observed
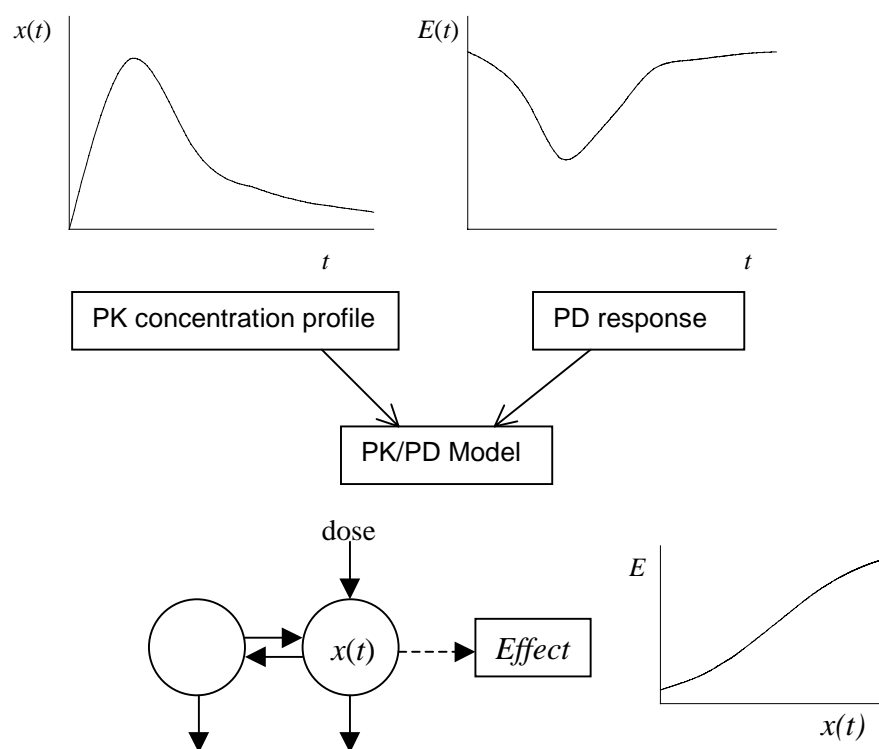

Figure 4. Structure of the PK/PD model.

response as quantified by pharmacodynamics. Thus, the resulting integrated PK/PD model allows the description of the complete time course of drug effects in response to a drug therapy. The PK/PD modeling can elucidate the causative relationship between drug exposure and response, and provide a better understanding of the sequence of

events those results in the observed drug effect. This information can be used to streamline the drug development process and dose optimization (Woo et al., 2002).

In the PK/PD study lots of attention should be paid to the appropriateness of the PD response, and the intended analysis and interpretation of the data. Drug response can be modeled by the linear model, the E_{max} model and the sigmoid E_{max} model.

In the linear model the observed pharmacological effect (E) is directly proportional to a drug exposure (x_E). The relationship is described as:

$$E = E_0 + P\, x_E \qquad\qquad\qquad\qquad (1)$$

Where E_0 indicates the baseline level and the proportionality constant, P, can be obtained as the slope term corresponding to linear regression of response on a drug exposure.

The E_{max} model is a family of functions describing nonlinear drug exposure-effect relationship. The minimal model capable of accounting for constraints on drug action over the entire dose range is a hyperbolic function:

$$E(t) = \frac{E_{max}\, x_E(t)}{EX_{50} + x_E(t)} \qquad\qquad\qquad\qquad (2)$$

Where E_{max} is the maximal effect that can be elicited by the drug, and EX_{50} is the value of drug when response is half maximal ($E_{max}/2$). This equation is a model of a saturable process: as x_E becomes large, E approaches E_{max} asymptotically, and no further increase in effect is possible. Absence of effect is predicted in the absence of drug. These constraints on the model are intuitively reasonable. When $x_E \ll EX_{50}$, the equation can reduce $E = E_{max}\, x_E / EX_{50}$, and a linear relationship is described. In the range of 20-80% E_{max}, the E_{max} model is well approximated by the linear model, but if E_{max} cannot be estimated, then the range represented by the data is undetermined(Holford and Sheiner, 1982).

Addition of a power term (N) to form the sigmoidal E_{max} model allows one to describe more diverse data sets:

$$E(t) = \frac{E_{max}[x_E(t)]^N}{EX_{50}^N + [x_E(t)]^N} \tag{3}$$

where the N exponent is termed the sigmoidity or slope factor, because it markedly affects curve slope without alteration in E_{max} or EX_{50}. When $N = 1$, the function is the basic E_{max} model. When $N > 1$, the slope curve in the region of EX_{50} (i.e., the sensitivity of response to a change in amount of drug) is increased (Figure 5).

Once initial estimates of the values of N, E_{max} and EX_{50} are determined, best estimates of the model parameters are readily obtained by fitting corresponding $x_E(t)$ and $E(t)$ data points by means of an iterative least-squares nonlinear regression program. The ability to fit data to the sigmoidal E_{max} equation does not necessarily mean that it is the correct model. Equations with many variables are flexible. Complex models may not be justified by the quantity and variability of the data, which will be apparent in the curve-fitting statistics (e.g., a high correlation between ostensibly independent variables) (Welling et al., 1991).
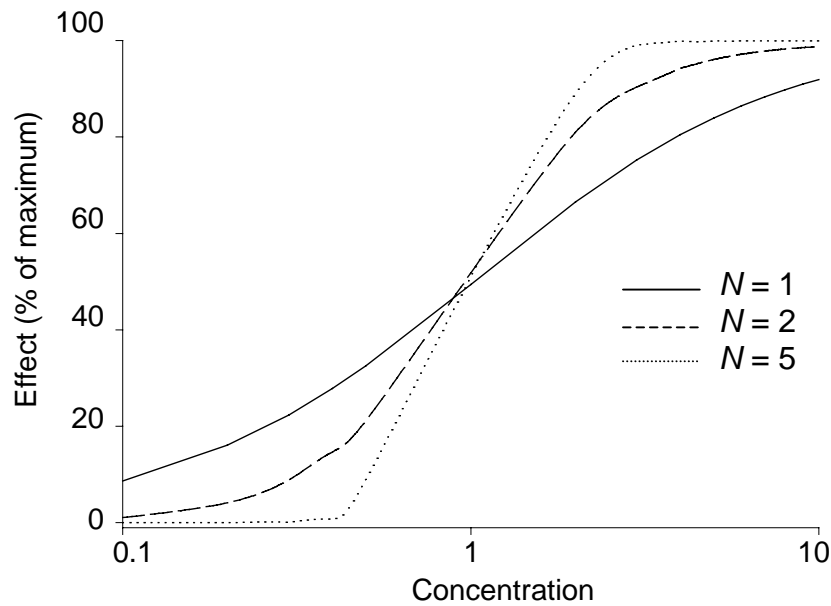

Figure 5. Sigmoid E_{max} model ($E_{max} = 100$, $EX_{50} = 1$). Change of the drug exposure-effect relationship curve according to the different values of the N power term corresponding to sensitivity (slopes).

Methods

Chapter 4. Isolated perfused rat heart

Following the onset of general anesthesia with pentobarbital (50 mg/kg, intraperitoneally) adult male Sprague-Dawley rats (300-350 g) were fixed on an operating table on their back. A cannula is bound into trachea for ventilation. The skin is incised by a longitudinal cut from the middle of the abdomen up to the throat. Then the abdomen is opened up to the diaphragm. The diaphragm is cut off the ribs following the anterior part of the inferior thoracic aperture. The thorax is cut open on the left and right side following the bone-cartilage-border on a line parallel to the sternum starting at the diaphragm and proceeding as far cranial as to the first rib. The complete anterior thoracic wall is turned upwards over the rat's head and the sternum is splitted from the xiphoid process exactly in the middle. The ribs are cut as far lateral as possible and the two thorax halves are turned upwards. The pericardium is removed as far as its attachment at the vascular system and any connective tissue around the ascending aorta is discarded. An aortic cannula filled with perfusate was rapidly inserted into the aorta and the pulmonary artery was incised to allow outflow of perfusate. Retrograde perfusion was started with an oxygenated perfusate consisted of Krebs-Henseleit buffer solution, pH 7.4, containing NaCl (118 mM), KCl (4.7 mM), $CaCl_2$ (2.52 mM), $MgSO_4$ (1.66 mM), $NaHCO_3$ (24.88 mM), KH_2PO_4 (1.18 mM), glucose (5.55mM), and Na pyruvate (2.0 mM).

A latex balloon attached to the end of a steel catheter was placed in the left ventricular through mitral valve. The catheter and the balloon are filled with a mixture of ethanol and water (50:50), and the other end is linked to a physiograph via a P23Db transducer. The balloon is inflated with water to create a diastolic pressure of 5 to 6 mmHg. Langendorff apparatus is depicted in Figure 6. The heart is perfused with a Krebs-Henseleit bicarbonate buffer at 37°C with a 60 mmHg pressure. After stabilization, the system is changed to constant flow condition maintaining a coronary flow of 9.5 ± 0.4 ml/min. The hearts are beating spontaneously at an average rate of 280 ± 20 beats/min.
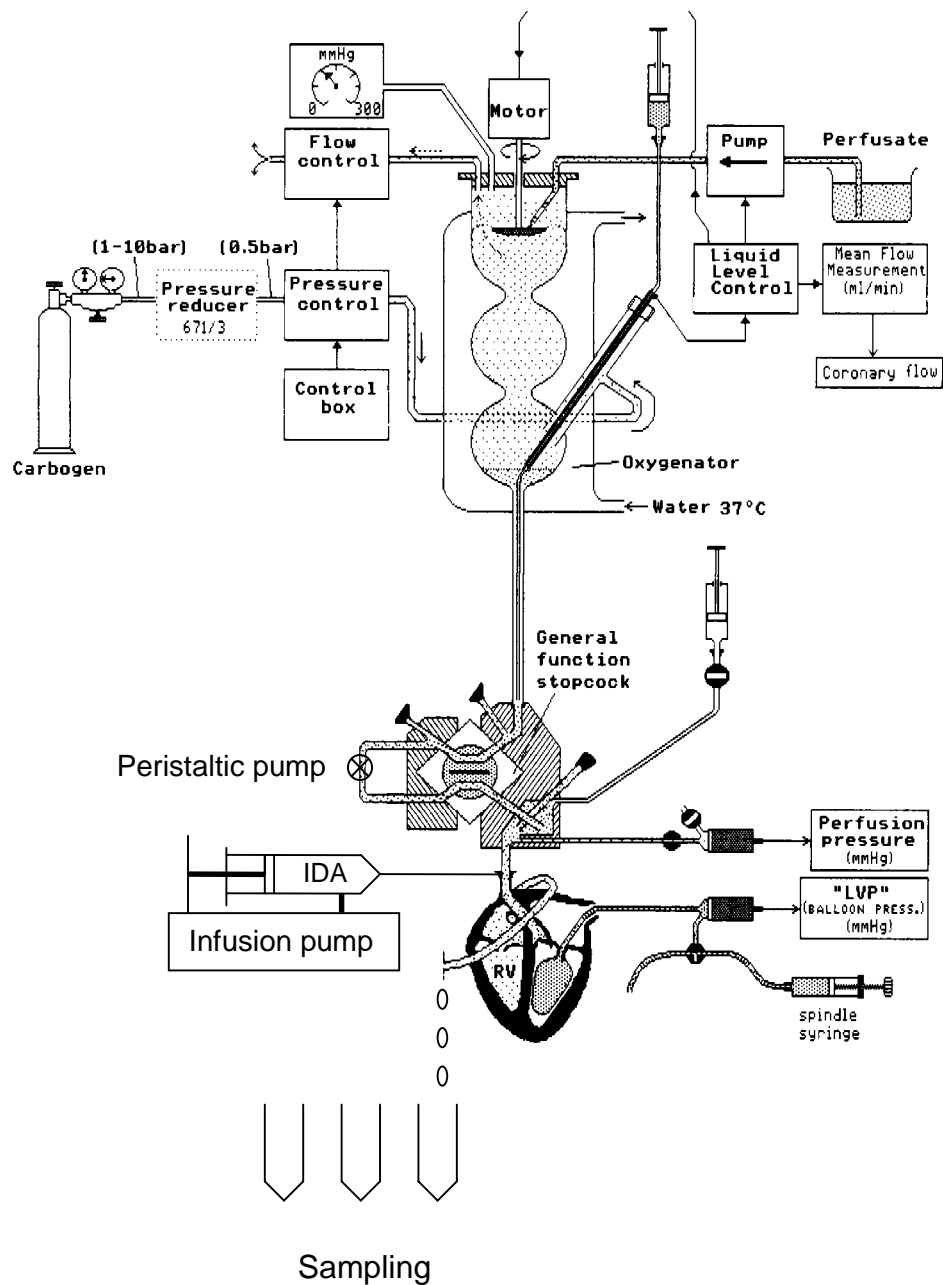
Figure 6. Langendorff apparatus for isolated perfused heart.

Left ventricular (LV) pressure and heart rate are continuously monitored by means of the balloon. Coronary perfusion pressure is regulated by a perfusion pressure control module and measured by a P23Db transducer connected to the aortic infusion cannula.

A physiological recording system (Hugo Sachs Elektronik, March, Germany) is used to monitor left ventricular systolic pressure (*LVSP*), left ventricular enddiastolic pressure (*LVEDP*), maximum and minimum values of rate of left ventricular pressure development (*LVdP/dt$_{max}$* and *LVdP/dt$_{min}$*), heart rate and coronary perfusion pressure.

Chapter 5. Experimental Design

5 - 1. Materials

Idarubicin was purchased from Pharmacia & Upjohn (Erlangen, Germany) and the other substances (verapamil, amiodarone, rutin, phenobarbital, caffeine, theophylline) are from Sigma (Deisenhofen, Germany). Doxorubicin and idarubicinol is kindly donated by Pharmacia & Upjohn (Erlangen, Germany), and PSC 833 is obtained from Novartis Pharma (Basel, Switzerland). All other chemicals and solvents are of the highest grade available.

5 - 2. Experimental Protocol

5-2-1. Control groups

Hearts are allowed to equilibrate for 20 min with Krebs-Henseleit solution. After stabilization, 5 ml (0.1 mg/ml, n=5) or 0.5 ml (1 mg/ml, n=5) of IDA solution is infused for ten or one minute with an infusion device (IVECO), respectively. The IDA dose is selected to induce submaximal negative inotropic and vasoconstrictive effects. Outflow samples are collected every 10 s for 3 min, every 30 s for the next 7 min, every 60 s for the next 10 min, and every 5 min for the next 60 min (total collection period 80 min). The outflow samples and hearts are kept frozen at -20°C until analysis.

5-2-2. Treatment groups

In a 10-min infusion protocol treatment studies are performed under perfusion with Krebs-Henseleit buffer containing verapamil (1 nM), amiodarone (1 µM), caffeine (1 µM), theophylline (3 µM), doxorubicin (20 µM), where IDA is infused at 20 min after start of perfusion of treatment. In hypothermic condition perfusate is cooled from 37° to 30°C, and IDA infused at 20 min thereafter.

In a 1-min infusion study IDA is infused in the same way described above under 20 min preinfusion of verapamil (1 nM), PSC 833 (1 µM), rutin (10 µM), and phenobarbital (100 µM), respectively.

The doses of substances treated are below the threshold value that leads to changes in the measured cardiovascular effects except doxorubicin treatment. To evaluate the

pharmacodynamic effects produced by doxorubicin alone, doxorubicin (20 µM) is infused for 100 min following a 20-min stabilization period. In each group independent experiments are performed in 5 hearts.

5-3. Determination of Idarubicin and Idarubicinol

The high-performance liquid chromatography from Merck consists of a pump (L-6200A), an autosampler (AS-2000A) and a fluorescence detector (RF-551) from Shimadzu. Chromatographic separation is performed using a LiChrospher 100 RP-18 (5µm; length: 4 mm, Merck). The mobile phase consists of water – acetonitrile – tetrahydrofuran - H_3PO_4 -triethylamine (312:165:20:1:2) and is adjusted to pH 2.2 with 5 M of HCl. The filtered mobile phase is degassed for 10 min with sonicator (Supersonic, Branson 2210, Danbury, CT, USA). Flow-rate is 1.0 ml/min, the excitation and emission wavelengths for fluorescence detection are set at 485 and 542 nm, respectively (Kuhlmann et al., 1999).

All hearts are randomly divided into four pieces and weighted. Each piece is homogenized in 2ml of Na_2HPO_4 (0.5 M, pH 8.2) on ice with a tissue homogenizer (Ultra-Turrax T 25, IKA®-Labortechnik). Homogenates, 300-400 mg, are taken from each fraction. Daunorubicinol (100 µl, 10 µg/ml), an internal standard, and 1 ml of Na_2HPO_4 are added and mixed with the homogenate. IDA and IDOL are extracted with 7 ml of chloroform/2-propanol [9/1]. After vortexing for 1 min and centrifuging (10 min at 3000 rpm), the organic layer is recovered, evaporated for dryness under vacuum at 40°C and finally reconstituted in 2 ml of methanol (Looby et al., 1997).

Chapter 6. Model Development and Data Analysis

6-1. Model Development for IDA

A model must be constructed that not only describes the measured outflow concentration-time profiles of IDA, but is also simple enough that it can be identified on the basis of the experimental data. Compartmental modeling allows the necessary complexity reduction, the evaluation of saturable transport processes. A minimal model is developed to describe the myocardial distribution kinetics of IDA. The model development is an iterative process both with regard to the underlying data sets and the selected model structures. Models are constructed as a series of differential equations which are solved numerically and fitted to the data using the ADAPT II-software package (D'Argenio and Schumitzky, 1997). As shown in Figure 7, 53 compartmental model structures are tested until the best model for the data of a 10-min infusion of IDA is selected. Any model showing a noninvertible Fisher's information matrix is discarded as nonidentifiable. Of the identifiable models, preference is given to those with low Akaike information criterion (Akaike, 1976) and to those whose pattern of residuals better approximated a random scatter. Parameter uncertainties and independence among parameters are verified using fractional standard deviations (*FSD*) and correlations obtained from the fitting procedure. A parameter with a *FSD* more than 0.5 is considered to indicate that the parameter has not estimated with sufficient statistical certainty. Although Model 28 is better than Model 25 in terms of AIC value, Model 25 is finally selected as the best model for a 10-min infusion of IDA, because it can describe both the IDA outflow concentration time profile and inotropic response better than Model 28.

For the model structure, the differential equations that describe changes in the amounts of IDA in compartments after a 10-min infusion of IDA at the inflow side of the heart (single-pass mode) are given by following equations:

$$dx_1(t)/dt = -(Q/V_1 + V_{max,12}/[K_{M,12} + x_1(t)])x_1(t) + k_{21}x_2(t) + R_{10min} \tag{4}$$

$$dx_2(t)/dt = V_{max,12}/[K_{M,12} + x_1(t)]) x_1(t) - (k_{21} + k_{24} + V_{max,23}/[K_{M,23} + x_2(t)]) x_2(t)$$
$$+ k_{32} x_3(t) \tag{5}$$

$$dx_3(t)/dt = V_{max,23}/[K_{M,23} + x_2(t)]) x_2(t) - k_{32} x_3(t) \tag{6}$$

Note that perfusate flow, Q (and drug input rate, R_{10min}) as well as drug outflow are always assumed to occur in Compartment 1 (distribution volume V_1) representing the vascular space and rapidly equilibrating tissue regions with respect to the myocardial disposition of IDA. First order rate constants describing (passive) inter-compartmental transport are denoted by k_{ij} and the flux J_{ij} due to active transport with Michaelis-Menten type kinetics is given by

$$J_{ij}(t) = \frac{V_{max,ij} x_i(t)}{K_{M,ij} + x_i(t)} \tag{7}$$

The associated concentration of drug at time t, denoted $y_1(t)$, is given by the following output equation.

$$y_1(t) = x_1(t) / V_1 \tag{8}$$

It is necessary to specify a model for the variance of the additive error of the measured data (i.e., variance model). Measurements are generally collected at discrete times, t_j, and include additive error as follows:

$$z_1(t_j) = y_1(t_j) + v_1(t_j) \tag{9}$$

where $z_1(t_j)$ represents the measured value of the model output $y_1(t_j)$ at time t_j, and $v_1(t_j)$ is the associated error. A portion of $v_1(t_j)$ is generally attributed to errors in the measurement process.

$v_1(t)$ is assumed to be normally distributed, an error variance model relates the variance of $v_1(t)$ [$var(v_1(t))$] to the model output $y_1(t)$ as follows:

$$\text{var}\{v_1(t)\} = (\sigma_{inter} + \sigma_{slope} y_1(t))^2 \tag{10}$$

where σ_{inter} and σ_{slope} are referred to as the variance model parameters(D'Argenio and Schumitzky, 1997).

Combined kinetic-dynamic modeling is performed linking the time course of IDA amount in the effect site compartment $x_E(t)$ described by the following equation:

$$dx_E/dt = (x_2 - x_E)/\tau_{eff} \tag{11}$$

with the time course of its negative inotropic action of IDA, $E(t)$. The response or transit time τ_{eff} ($1/k_{eff}$) characterizes the disequilibrium between the functional effect site (x_E) and compartment 2 (Holford and Sheiner, 1981; D'Argenio and Schumitzky, 1997). The effect $E(t)$ is defined as the decrease of LVDP as fraction of the baseline response LVDP(0):

$$E(t) = -\frac{LVDP(0) - LVDP(t)}{LVDP(0)} \tag{12}$$

The effect site concentration (amount) induces the effect $E(t)$ by a sigmoid E_{max} model (Holford and Sheiner, 1981). The associated negative inotropic effect at time t, denoted $y_2(t)$, is given by the following output equation.

$$y_2(t) = \frac{E_{\max}\left[x_E(t)\right]^N}{EX_{50}^N + \left[x_E(t)\right]^N} \tag{13}$$

where EX_{50} is the effect site amount that corresponds to 50 % of the maximum effect ($E_{\max}$) and N is the Hill coefficient that determines the sigmoidicity of the curve. The variance is assumed to be normally distributed and as the additive error of the measured data as described above.

Since the kinetic model of a 1-min infusion of IDA is selected according to the principle of parsimony as a minimal model, the model structure and parameter estimates differ slightly from those reported in a 10-min protocol. Thus, the second nonlinear transport process is now replaced by passive transport (k_{23}). The differential equations for IDA after a 1-min infusion of IDA are represented as follow:

$$dx_1(t)/dt = -(Q/V_1 + V_{max,12}/[K_{M,12} + x_1(t)])x_1(t) + k_{21}x_2(t) + R_{1min} \tag{14}$$

$$dx_2(t)/dt = V_{max,12}/[K_{M,12} + x_1(t)])x_1(t) - (k_{21} + k_{24} + k_{23})x_2(t) + k_{32}x_3(t) \tag{15}$$

$dx_3(t)/dt = k_{23}\, x_2(t) - k_{32}\, x_3(t)$ (16)

Fitting is performed with average data values (with 5 hearts in each group) using maximum likelihood estimation and assuming that the measurement error has a standard deviation which is a linear function of the measured quantity. When the additive error is normally distributed, both system and variance model parameters (α and β) can be estimated by maximizing the likelihood function. This is done by minimizing, over α and β, the negative of the log of the likelihood (O_{NLL}) which is given as follows:

$$O_{NLL} = l \cdot m \cdot \ln(2\pi)/2 + \frac{1}{2}\sum_{i=1}^{l}\sum_{j=1}^{m}\left[\frac{(z_i(t_j) - y_i(\alpha,t_j))^2}{g_i(\alpha,t_j,\beta)} + \ln g_i(\alpha,t_j,\beta)\right]$$ (17)

The resulting maximum likelihood estimates are denoted $\hat{\alpha}$ and $\hat{\beta}$.
For maximum likelihood estimator, AIC is:

$AIC = 2\, O_{NLL} + 2\,(p + q)$ (18)

where p and q denote the number of parameter and variance, respectively.

The Fisher information matrix (F) expresses the information content of experimental data and equals (Seber and Wild, 1989):

$$F = \sum_{j=1}^{N}(\frac{\partial y}{\partial \theta_i}(t_j))^T Q_j (\frac{\partial y}{\partial \theta_i}(t_j))$$ (19)

y: vector of model predictions at time t_j (j=1 to N)
Q: vector containing weighting coefficients
θ: vector of model parameter (i=1 to P)

The fisher information matrix is therefore a P X P matrix with diagonal elements of the form:

$$f_{i,j} = \sum_{j=1}^{N}(\frac{\partial y}{\partial \theta_i}(t_j))^2$$ (20)

and off-diagonal elements of the form:

$$f_{i,k} = \sum_{j=1}^{N} \left(\frac{\partial y}{\partial \theta_i}(t_j) \right) \left(\frac{\partial y}{\partial \theta_k}(t_j) \right) \tag{21}$$

The corelation coefficients ρ_{ij} are computed from the covariance matrix (X), which is the inverse of F (Chandran and Smets, 2000):

$$\rho_{i,k} = \frac{x_{i,k}}{(x_{i,j} \cdot x_{k,k})^{0.5}} \tag{22}$$

where:

$x_{i,k}$: off-diagonal element of the covariance matrix X

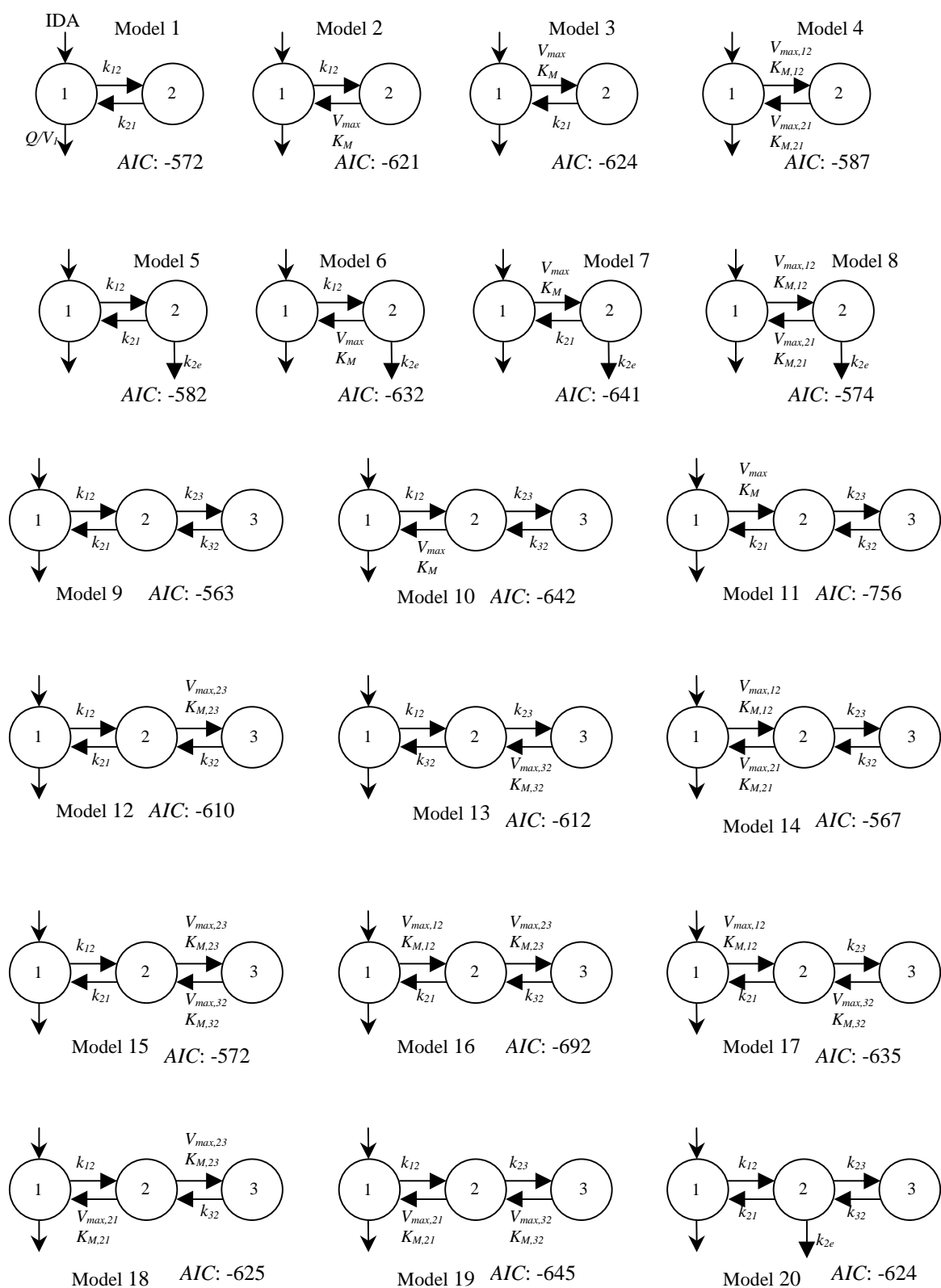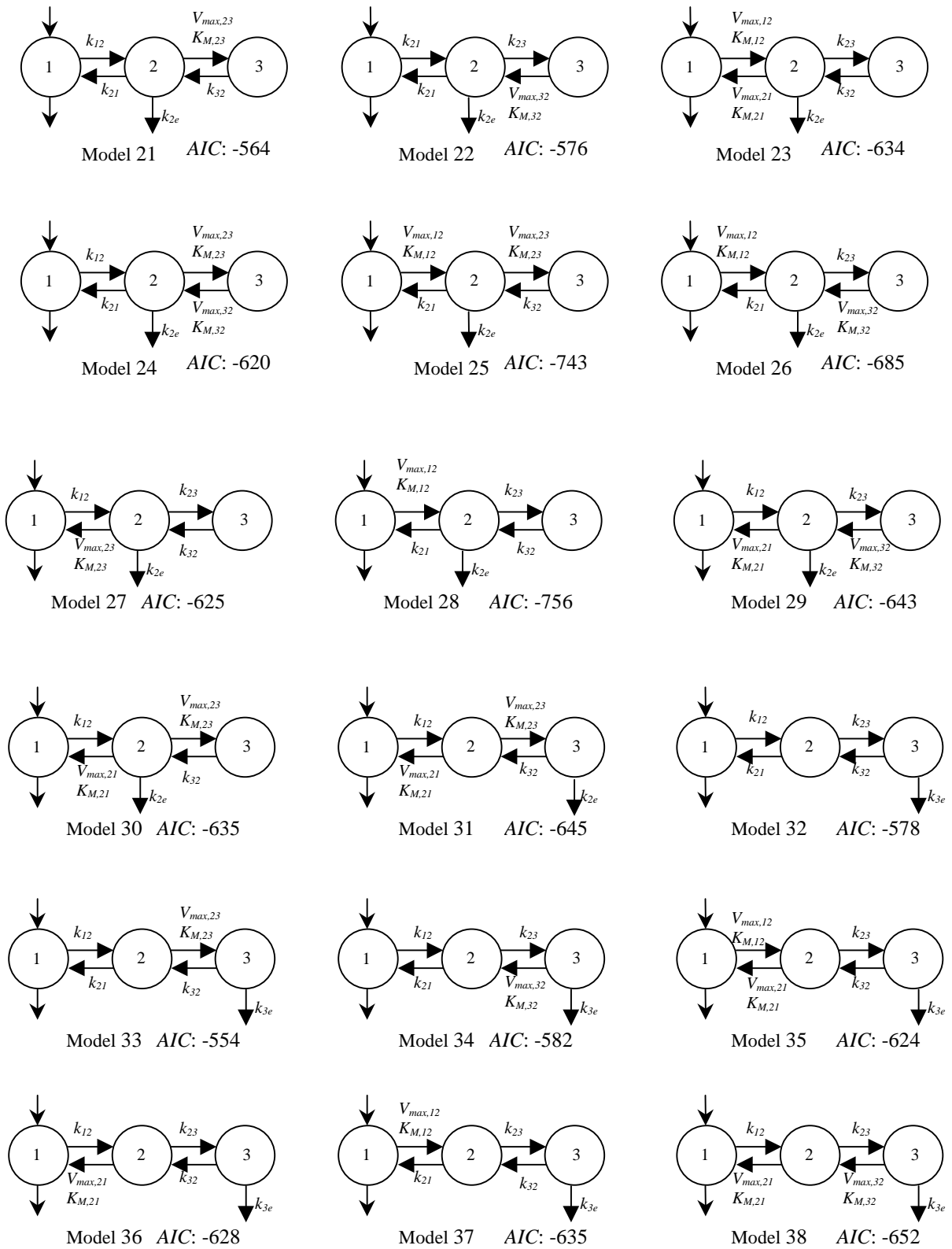$x_{i,i}$: and $x_{k,k}$: mean diagonal elements of the covariance matrix X.

Figure 7. AIC values of tested compartmental structures for idarubicin.
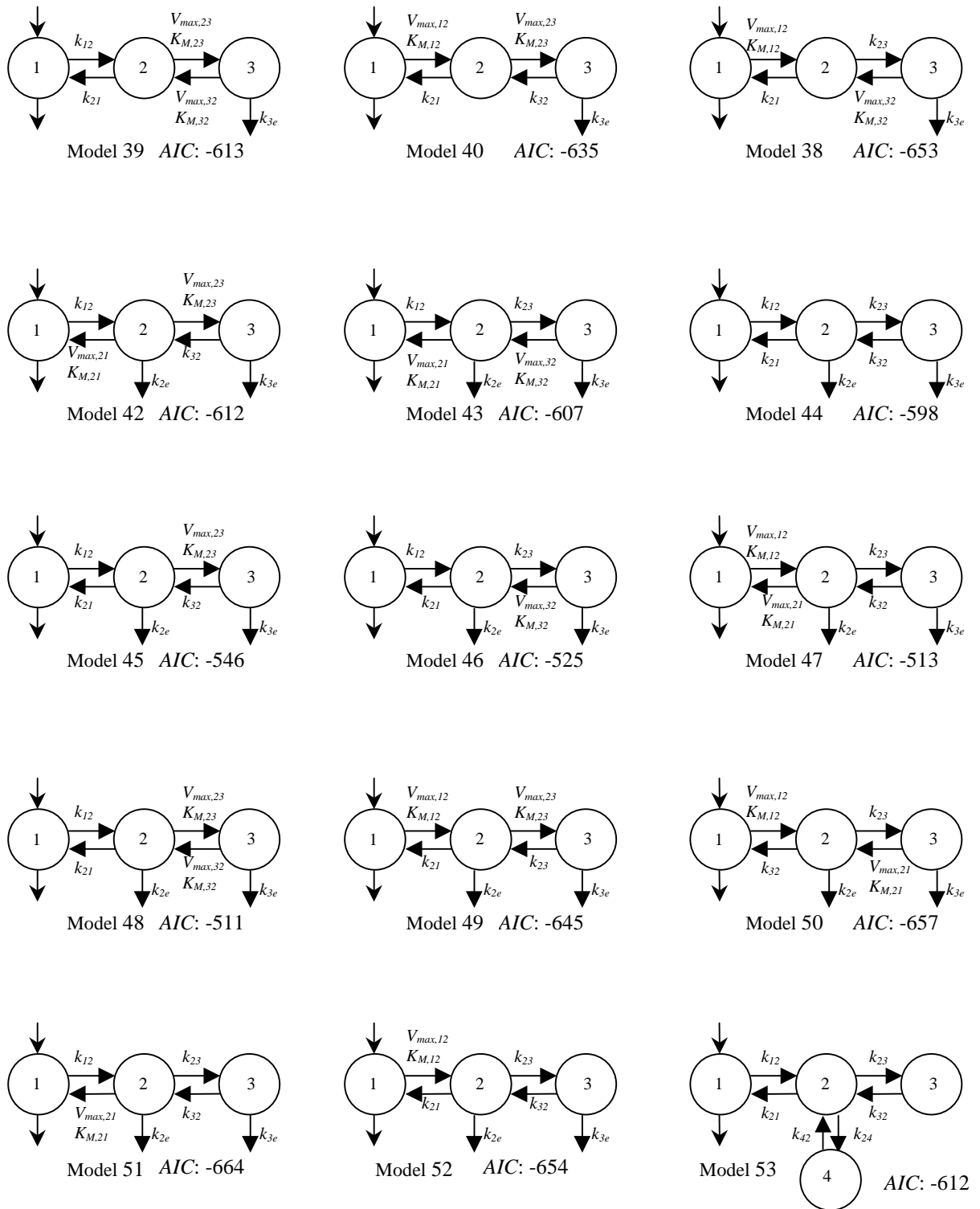
Figure 7. Continued.

Figure 7. Continued.

6-2. Simultaneous Nonlinear Regression (SNLR)

The crucial associated question is concerned with the uncertainties in the estimated parameter values since model identifiability is a central problem in using models with saturable transport processes (nonlinear systems). An analysis often yields many parameter value sets ("solutions") that fits the data of one experiment nearly equally well. In other words, the information content of the experiment is insufficient to resolve the parameters into a unique set of most probable values. A practical method to overcome this problem is simultaneous nonlinear regression (SNLR) (e.g., Kakkar et al., 2000) where the regression process is conducted for different experiments simultaneously and the modeling function shares parameters that are independent of the specific experimental condition. SNLR can be successful when complete data sets (with replicates) are obtained from experiments performed under different conditions as, for example, in the absence and presence of P-gp inhibitors.

Nonlinear regression is performed with the average data of the control group and the treatment groups. Thereby, the parameters described the kinetics in the control group and factors f_i accounts for a potential change in parameters P_i due to the treatments (i.e., in the model of the treatment groups model parameters P_i were replaced by $f_i P_i$). In the experiments in the presence of P-gp inhibitor (verapamil, amiodarone) 9 equations (control, eq. 4-6; verapamil, eq. 23-25; amiodarone, eq. 26-28) are solved and simultaneously fitted to the data.

$$dx_1(t)/dt = -(Q/V_1 + f_{Vmax12,vera}V_{max,12}/[f_{Km12,vera}K_{M,12} + x_1(t)])x_1(t) + f_{k12,vera}k_{21}x_2(t) + R_{10min} \tag{23}$$

$$dx_2(t)/dt = f_{Vmax12,vera}V_{max,12}/[f_{Km12,vera}K_{M,12} + x_1(t)])\,x_1(t) - (f_{k21,vera}k_{21} + f_{k24,vera}k_{24} + f_{Vmax23,vera}V_{max,23}/[f_{Km23,vera}K_{M,23} + x_2(t)])\,x_2(t) + f_{k32,vera}\,k_{32}\,x_3(t) \tag{24}$$

$$dx_3(t)/dt = f_{Vmax23,vera}V_{max,23}/[f_{Km23,vera}K_{M,23} + x_2(t)])\,x_2(t) - f_{k32,vera}k_{32}\,x_3(t) \tag{25}$$

$$dx_1(t)/dt = -(Q/V_1 + f_{Vmax12,amio}V_{max,12}/[f_{Km12,amio}K_{M,12} + x_1(t)])x_1(t) + f_{k12,amio}k_{21}x_2(t) + R_{10min} \tag{26}$$

$$dx_2(t)/dt = f_{Vmax12,amio}V_{max,12}/[f_{Km12,amio}K_{M,12} + x_1(t)])\,x_1(t) - (f_{k21,amio}k_{21} + f_{k24,amio}k_{24} + f_{Vmax23,amio}V_{max,23}/[f_{Km23,amio}K_{M,23} + x_2(t)])\,x_2(t) + f_{k32,amio}\,k_{32}\,x_3(t) \tag{27}$$

$$dx_3(t)/dt = f_{Vmax23,amio}V_{max,23}/[f_{Km23,amio}K_{M,23} + x_2(t)])\,x_2(t) - f_{k32,amio}k_{32}\,x_3(t) \tag{28}$$

where "vera" and "amio" indicate verapamil and amiodarone, respectively.

All possible combinations of factors are tested with the aim to describe treatment groups by a minimum number of factors, i.e. free model parameters. The factor selection is made according to the model selection criteria.

6-3. Pharmacodynamic Effect

Left ventricular pressure and coronary perfusion pressure (coronary vascular resistance, CVR) are recorded on a computer that allows continuous monitoring of heart rate, left ventricular systolic pressure (LVSP), left ventricular enddiastolic pressure (LVEDP), maximum and minimum values of rate of left ventricular pressure development (LVdP/dt$_{max}$ and LVdP/dt$_{min}$). Left ventricular developed pressure is defined as LVDP = LVSP - LVEDP. The change of effect parameters (LVDP, Heart rate, CVR) induced by IDA, $\Delta E(t)$ is given by

$$\Delta E(t) = \frac{E(t) - E(0)}{E(0)} \tag{29}$$

where $E(0)$ presents the baseline value of each parameter before IDA administration. Numerical integration is used to calculate the area under the effect curve (AUE), which acts as a measure of the overall effect of IDA in the presence situation of bolus injection where the pharmacological effect changes with time:

$$AUE = \int_0^{t_n} \left[E(t) - E_0 \right] \tag{30}$$

where t_n denotes the time of the last measurement.

6-4. Noncompartmental pharmacokinetic analysis

The time course of amount of IDA (or IDOL) recovered in outflow perfusate, $A_R(t)$, is

calculated from the outflow concentration versus time data, $C(t)$, and perfusate flow, Q, using a numerical integration method

$$A_R(t) = Q \int_0^t C(\tau) d\tau \qquad (31)$$

and the fraction of dose recovered at the end of experiment ($t_{last} = 80$ min) is obtained as $Recovery = A_{R,}(t_{last})/\text{Dose}$.

6-5. Statistics

The results are expressed as mean ± S.D. The significance of changes in the time course of outflow concentration in treatment is tested by repeated measurement ANOVA. P-values of less than 0.05 are considered statistically significant.

Since in the present case global analysis (SNLR) can be performed only with pooled data, asymptotic standard errors of parameter estimates are obtained by nonlinear regression which are generally over-optimistic. Thus, the likelihood ratio test (Huet et al., 1996) is used to determine the significance of parameter changes in the nested models due to the treatment.

In the likelihood ratio test O_{NLL} values of the control ("*Control*") and an alternative ("*Alternative*") model which has a different parameter value are calculated from each AIC value (eq. 17).

$$S_L = -2 \left(O_{NLL}^{Alternative} - O_{NLL}^{Control} \right) \qquad (32)$$

If S_L is bigger than the value in the chi-square distribution table, then the parameter change is significant.

Results and Discussion

Chapter 7. PK/PD Modeling of IDA and Effect of P-gp Inhibitors (Verapamil, amiodarone, PSC 833)

7 - 1. Control, verapamil-, amiodarone-treatment in a 10-min infusion of IDA

Clarification of the transport mechanism of drugs into the heart is important regarding the efficacy or toxicity of cardioactive drugs. To better understand the physiological and pharmacological role of P-gp in the heart, the uptake kinetics and negative inotropic action of IDA are investigated in the absence and presence of P-gp inhibitors, verapamil and amiodarone.

Simultaneous nonlinear regression (SNLR) is performed following: IDA data obtained during a control perfusion and when P-gp antagonists are added to the perfusion, i.e., three sets of average data "control", "verapamil" and "amiodarone" are fitted simultaneously whereby factors f_{inh} accounted for a potential change in parameters due to the presence of P-gp inhibitor. Then, the pharmacokinetic parameters are fixed in fitting the effect data to estimate k_{eff}, EX_{50}, E_{max}, and N.

7-1-1. Uptake Kinetics of IDA and Effect of Verapamil and Amiodarone

Figure 8A shows the average outflow concentration-time profiles obtained for a 10-min infusion of IDA in the absence and presence of the P-gp inhibitors verapamil or amiodarone (n = 5 independent experiments in each group). After reaching their peaks at the end of infusion, the curves decays rapidly within 10 s, followed by a slow decline. Compared with control, the outflow concentration curve is shifted downward during the infusion period in the presence of verapamil (1 nM) or amiodarone (1 μM) (P < 0.05) indicating increased uptake of IDA.

A series of different compartment models describing the myocardial kinetics of IDA is evaluated. The best model selected according to the criteria described above is schematically shown in Figure 9.

Figures 8B and C show the resulting simultaneous fit of average IDA outflow concentration-time profiles for the three groups. The parameter estimates describing

cardiac disposition of IDA in the absence and presence of P-gp inhibitors are listed in Table 1. The compartment model and the measured data are concordant. The apparent distribution volume of Compartment 1 (14 mL) is larger than the distribution volume of an intravascular indicator indicating rapid equilibration with a tissue region surrounding the vascular space. The saturable, Michaelis-Menten type, uptake process into the heart is characterized by the apparent maximal transport rate $V_{max,12}$ and the apparent Michaelis constant $K_{M,12}$, (x_1 at which this uptake rate is at its half-maximal level) equal to 644 nmol/min and 42.8 nmol, respectively (alternatively, 46.0 µmol/L/min and 3.06 µmol/L in terms of concentration $C_1 = x_1/ V_1$). Kinetic analysis of the data indicates the existence of a second carrier-mediated transport process which governs distribution from Compartment 2 to Compartment 3 ($V_{max,23} = 347$ nmol/min, $K_{M,23} = 215$ nmol). The sequestration rate constant k_{24} accounts for quasi-irreversible binding and metabolism of IDA. P-gp inhibition causes a nearly 2-fold increase in the maximal uptake rate (P < 0.01), i.e., an increase in $V_{max,12}$ by factors $f_{Vmax12,vera} = 1.77$ and $f_{Vmax12,amio} = 1.80$ for verapamil and amiodarone, respectively. These factors completely describe the effect of verapamil and amiodarone on pharmacokinetics of IDA since all data are simultaneously fitted by a single set of parameter values (Table 1). The predicted amount of IDA in the heart is significantly increased by verapamil corresponding to the enhancement of IDA uptake rate (Figure 8D). The total amount in the heart is mostly dependent on the amount sequestrated to Compartment 4. The simulation result of the amount-time profile of IDA at each compartment is dipicted in Figure 10. The cardiac kinetics of IDA is characterized by high intracellular accumulation, with a predicted steady-state partition ratio for linear kinetics [$k_{in}/k_{out} = (V_{max,12}/ K_{M,12})/ k_{21}$] of 5.6 (which would increase nearly 2-fold in the presence of P-gp inhibitors). Fractional standard deviations for the parameter estimates and approximate correlation coefficients are mostly less than 0.25 and 0.8, respectively. Only the parameters V_1 and $K_{M,23}$ are relatively "poorly determined".
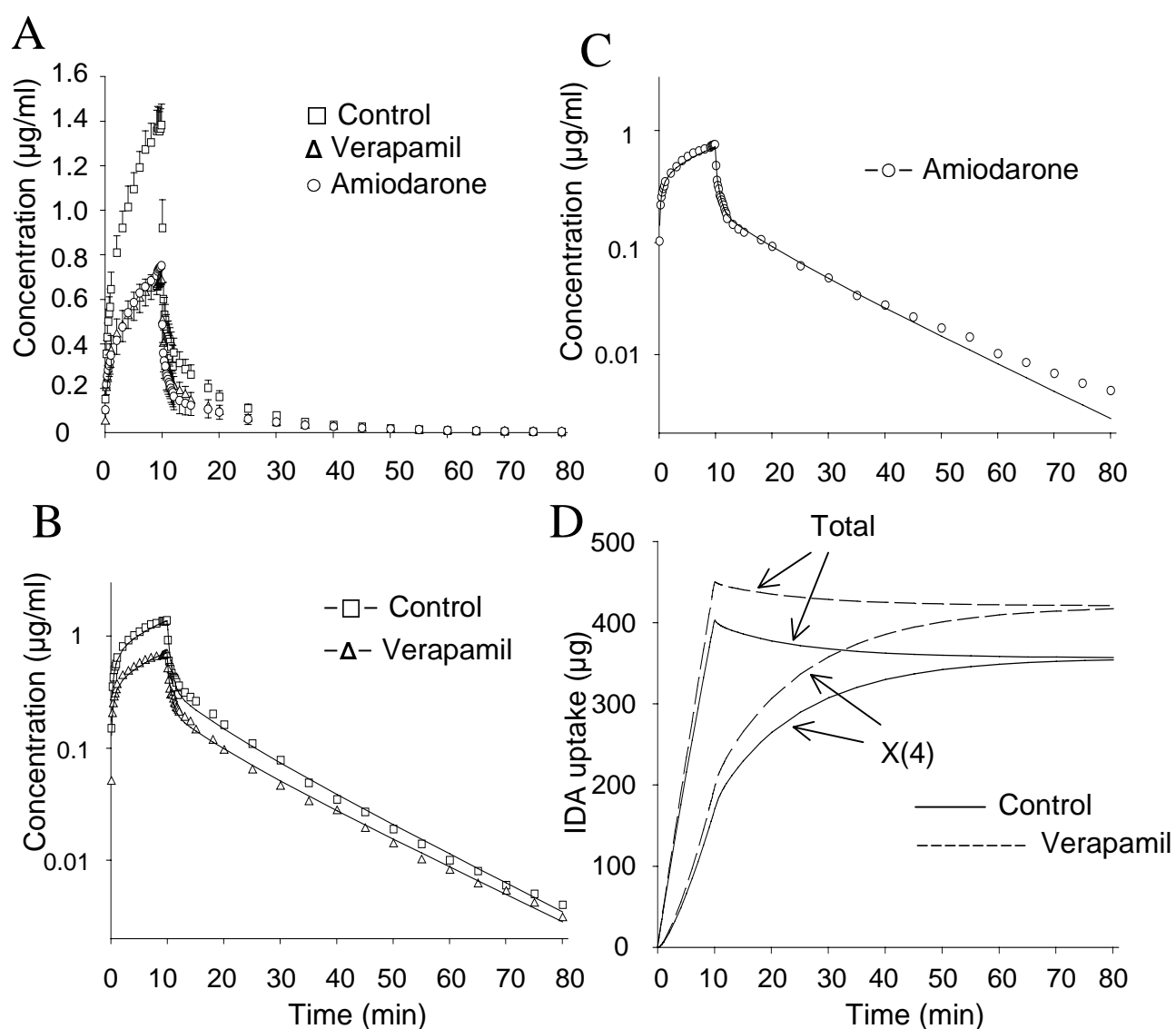
Figure 8. Panel A: IDA outflow profiles in hearts perfused with Krebs-Henseleit solution (control), verapamil (1 nM), and amiodarone (1 µM) after a 10 min infusion of 0.5 mg IDA; average ± S.D., n = 5 in each group). In the presence of P-gp inhibitors, the outflow concentration is significantly reduced during the infusion period (P<0.05). Panels B-C: Simultaneous fit to the average outflow data of the control, verapamil (B) and amiodarone (C) experiments. D: Predicted time course of total amount and compartmental amount (Compartment 4) of IDA and other generated metabolites except IDOL in the heart.

In — inflow → $x_1(t)$ — outflow → Q/V_1

P-gp

extracellular

intracellular

$V_{max,12}, K_{M,12}$ k_{21}

k_{32}

$x_3(t)$ $x_2(t)$ τ_{eff} $x_E(t)$

$V_{max,23}, K_{M,23}$

negative inotropic effect

k_{24}

$$E(t) = \frac{E_{\max}[x_E(t)]^N}{EX_{50}^N + [x_E(t)]^N}$$

$x_4(t)$

Figure 9. The model finally selected to describe the disposition of IDA in the isolated perfused rat heart. (V_1, initial distribution volume; Q, perfusate flow; Q/V_1, outflow rate constant; k_{ij}, first order rate constants; $V_{max,ij}$ and $K_{M,ij}$, Michaelis-Menten transport parameters; $x_i(t)$, compartmental amounts; P-gp, P-gp-mediated influx hindrance).

Table 1. Model parameter estimates for the pharmacokinetics and pharmacodynamics of a 10-min infusion of IDA in hearts from control, verapamil-(1 nM), and amiodarone-(1 µM) treated groups.

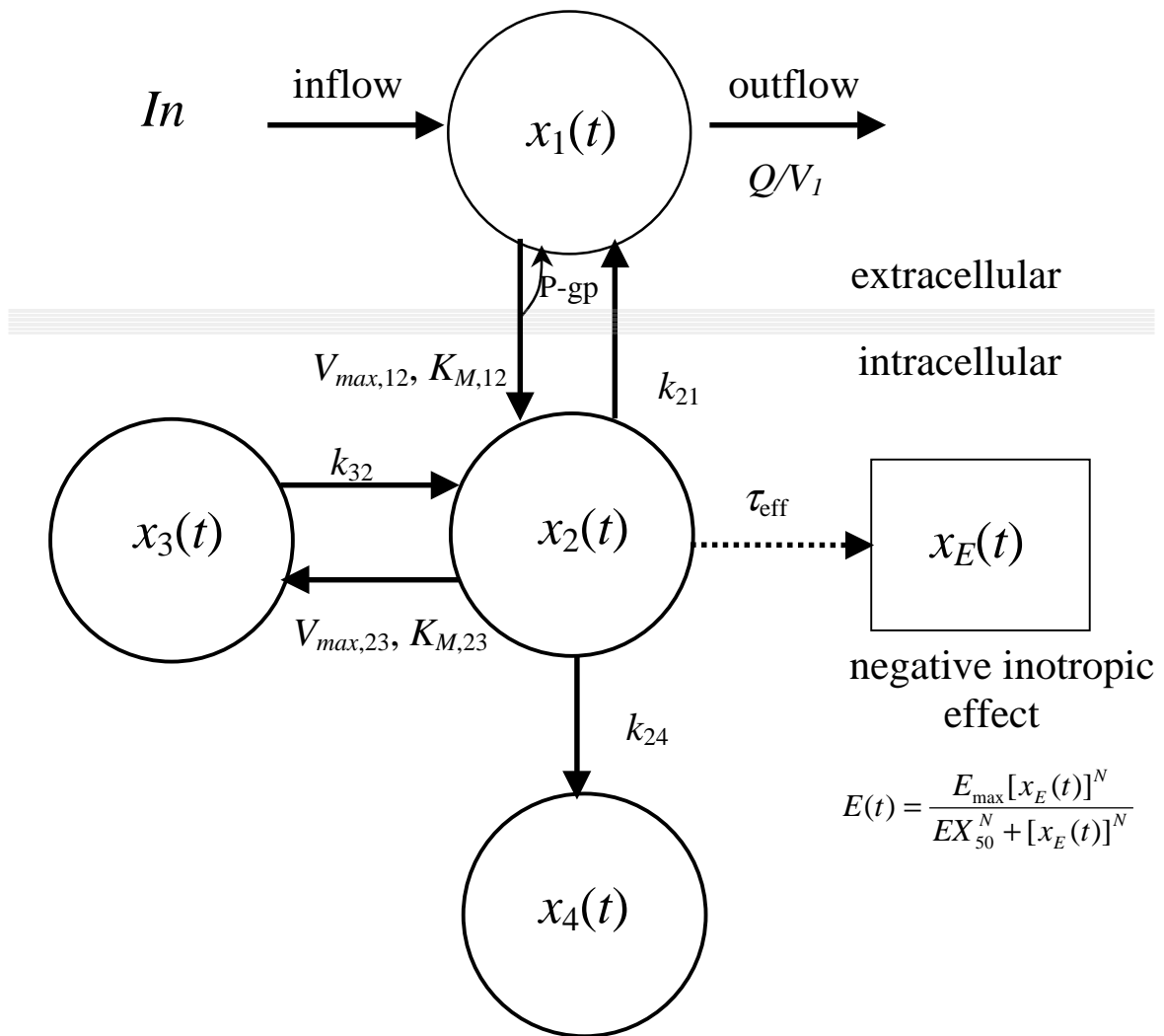| Pharmacokinetics[a]		FSD[c]	Pharmacodynamics[b]		FSD
Parameter	Estimate		Parameter	Estimate	
$V_{max,12}$ (nmol/min)	644	0.18	Control		
$f_{Vmax12,vera}$	1.76	0.03	τ_{eff} (min)	0.52	0.18
$f_{Vmax12,amio}$	1.80	0.03	E_{max} (%)	54.1	0.04
$K_{m,12}$ (nmol)	42.8	0.17	EX_{50} (µg)	19.2	0.07
k_{21} (min^{-1})	2.6	0.26	Verapamil		
k_{24} (min^{-1})	0.55	0.17	τ_{eff} (min)	1.67	0.04
$V_{max,23}$ (nmol/min)	347	0.23	E_{max} (%)	65.4	0.12
$K_{m,23}$ (nmol)	215	0.44	EX_{50} (µg)	40.8	0.11
k_{32} (min^{-1})	0.22	0.08	N	2.3	0.09
V_1 (ml)	14		Amiodarone		
$\sigma_{0,i}$ (µg/ml)	$< 10^{-7}$		τ_{eff} (min)	2.36	0.06
$\sigma_{1,cont}$	0.14		E_{max} (%)	45.9	0.09
$\sigma_{1,vera}$	0.12		EX_{50} (µg)	28.6	0.10
$\sigma_{1,amio}$	0.09		N	2.4	0.11

[a] Simultaneous nonlinear regression of three IDA outflow concentration-time profiles (mean curves of control, verapamil, and amiodarone group, see Figure 8B and C), where one additional parameter in the model equationa accounted for the effect of verapamil ($f_{Vmax12,vera}$) or amiodarone ($f_{Vmax12,amio}$), respectively (e.g., $V_{max,12, vera} = f_{Vmax12,vera} V_{max,12}$).
[b] Final estimates (fit of LVDP data) with fixed pharmacokinetic parameters.
[c] Fractional standard deviations.
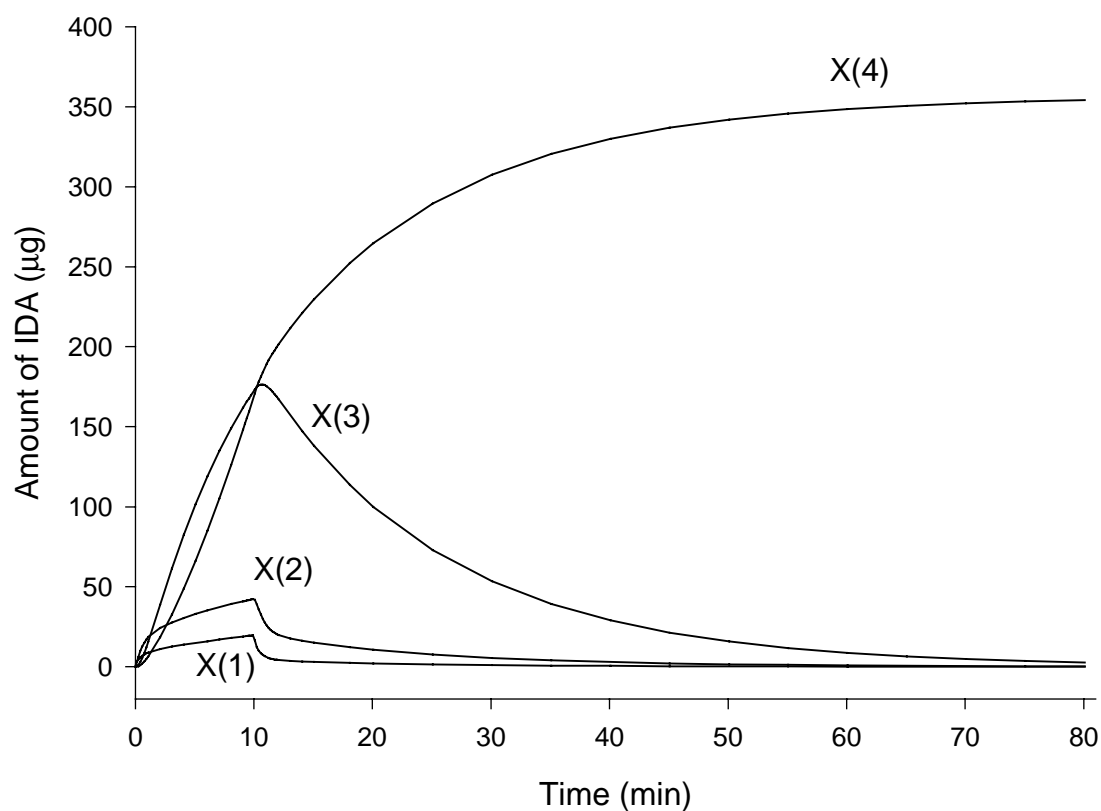
Figure 10. Time course of IDA-amounts in Compartment 1 to 4 after 10 min infusion of 0.5 mg IDA.

7-1-2. Pharmacodynamic response of IDA and Effect of verapamil and Amiodarone

IDA (0.5 mg) decreases myocardial contractility (LVDP, LVdP/dt$_{max}$), with maximum effects at the end of infusion. The LVDP and LVdP/dt$_{max}$ are decreased to 48.7 % and 51.2 % of baseline level, respectively, and recovered within 30 min. Figures 11A-C display the time course of observed and model-predicted negative inotropic action, $E(t)$, of IDA. The effect as a function of drug amount at the effect site is depicted for the three experimental groups in Figure 11D. The response is described adequately by the sigmoid E_{max} model; both verapamil and amiodarone attenuate the negative inotropic effect of IDA shifting the amount (or concentration)-effect relationship downwards. The equilibration time τ_{eff} of 0.52 min between cytosolic IDA concentration and effect increases more than 3-fold in the presence of P-gp inhibitors (1.67 and 2.36 min for verapamil and amiodarone, respectively).

A

B

C

D

Figure 11. Negative inotropic effect of IDA. A-C: The time course of effect as reduction of LVDP in % of baseline and fit by the combined kinetic-dynamic model for the control (A), verapamil (B), and amiodarone (C) group (average ± S.E., n = 5 in each group). D: Relationship between LVDP and the effect site amount predicted by the model for control, verapamil and amiodarone experiments.

7 - 2. Control, Verapamil-, PSC 833-treatment in a 1-min infusion of IDA

7-2-1. Uptake Kinetics of IDA and Effect of Verapamil and PSC 833

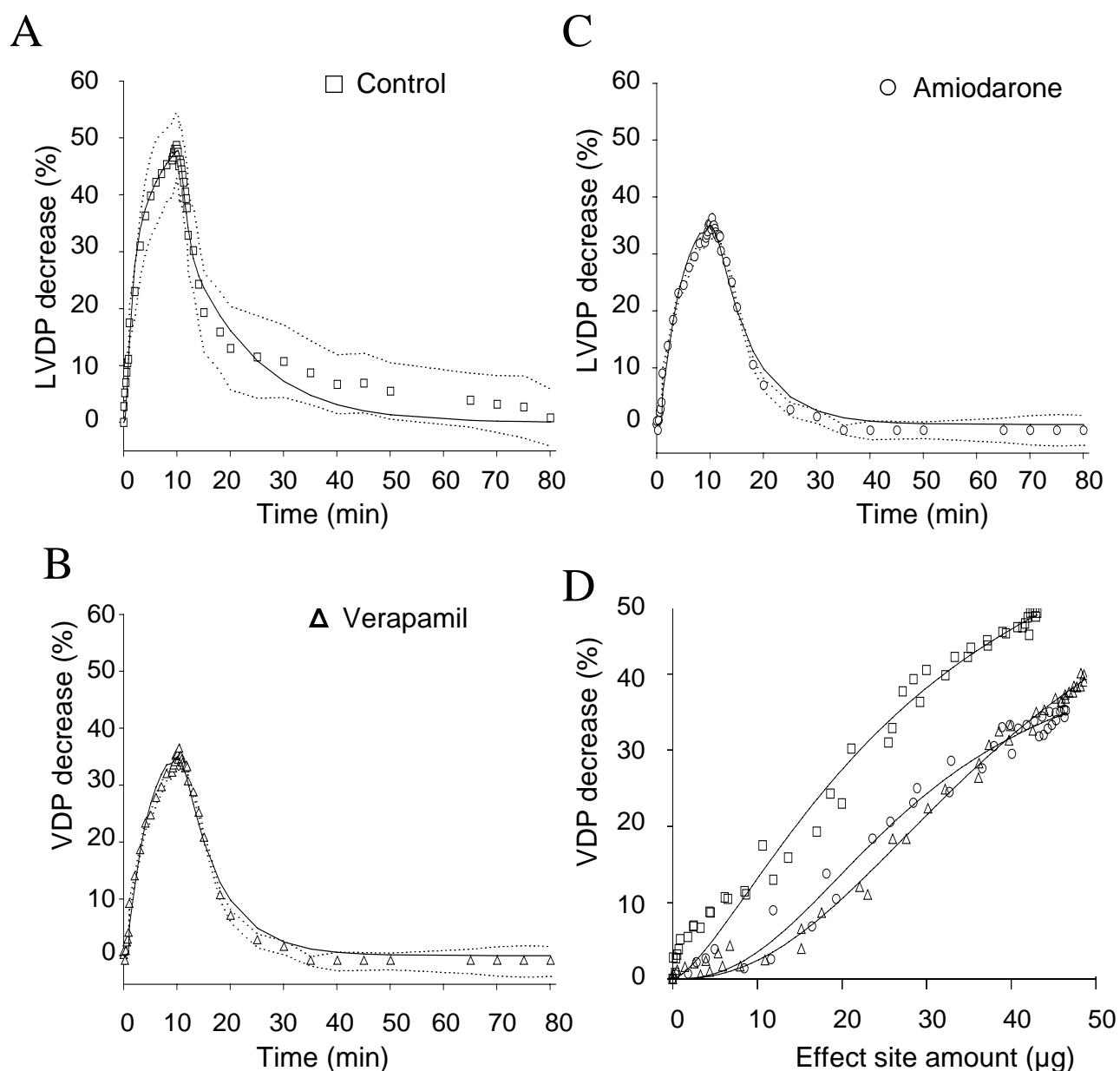Figure 12A shows the average outflow concentration-time profiles for IDA obtained for a 1-min infusion of IDA. The recoveries of IDA in the outflow perfusate (up to 80 min) are 53.9 ± 8.5 % of the dose, while 15.9 ± 1.71 % remained in the heart; leading to a total recovery (cumulative outflow plus amount in tissue) of 69.7 ± 8.6 % (Figure 12B). As shown in Figure 12B, verapamil (1 nM), in contrast to PSC 833 (1 μM), significantly increases cardiac uptake of IDA. The outflow recovery is decreased by 34.1 % and residual amount is increased by 45.1 %; while for PSC 833 no effect on residual amount could be detected, the outflow recovery is significantly increased by 43.8 %.

In modelling approach, firstly, average data of control is fitted (Figure 14A), and the parameter estimates are utilised to fit the treatment data sets, e.g. "verapamil", " PSC 833". Maximum likelihood estimator is used and the criteria for model selection and validity are as previously described. The parameter estimates of control data are listed in Table 2. The compartment model (Figure 13) describes the measured data very well. The apparent distribution volume of Compartment 1 is 3 ml. The apparent maximal transport rate $V_{max,12}$ and the apparent Michaelis constant $K_{M,12}$ equal to 760 nmol/min and 3.6 nmol, respectively.

Model validation in terms of fractional standard deviations shows that most parameters are estimated with sufficient validity. In compartmental modeling analysis verapamil increases the maximal uptake rate by 15 % ($fVmax,12$ = 1.15) and decreases back transport from Compartment 3 to Compartment 2, i.e., a decrease in k_{32} by factor of 0.03 (Figure 14B). On the other hand, PSC 833 hinders the uptake of IDA in a competitive manner and decreases the sequestration rate: $K_{M,12}$ of IDA increases by 1.8-fold, while the sequestration rate constant, k_{24} is decreased by factor of 0.4 (Figure 14C). The time courses of the total cardiac amount of IDA (plus formed metabolites) and the amount at Compartment 4 are depicted in Figure 14D.
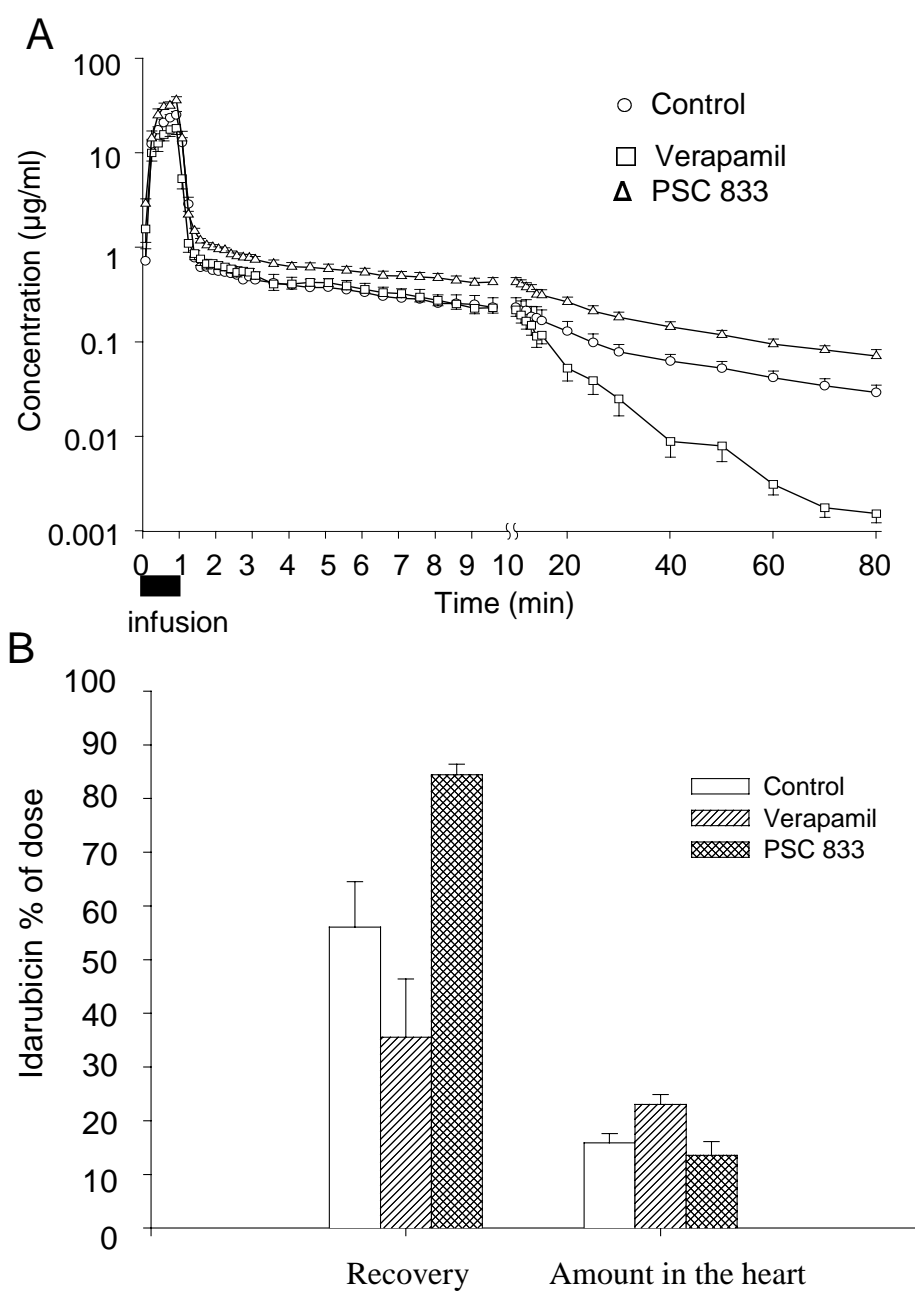
Figure 12. Panel A: IDA outflow profiles in heart perfused with Krebs-Henseleit buffer (control), verapamil (1 nM), and PSC 833 (1 µM) after a 0.5mg dose of IDA. Panel B: Recovery of IDA (in perfusate and amount in heart at 80 min after infusion of IDA in heart perfused with buffer (control), verapamil (1 nM), and PSC 833 (1 µM) (mean ± SEM; n=5 in each group; *$P<0.05$; **$P<0.005$; ***$P<0.001$, compared to control).
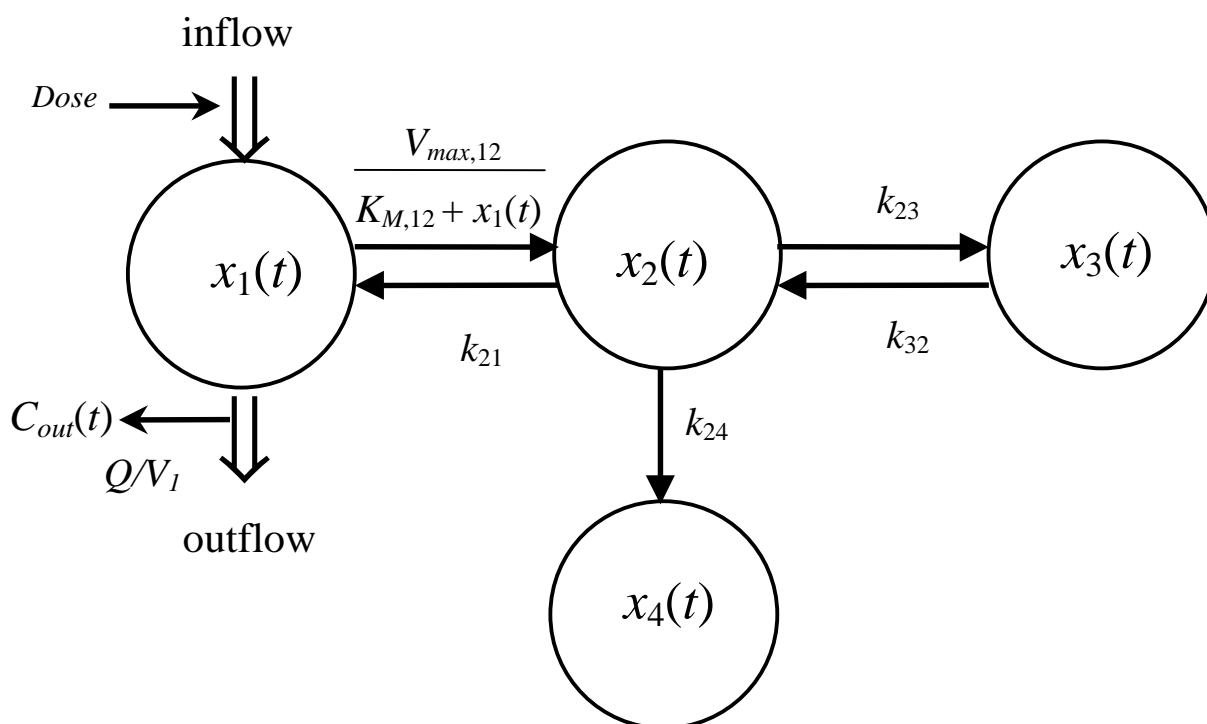
Figure 13. Compartmental model of IDA kinetics in the isolated perfused rat heart (V_1, initial distribution volume; Q, perfusate flow; Q/V_1, outflow rate constant; k_{ij}, first order rate constants; $V_{max,12}$ and $K_{M,12}$, Michaelis-Menten parameters of the uptake transport process; $x_i(t)$, compartmental amounts.

Table 2. Model parameter estimates for the pharmacokinetics of a 1-min infusion of IDA in hearts from control, verapamil-(1 nM), and PSC 833- (1 µM) treated groups.

Idarubicin		FSD^a	Treatments			FSD
Parameter	Estimate		Factor	Verapamil	PSC 833	
$V_{max,12}$ (nmol/min)	760.0	0.21	$fV_{max,12}$	1.15		0.02
$K_{M,12}$ (nmol)	3.6	0.46	$fK_{M,12}$		1.8	0.05
k_{21} (min^{-1})	0.7	0.30				
k_{23} (min^{-1})	0.04	0.32				
k_{32} (min^{-1})	0.06	0.33	fk_{32}	0.03		0.18
k_{24} (min^{-1})	0.03	0.21	fk_{24}		0.4	0.17
V_1 (ml)	3.0	0.15				

[a] Fractional standard deviations.
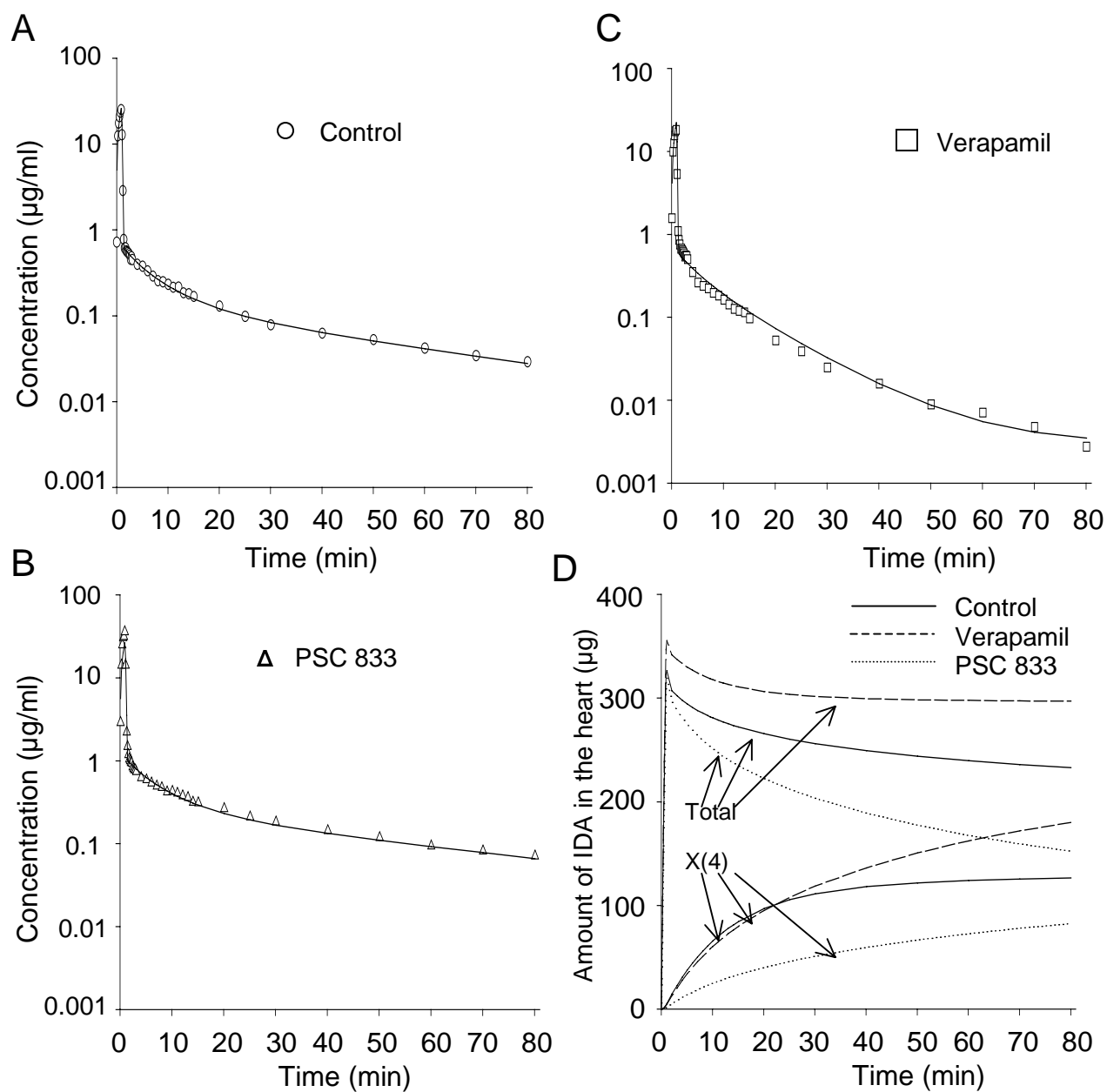
Figure 14. Panels A-C: Fits to the IDA average outflow data of the control (A), verapamil- (1 nM, B), and PSC 833- (1 µM, C) treatments. D: Predicted time course of total amount and compartmental amount (Compartment 4) of IDA in the heart.

7-2-2. Pharmacodynamic response of IDA and Effect of Verapamil and PSC 833

IDA (0.5 mg) decreases myocardial contractility (LVDP, LVdP/dt$_{max}$), with maximum effects at the end of infusion. The LVDP and LVdP/dt$_{max}$ are decreased to 39.3 % and 36.2 % of baseline level, respectively, and recovered within 30 min (Figure 15A). IDA impaires the diastolic relaxation; LVEDP increases from 5.3 ± 1.3 to 11.9 ± 3.4 mmHg after 2.4 min (Figure 15B) and LVdP/dt$_{min}$ decreases to 34.7 % of baseline level. The time course of the IDA-induced change in coronary vascular resistance (CVR) is biphasic: after an initial increase to 138.2 %   (reaching a peak value at 2 min), it decreases to a minimum of -7.3 % at 10 min and then increases again to 127.3 % of the basal value at 80 min (Figure 16). All these pharmacodynamic effects of IDA are significant at $P < 0.05$ level by one-way RM ANOVAs.

Verapamil (1 nM) attenuates the negative inotropic effect of IDA (Figure 15A), and the area under the effect curve AUE_{LVDP} changes from -324.4 ± 9.8 to -221.0 ± 28.2 mmHg min ($P < 0.05$). PSC 833 (1 μM), in contrast, impaires the recovery of LVDP to baseline ($AUE_{LVDP} = -1724.6$ mmHg min, $P < 0.05$ compared to control). The vasoconstrictive effect of IDA is markedly potentiated by PSC 833; both the maximum effect and the area under the effect curve AUE_{CVR} are significantly increased 2- and 3-fold, respectively. Verapamil significantly enhances the secondary increase in CVR after 80 minutes (Figure 16).

Figure 15. Effect of IDA (0.5 mg) on time course of LVDP (A) and LVEDP (B) in hearts perfused with buffer (control), verapamil (1 nM), and PSC 833 (1 μM) (mean ± SEM; n=5 in each group).

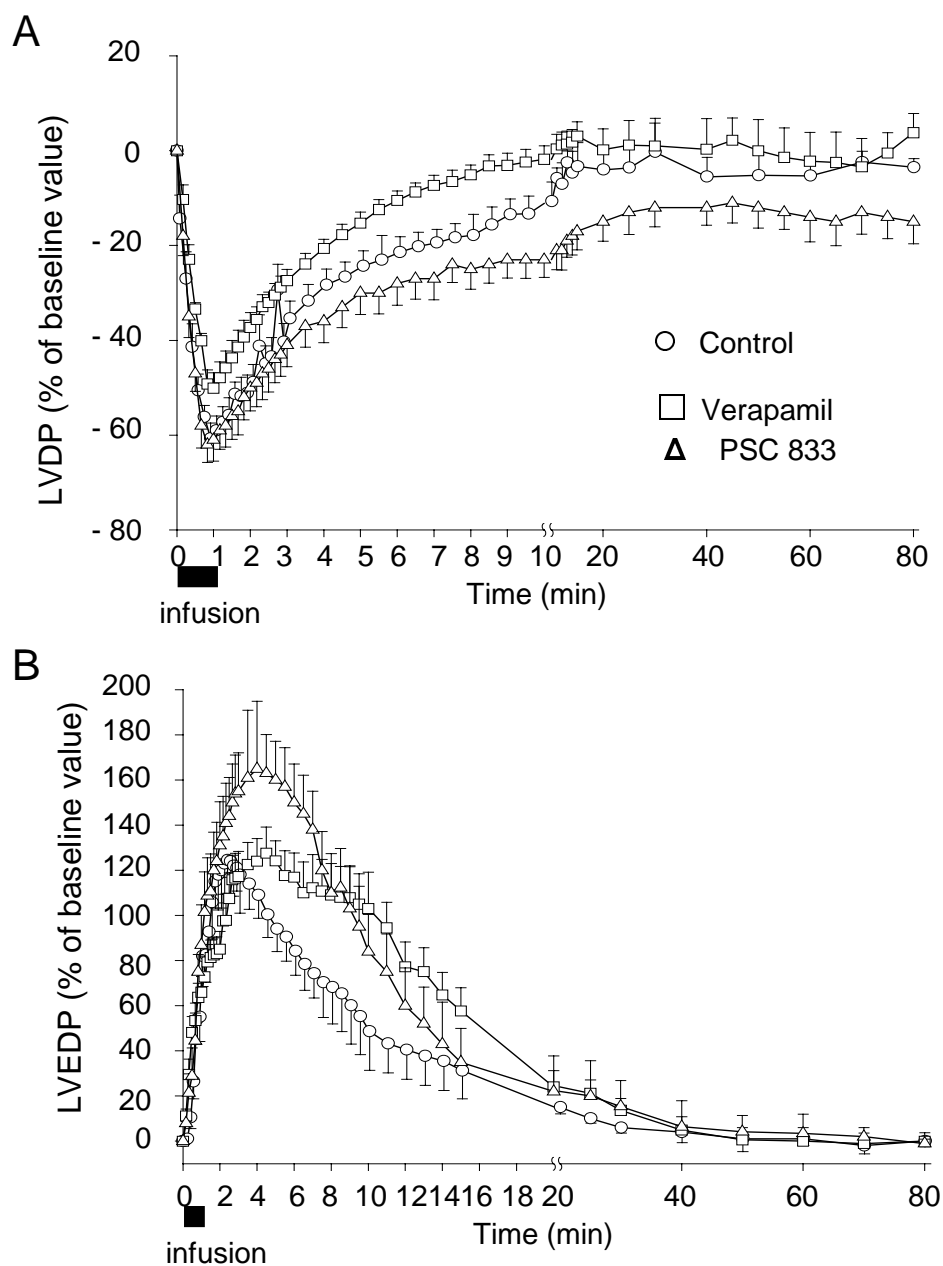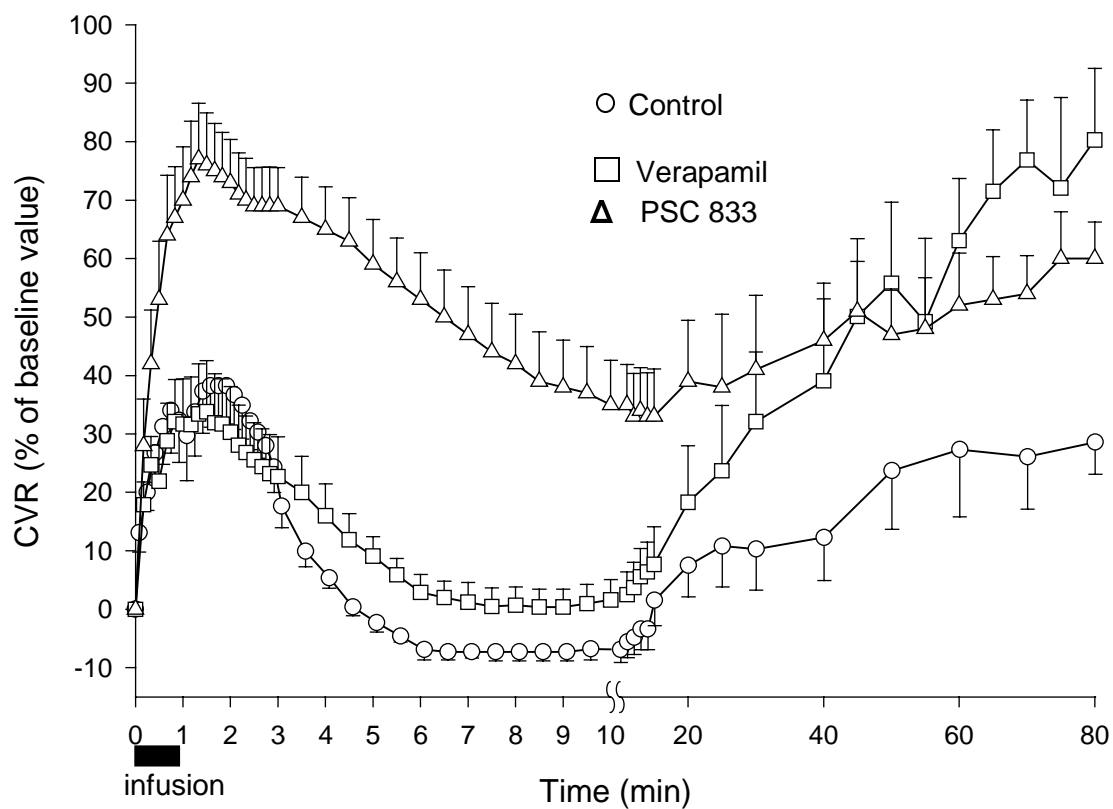**Figure 16.** Effect of IDA (0.5 mg) on coronary vascular resistance in hearts perfused with buffer (control), verapamil (1 nM), and PSC 833 (1 μM) (mean ± SEM; n=5 in each group).

7 - 3. Discussion

This study provides evidence 1) that uptake of the lipophilic anthracycline IDA in rat heart is through a saturable transport process, 2) that verapamil and amiodarone increase the maximal uptake rates of IDA, while PSC 833 decreases the myocardial uptake of IDA, and 3) that intracellular kinetics of IDA is closely related to its negative inotropic action whereby both P-gp inhibitors attenuate the cellular concentration-response relationship.

Uptake kinetics of anthracyclines including IDA has been previously studied in various cell lines; however, the transport mechanism is not completely clear. In this chapter, the uptake kinetics of a P-gp substrate, IDA into the intact heart is investigated for the first time. The observed nearly 2-fold increase in $V_{max,12}$ by P-gp antagonists in a 10-min infusion of IDA suggests that under control conditions P-gp pumps IDA out of the membrane, thus limiting its uptake (Figure 9). The observed (net) rate of myocardial IDA uptake represents a balance between two opposing processes; active pumping by P-gp back to the extracellular space and saturable transport of drug across the membrane. This finding is consistent with the "hydrophobic vacuum cleaner" model (Gottesman and Pastan, 1993), where P-gp interacts directly with substances in the

Figure 17. Schematic diagram of "hydrophobic vacuum cleaner" model.

plasma membrane accounting for decreased drug influx rates (P-gp removes drugs directly from the membrane, Figure 17); i.e., P-gp substrates probably gain access to the protein after partitioning into the membrane rather than from the aqueous phase. The fact that only $V_{max,12}$ but not $K_{M,12}$ is affected suggests a noncompetitive interaction in

accordance with the interaction between anthracyclines and verapamil in MDR cells (Nielsen et al., 1995; Stein, 1997). It has been shown that P-gp is expr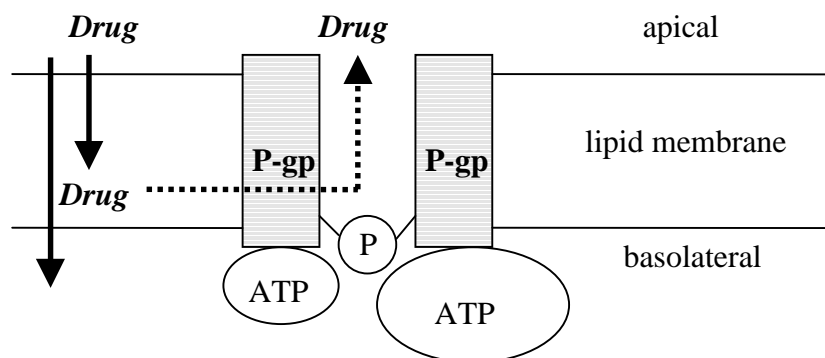essed in heart tissue (van der Valk et al., 1990; Cayre et al., 1996; Beaulieu et al., 1997; Estevez et al., 2000), and that P-gp has a role in the cardiac uptake of anthracyclines was recently suggested by pharmacokinetic studies in mice lacking *mdr1a* P-gp (*mdr1a* (-/-) mice) (van Asperen *et al*., 1999). That P-gp inhibition primarily increased cardiac uptake but not efflux from the heart ("influx hindrance") is in accordance with findings by Decleves et al. (1998) in leukemia HL-60 cells, who suggested that intracellular trapping of molecules could limit their availability for P-gp-mediated efflux. In contrast to the brain, where the P-gp pump is located on the luminal side of the capillary endothelial cell (Beaulieu et al., 1997), its location is less clear in the heart. Although P-gp is present in the plasma membrane of cardiomyocytes (Cayre et al., 1996; Estevez et al., 2000) and this kinetic-dynamic model indicates that Compartment 2 represents the cytosol (see below), one cannot differentiate between capillary wall and sarcolemma as permeability barriers.

The observation of Michaelis-Menten kinetics for uptake of the hydrophobic compound IDA in the intact heart is an interesting, novel result because the underlying mechanism is still poorly understood. There seems to be contradicting and confusing evidence in the literature with regard to anthracycline transport in cancer cell lines. On the one hand, it is suggested that passive membrane permeation plays a substantial role in controlling cellular accumulation together with P-gp-mediated efflux (reviewed in Refs. Stein, 1997;Wielinga et al., 2000). On the other hand, saturable uptake transport of anthracyclines into normal and MDR cells has been reported by several groups (Skovsgaard et al., 1978; Kerr et al., 1986; Usansky et al., 1991; Nielsen et al.,1995; Nagasawa et al., 1996, 1997; Decorti et al., 1998). Thus, in human mononuclear cells and HL60 cells, uptake of IDA was primarily carrier-mediated with a contribution of passive diffusion of about 10 % (Nagasawa et al., 1997). Similar to these results verapamil in MDR cells affected preferentially influx of daunorubicin increasing V_{max} by about 50% (Nielsen et al., 1995). However, the discussion of the underlying mechanisms is controversial (Kerr et al., 1986; Decorti et al., 1998; Nielsen et al., 1995); Decorti et al. (1998) suggested that saturation of nonspecific binding sites on the cell could mimic carrier-mediated transport.

The role of the intracellular transporter with lower capacity ($V_{max,23} \approx 0.5\ V_{max,12}$) and affinity ($K_{M,23} \approx 5K_{M,12}$) is less clear. One may speculate that Compartment 3 represents a sub-cellular pool, e.g., cytoplasmic organelles (Larsen et al., 2000), but in contrast to the uptake transporter, the estimation of the parameters $V_{max,23}$ and $K_{M,23}$ is less reliable (see discussion below). Figures 8D and 10 show that more than 90 % of the IDA amount which is taken up remains in the heart (or is metabolized) after the 80 min washout period demonstrating the strong binding to intracellular constituents (DNA) and trapping in acidic vesicles.

The effect of PSC 833 on cardiac uptake of IDA is unexpected. This finding is in contrast to that a well-known P-gp inhibitor, PSC 833 significantly increased the cardiac accumulation of doxorubicin administered intravenously to mice (Colombo et al., 1996), and that the combination of IDA and PSC 833 reversed P-gp mediated MDR in leukemia cells (Fukushima et al., 1999). In modeling analysis the IDA uptake inhibition is due to both an increase of $K_{M,12}$ and a decrease of k_{24}, sequestration rate constant implying irreversible binding and/or converting to aglycone. However, the latter dominantly affects the decrease of accumulation of IDA in the heart rather than the former from the simulation results. Since PSC 833 had no effect on the removal of daunosamine sugar by the microsomal P450 reductase (Fischer et al., 1998), the decrease of sequestration rate by metabolic interaction between IDA and PSC 833 could be excluded. On the other hand, one may speculate that PSC 833 influences the intracellular trapping of IDA probably due to change of intracellular pH, and further investigation would be important.

Although it has been suggested that the acute cardiac effects of anthracyclines are due to impaired myocardial Ca^{2+} handling, the mechanism appears still unclear (Matsushita et al., 2000). Several studies indicated that anthracyclines activate the cardiac sarcoplasmic reticulum (SR) Ca^{2+} release channel (ryanodine receptor) leading to an intracellular Ca^{2+} overload associated with an impairment of Ca^{2+} transients and a decrease in myocardial contractility (Holmberg and Williams, 1990; Earm et al., 1994; Temma et al., 1994; Temma et al., 1996; Maeda et al., 1999). Recently, it has been suggested that this negative inotropic action could also result from an inhibition of SR Ca^{2+} release (Olson et al., 2000). A dose-dependent decrease in the amplitude of

cytosolic Ca^{2+} transients has been observed for IDA in isolated rat myocytes (P. Wolna and M. Weiss, unpublished data). The present finding, that the effect $E(t)$, i.e., the decrease in contractility, is linked to the time course of IDA in Compartment 2, $x_2(t)$, with a relatively short lag time of 0.52 min, appears consistent with this concept (Figure 11A). Suggesting that $x_2(t)$ is the amount in the pharmacologically active pool, the kinetic-dynamic modeling sheds light on the possible anatomical/physiological role of the compartments, where Compartment 2 may represent the cytosol with trans-sarcolemmal IDA influx from Compartment 1. The model analysis allows, for the first time, a separation of the kinetic and dynamic effects determining the verapamil/amiodarone – IDA interaction. Theoretically, both cardioactive drugs interfere with stimulus-contraction coupling. The attenuation of the idarubicin-induced negative inotropic effect (Figure 11D) is in accordance with the protective effects of a calcium antagonist on doxorubicin-induced impairment of Ca^{2+} transients in rat cardiac myocytes (Maeda et al., 1999) and the inhibitory effect of amiodarone on the Na^{+}/Ca^{2+} exchanger, which has been suggested to prevent Ca^{2+} overload under pathological conditions (Watanabe and Kimura, 2000). However, because the complex mechanism of the negative inotropic action of IDA is not well understood and the available data are very limited, this empirical model is necessarily an oversimplification, which, for example, does not explain the physiological role of τ_{eff}.

PSC 833, on the other hand, shows an opposite effect in prolonging the recovery of the IDA-induced LVDP-decrease to baseline (Figure 15A). The same mechanisms that are responsible for the negative inotropic effects of cyclosporine A (Janssen et al., 2000) might be involved in this interaction. There is also a tendency for an increase in LVEDP after co-administration of PSC 833, but the variability is too high to achieve statistical significance (Figure 15B).

It has been long recognized that the acute anthracycline cardiotoxicity is characterized by an increase in coronary resistance (Pelikan et al., 1986). Current knowledge suggests that inhibition of nitric oxide (NO) synthesis is most likely responsible for the vasoconstriction produced by IDA, since there is no increasing evidence that 1) the release of NO contributes to the control of resting coronary blood flow (see e.g., Duffy et al., 1999) and 2) anthracyclines are potent nitric oxide synthase (NOS) inhibitors as shown for doxorubicin (Garner et al., 1999; Pomposiello et al., 1997), whereby the

endothelial NO-synthase (NOS III) was particularly susceptible to this inhibition. Thus, acute NOS-inhibition increased coronary vascular resistance in Langendorff-perfused hearts (Sudhir et al., 1994; Russo et al., 1996). The potentiation of the IDA-induced vasoconstriction in the presence of PSC 833 could be explained by the same mechanism since it has been suggested that the acute vasoconstriction induced by cyclosporine may be (partly) mediated by an impaired NO release (Watanabe et al., 1996). Less is known regarding vascular effects of PSC 833; a calcium potentiating effect similar to that of cyclosporine was found in vascular smooth muscle cells (Platel et al., 2000). In a pilot experiment a dose-dependent increase in CVR with PSC 833 is observed for concentrations above 0.1 mM. Thus, while PSC 833 in the concentration used in the present study (1 µM) did not affect CVR, it strongly potentiated the vasoconstrictive effect of IDA. The secondary increase in CVR in the presence of verapamil could be ascribed to the increase in the cardiac accumulation of IDA.

The importance of this study is the measurement of both myocardial kinetics and dynamics of the P-gp substrate IDA in the absence and presence of P-gp inhibitors. It should be noted that while our verapamil perfusate concentration of 1 nM is much lower than the concentrations used for MDR reversal *in vitro* and the therapeutic plasma concentrations, the concentration of PSC 833 (1 µM) is in the order of the effective concentration *in vitro* and *in vivo* (Estevez et al., 2000; Robert, 1999).

With regard to model identifiability and the precision of parameter estimates, it is encouraging that the fractional standard deviations and correlation coefficients between parameters are < 0.5 and < 0.8, respectively. Furthermore, a kinetic model will gain creditability if it can describe experimental data under different conditions (absence and presence of P-gp inhibitors) by adjustment of only one parameter ($V_{max,12}$ for uptake transport). Because this is the first report suggesting saturable uptake of a hydrophobic compound at the organ level, it is important to note that all tested alternative models based on passive influx completely failed to fit the data. The information obtained from IDA pharmacodynamics is necessary to identify the intracellular distribution kinetics, i.e., to obtain initial estimates of $V_{max,23}$ and $K_{M,23}$. As also obvious from the higher approximate coefficient of variation of $K_{M,23}$, less experimental evidence has been obtained in support of this intracellular uptake transporter. In view of the relatively slow

drug input rate used in this experiment, it is not surprising that the initial distribution volume V_1 is not uniquely identifiable. The value of 14.0 mL represents the optimal estimate which is then fixed to obtain the approximate *FSD*s for the other parameters (Table 1). (Note that the apparent extracellular distribution volume V_1 also accounts for rapid binding processes and has no direct anatomical meaning.) The estimate of apparent V_1 in a 1-min infusion of IDA is approximately one fifth of that in a 10-min infusion experiment indicating that the initial distribution process of rapid equilibration surrounding the vascular space decreases with increasing infusion rate. The necessarily simplified compartmental modeling approach taken herein represents a useful "minimal" heart model (Weiss, 1998), However, as any model, it does not provide a unique picture and must evolve with new acquired data and knowledge.

Chapter 8. Effect of Doxorubicin and Hypothermia

To date, uptake studies of anthracycline anticancer agents have been largely performed in vitro in tumour cell lines and it is doubtful whether these results accurately reflect the transport in intact organs. Furthermore, controversy exists as to whether cellular uptake of anthracyclines occurs via saturable transport mechanisms or passive diffusion (e.g., Speelmans et al., 1996; Decorti et al., 1998; Wielinga et al., 2000).

In previous chapter it has been suggested that 1) myocardial uptake of IDA appears to be characterized by Michaelis-Menten-type kinetics, 2) the saturable uptake rate is increased by P-gp inhibitors, probably because of impairment of P-gp mediated influx hindrance and 3) negative inotropic effect of IDA is closely related to its cellular pharmacokinetics. However, the nature of this saturable transport process is unknown. Because IDA is a hydrophobic molecule, it would be expected to cross the membrane barriers passively with relative ease in neutral form (Wielinga et al., 2000), but the mechanism by which anthracyclines are transported across cell membranes in cultured cells remains still rather unclear. Only previous results for the first time quantifies anthracycline uptake in an intact organ.

The purpose of this chapter is the investigation of temperature dependency and inhibitability by doxorubicin of myocardial uptake in order to elucidate further the underlying mechanisms. Like in previously described experiments, nonlinear regression is performed with the average data of the control group and those of the doxorubicin or hypothermia group, respectively.

8-1. Effect of Doxorubicin and Hypothermia on Pharmacokinetics of IDA

The average outflow concentration-time curves after infusion of 0.5 mg IDA for 10 min are shown in Figure 18A for the control and two treatment groups (n=5, independent experiments in each group). The curves show a maximum at the end of infusion and a rapid decay upon cessation of infusion is followed by a slower terminal phase. In the presence of doxorubicin (20 µM) the curve is shifted upwards in a nearly parallel fashion (P<0.01) suggesting reduced uptake during infusion. Mild hypothermia (30°C) changes the shape of the outflow, C(t), curve: following a steep increase within about 1

min (leaving the maximum at the end of infusion nearly unchanged), the concentration in the terminal phase is lower than that of control. Doxorubicin significantly inhibits net cardiac uptake of IDA as reflected by an increase in outflow recovery and a decrease in residual amount in the heart (Figure 18D).

Figures 18B and C show the fits of outflow concentration-time profiles of the doxorubicin and hypothermia group, respectively. Doxorubicin reduces both the maximal uptake rate $V_{max,12}$ and the cellular sequestration rate constant k_{24} (accounting for irreversible binding and metabolism) significantly to 65 and 35 %, respectively (Table 3), of the control value (P < 0.01). Hypothermia (30^oC), in contrast, reduces IDA uptake rate by increasing the Michaelis constant $K_{M,12}$ (~ 5.3-fold greater than that for control). But since also the efflux rate constant k_{21} decreases (to 8% of the control value), the net uptake remained unchanged (Figure 18D). The effect of temperature reduction on the model parameters $K_{M,12}$ and k_{21} is significant (P < 0.01). The presence of doxorubicin and hypothermia decreases the formation of idarubicinol from IDA in the heart by 85 % (P<0.01) and 34 % (P<0.05), respectively (Figure 18D).

Table 3. Parameters estimates for the disposition of IDA in the doxorubicin (20µM) and hypothermia (30^oC) group.

Doxorubicin	$fV_{max,12,Dox}$	$fk_{24,Dox}$
	0.65 [a] (0.08[b])	0.35 (0.09)
Hypothermia	$fK_{M,12,Hypotherm}$	$fk_{21,Hypotherm}$
	5.29 (0.02)	0.08 (0.02)

[a] Nonlinear regression of IDA outflow concentration-time profiles where two additional parameters accounted in the model equations for the effect of hypothermia (30^oC) and doxorubicin (20µM) on IDA (The parameter estimates of control are listed Table 1).
[b] Fractional standard deviations.
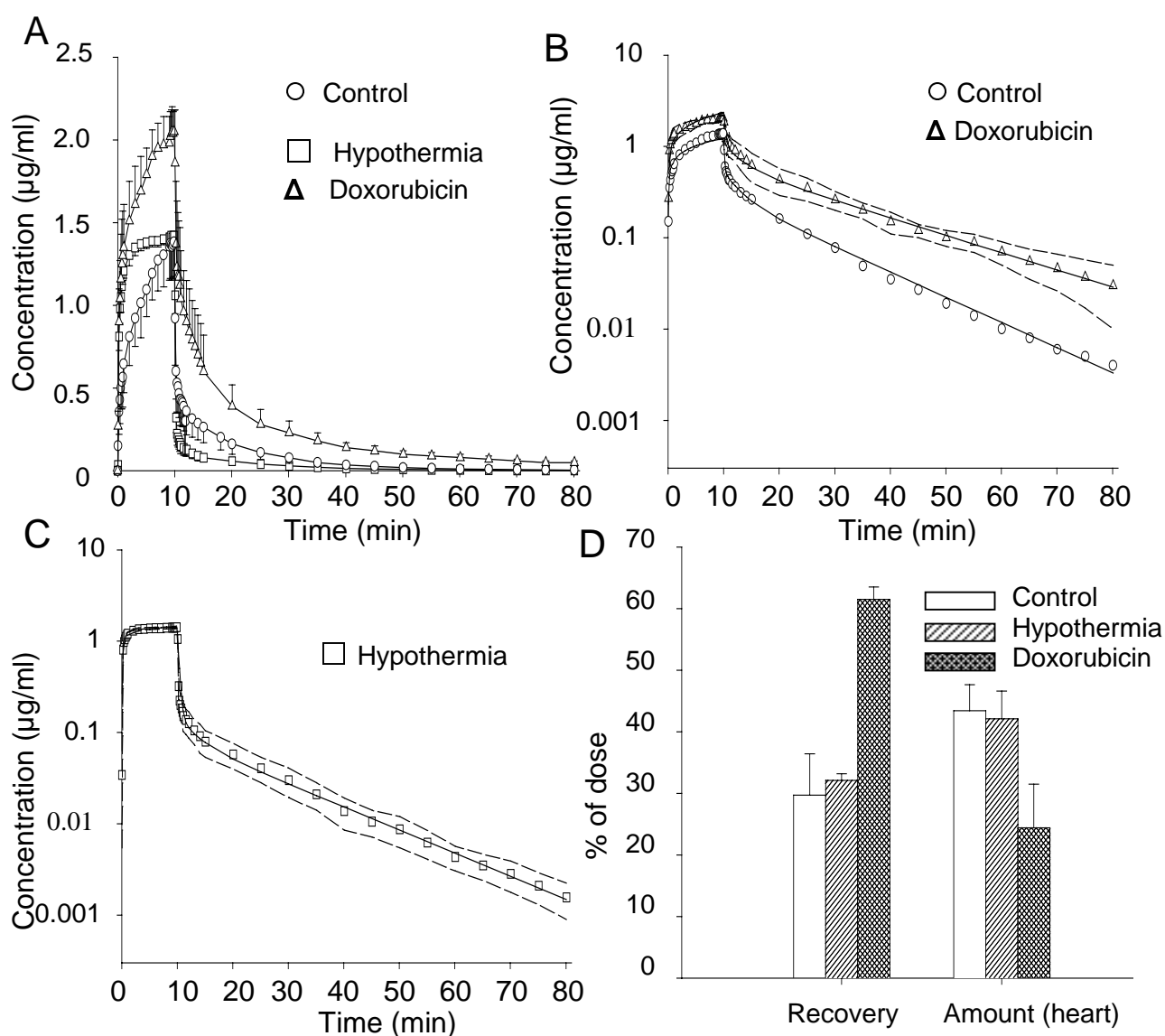
Figure 18. Panel A: IDA outflow profiles in hearts perfused with Krebs-Henseleit solution (control, 37°C), doxorubicin (20 µM), and hypothermia (30°C) for the 10-min infusion of 0.5 mg IDA (mean ± S.D., n = 5 in each group). Panels B-C: Fits of the mean outflow data of the control, doxorubicin (B) and low temperature experiments (C). Panel D: Outflow recoveries of IDA and residual amounts of IDA in the heart at the end of experiment ([*], $P<0.01$; [**], $P<0.005$ compare to control).

8-2. Effect of Doxorubicin and Hypothermia on Pharmacodynamics of IDA

While the presence of doxorubicin (20µM) in perfusate does not induce a significant change in LVDP within the first 20 min, infusion of IDA (0.5 mg) decreases LVDP to 49 ± 5 % of pre-infusion value at the end of infusion and recovery is completely impaired (after a transient increase to 64.4 ± 6 % of pre-infusion level) due to the delayed negative inotropic effect of doxorubicin. When administered alone, the relatively low concentration of doxorubicin (20µM) produces a maximum decrease in LVDP (to 56.1 ± 9 % of baseline level) about 100 min after start of infusion (Figure 19A). There is no significant change in coronary vascular resistance during the infusion of doxorubicin, and no further influence on IDA induces vasoconstriction compared to control (Figure 19C). In heart rate there is a delayed effect like LVDP, it is continuously decreased to 18 ± 9 % of baseline level at the end of experiment (Figure 19B).

After an increase in LVDP due to positive inotropism of hypothermia (to 160 ± 20 % of baseline level), infusion of IDA decreases myocardial contractility (LVDP) to 37 ± 3 % of pre-infusion level. The effect recovers within 30 min to 62 ± 7 % of pre-infusion level (Figure 20A). Heart rate is decreased to 50 ± 3 % of baseline value in hypothermic condition, but there is no significant change by the infusion of IDA (Figure 20B). Vasoconstriction is induced by hypothermia (Figure 20C), i.g., CVR is increased by 71 ± 15 % compared to that at $37^{o}C$. IDA induced increase of CVR is potentiated in hypothermic condition by 125 ± 18 and 98 ± 13 % of pre-infusion level at the end of IDA infusion and at 80 min, respectively. All these pharmacodynamic effects of IDA are significant at $P < 0.05$ level by one-way RM ANOVAs.
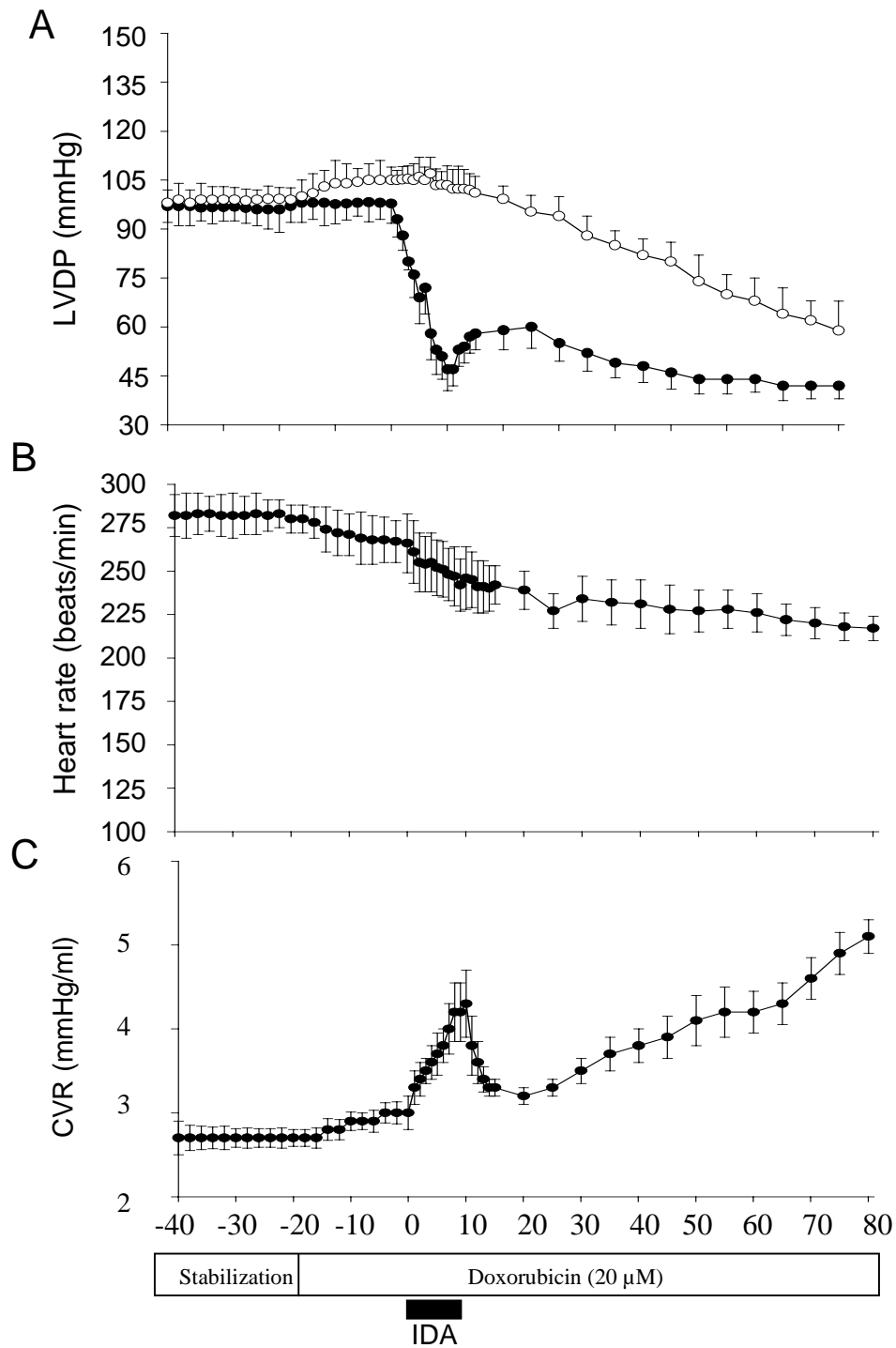
Figure 19. Time course of IDA-induced cardiac performances in the presence of doxorubicin (20 µM). A: left ventricular developed pressure (LVDP, ●) and the effect of doxorubicin alone (○), B: heart rate, C: coronary vascular resistance (CVR) (mean ± S.D., n = 5).

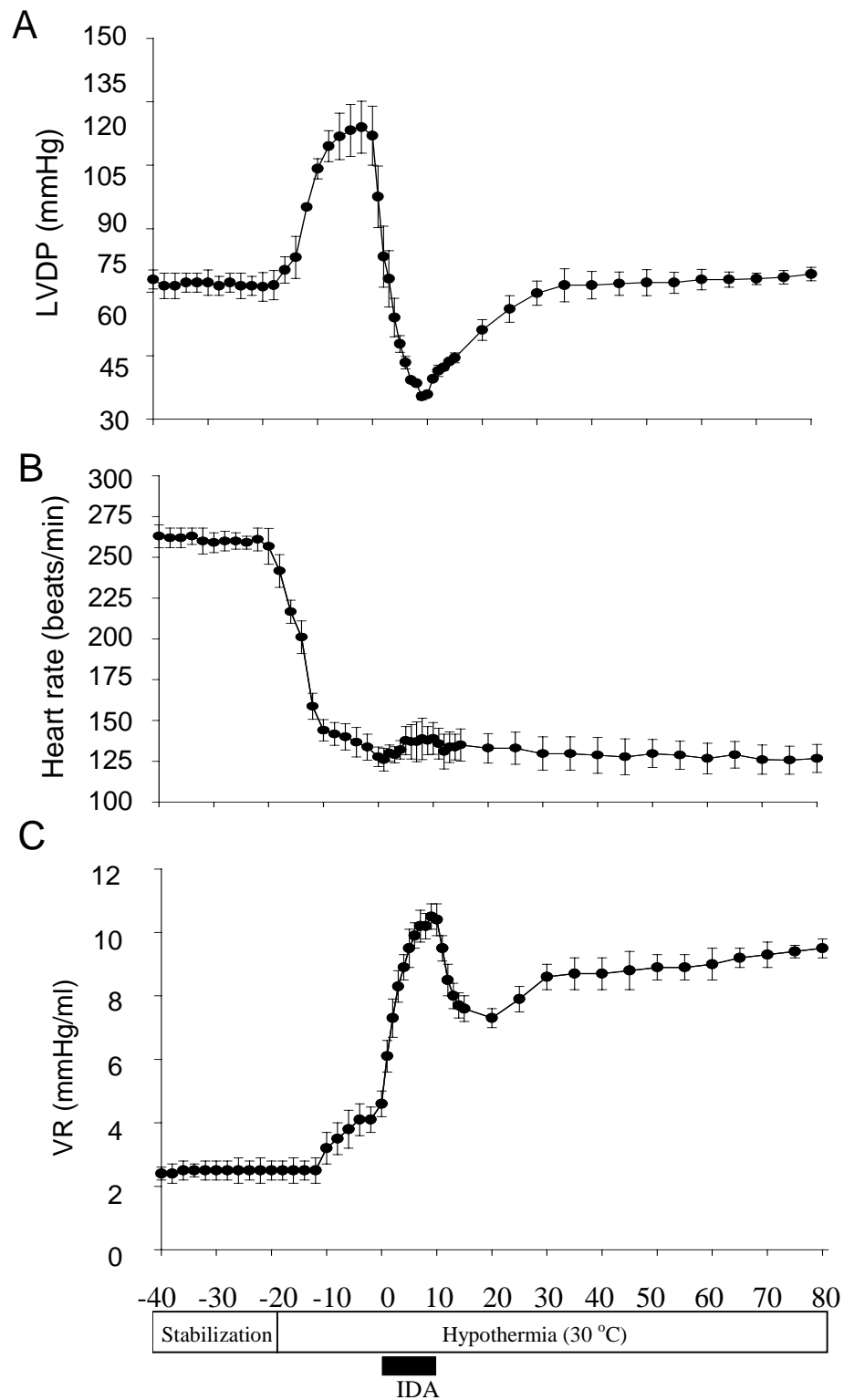**Figure 20.** Time course of IDA-induced cardiac performances in hypothermia (30°C). A: left ventricular developed pressure (LVDP), B: heart rate, C: coronary vascular resistance (CVR) (mean $\pm$ S.D., n = 5).

8-3. Discussion

At present, there is very little mechanistic understanding of anthracycline transport into the heart and other organs. The main outcome of this study is the inhibitability and temperature sensitivity of IDA uptake into the rat heart. The results indicate that the model adequately describes the effects of doxorubicin and hypothermia on IDA uptake by the rat heart. The myocardial uptake rate of IDA is noncompetitively inhibited by another anthracycline, doxorubicin due to a decrease in $V_{max,12}$, and the inhibition of uptake (increase in $K_{M,12}$) is observed upon cooling from 37° to 30°C. Kinetic analysis of IDA data reveals that the significant decrease in maximum uptake rate V_{max} in the presence of doxorubicin leads to a reduction of net uptake of IDA. The lower value of the elimination rate constant k_{24} reflects a decrease in intracellular trapping and metabolism. Hypothermia, in contrast, does not affect net uptake of IDA since the inhibition of uptake rate (increase in K_M) is counterbalanced by a decrease in the efflux rate constant (k_{21}).   Note that the factors $f_{Vmax12,Dox}$, $f_{k21,Dox}$ and $f_{KM12,Hypo}$, $f_{k24,Hypo}$ completely describe the effect of doxorubicin and temperature, respectively, on pharmacokinetics of IDA since all data are fitted by a single set of parameter values.

The noncompetitive inhibition of myocardial IDA uptake by doxorubicin is in accordance with observations in human leukaemia HL60 cells and mononuclear cells (Nagasawa et al., 1997). Interestingly, a competitive inhibition was observed for daunorubicin suggesting that the latter, in contrast to doxorubicin, binds to the same site as IDA. A qualitatively similar effect of hypothermia was found for anthracycline uptake in cultured fibroblasts where cellular accumulation of daunorubicin and doxorubicin was significantly inhibited by a decrease in incubation temperature from 37 to 30°C (Peterson and Trouet, 1978). Hyperthermia, on the other hand, increased the cellular uptake of doxorubicin in cultured cells (Nagaoka et al., 1986; Bates and Mackillop, 1986). The decrease in the efflux rate constant (k_{21}) with temperature is in line with observations in cultured cells, where the efflux rate of doxorubicin increased with temperature (Bates and Mackillop, 1986).
 It is well known that mild hypothermia exerts a positive inotropic effect (e.g., Weisser et al., 2001). The negative inotropic effect of IDA under hypothermia or doxorubicin is

similar to that under control conditions. The complete impairment of LVDP recovery to pre-infusion levels in the doxorubicin group is caused by the delayed development of the doxorubicin induced negative inotropism. An explanation of this phenomenon is lacking, however, for the hypothermia group, where similarly to the control experiments, LVDP recovered within 30 min, but reached only 62 % of the pre-infusion level.

In summary, these results provide strong evidence for the existence of a specific, saturable myocardial uptake process for anthracyclines in the rat heart.

Chapter 9. Effects of Caffeine and Theophylline

Based on in vitro data suggesting an enhancement by methylxanthines of IDA influx in leukemia cells (Sadzuka et al., 2000), the experiments described in this chapter are aimed at testing the hypothesis that a commonly used methylxanthine, caffeine, might influence the myocardial uptake of IDA. Furthermore, since caffeine is a well-known ryanodine receptor agonist, it is expected to affect pharmacodynamics of IDA due to its influence on anthracyline-induced Ca^{2+} release from sarcoplasmic reticulum (SR) (Pessah et al., 1990; Olson et al., 2000). The latter mechanism was suggested to cause the acute inotropic effect of anthracyclines (Matsushita et al., 2000) and might be involved in the cardiotoxic action of IDA. To address this issue, cardiac pharmacokinetics and pharmacodynamics of IDA is investigated in the presence of caffeine or theophylline in perfusate.

9-1. Effect of Caffeine and Theophylline on Pharmacokinetics of IDA

Figure 21A shows the average outflow concentration-time profiles obtained for a 10 min infusion of IDA (0.5 mg) in the absence and presence of caffeine (1 µM) or theophylline (3 µM), respectively. Caffeine, in contrast to theophylline, shifts the outflow concentration curve downward in a nearly parallel fashion (P<0.01) indicating increased uptake of IDA. Caffeine significantly decreases the outflow recovery of IDA from 29.7 ± 6.7 to 11.4 ± 0.97 % (*P*<0.01) and increases the residual amount of IDA in the heart from 43.4 ± 4.2 to 61.6 ± 4.2 % of dose (*P*<0.01). Theophylline has no significant effect on both recovery (33.7 ± 5.1 %) and residual amount of IDA (49.7 ± 6.9 %). The fits of IDA outflow concentration-time profiles of caffeine- and theophylline-treated groups are shown in Figure 21B. A perfect fit of IDA is obtained with only one factor, i.e., by changing one model parameter value, namely $V_{max,12}$ in the caffeine and k_{24} in the theophylline group, respectively (Table 4). While caffeine causes 2.7-fold increase in the maximal uptake rate (P<0.01), ($f_{Vmax,12} = 2.65$ with *FSD* of 0.04), theophylline leads to a 19 % reduction of the sequestration rate constant, k_{24} ($f_{k24} = 0.81$ with *FSD* of 0.03). The latter is reflected by the slightly lower decay (i.e., decreased slope) of the outflow curve in the terminal phase (Figure 21B).
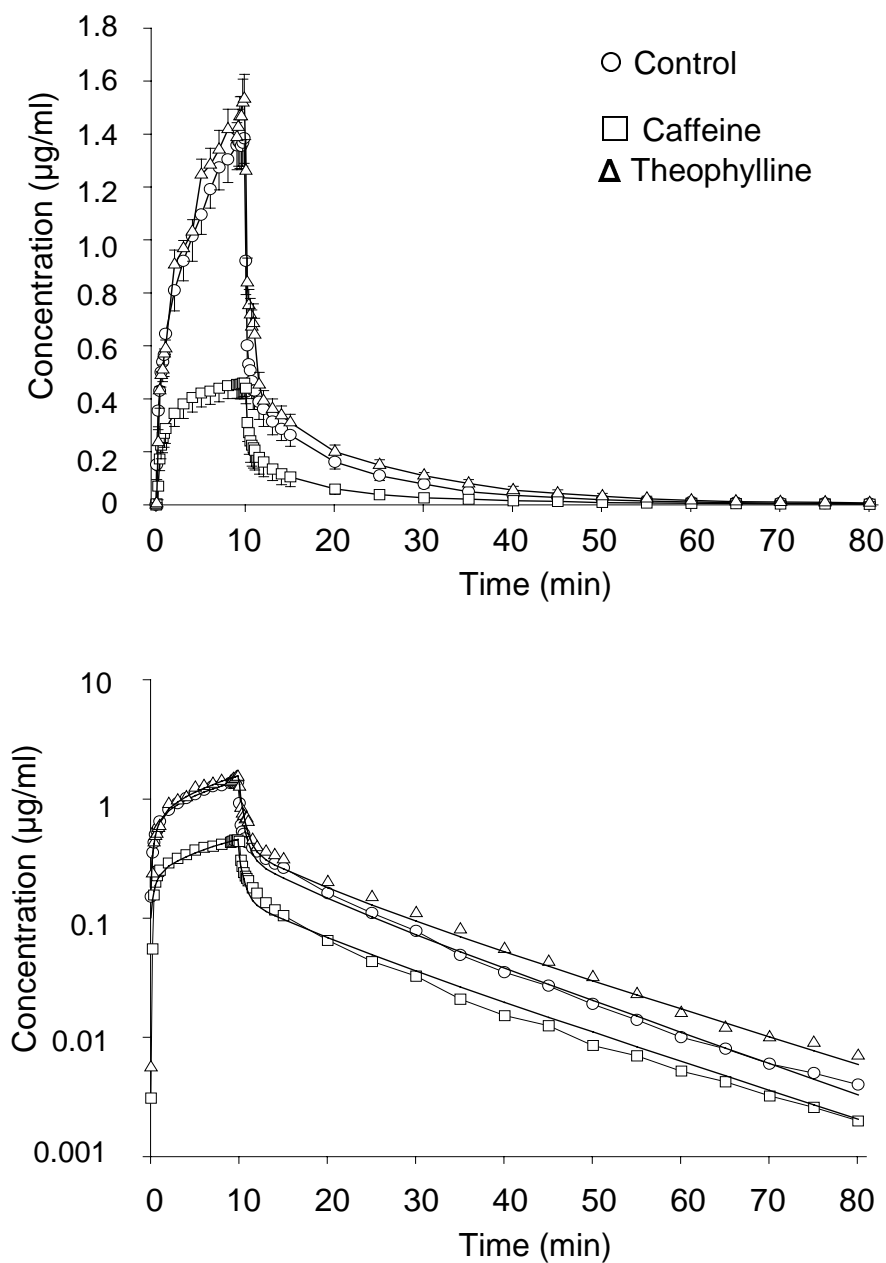
Figure 21. Panel A: outflow profiles of IDA in hearts perfused with buffer (control), caffeine (1 µM), and theophylline (3 µM) after a 10 min infusion of 0.5mg IDA (average ± S.E. n=5 in each group). Panel B: Fits to the IDA average outflow data of the control, caffeine- and theophylline-treatment.

Table 4. Parameters estimates for the disposition of IDA in the presence of caffeine (1 µM) and theophylline (3 µM).

	Parameter	Estimate	*FSD*
Caffeine	$fV_{max,12}$	2.65[a]	0.04[b]
Theophylline	$fk_{24,}$	0.81	0.03

[a] Nonlinear regression of IDA outflow concentration-time profiles where an additional parameter accounted in the model equations for the effect of caffeine and theophylline on IDA (The parameter estimates of control are listed Table 1).
[b] Fractional standard deviations.

9-2. Effect of Caffeine and Theophylline on Pharmacodynamics of IDA

The effect of caffeine (1 µM) or theophylline (3 µM) on the IDA-induced negative inotropic effect with maximal 49% decrease in LVDP at the end of a 10-min infusion of a 0.5 mg dose of IDA is depicted in Figure 22. While in the presence of caffeine the cardiodepressive action of IDA is completely reversed with rapid development of a positive inotropic effect within 2 min (18.2 ± 4.9 % increase in LVDP), theophylline significantly attenuates the negative inotropic effect of IDA at the end of infusion (only 20.6 ± 2.5% instead of 48.7 ± 5.8 % decrease in LVDP, P<0.001) shifting the response curve upwards. However, the slow increase and a sustained plateau of LVDP during the washout phase is higher for theophylline than for caffeine (21.3 ± 6.5 % vs. 10.0 ± 4.2 % of baseline at the end of experiment, P < 0.05). There is no change in LVEDP in both control and treatment groups. Caffeine significantly potentiates the decrease in heart rate during IDA infusion (Figure 23A). Theophylline, in contrast, is without effect in the infusion period but the heart rate is further significantly reduced to –14.9 ± 2.2 % instead of –6.9 ± 2.9 % (control) at 80 min. The maximum vasoconstrictive effect of IDA (75.4 ± 16.4 % increase in CVR at the end of infusion) is not significantly influenced by caffeine (94.9 ± 30.2 %) (Figure 23B). However, the secondary increase of CVR is inhibited by caffeine (P<0.01). Theophylline, on the other hand, significantly attenuates IDA-induced vasoconstriction (35.0 ± 4.8 % increase in CVR) and abolishes the secondary increase of CVR completely.

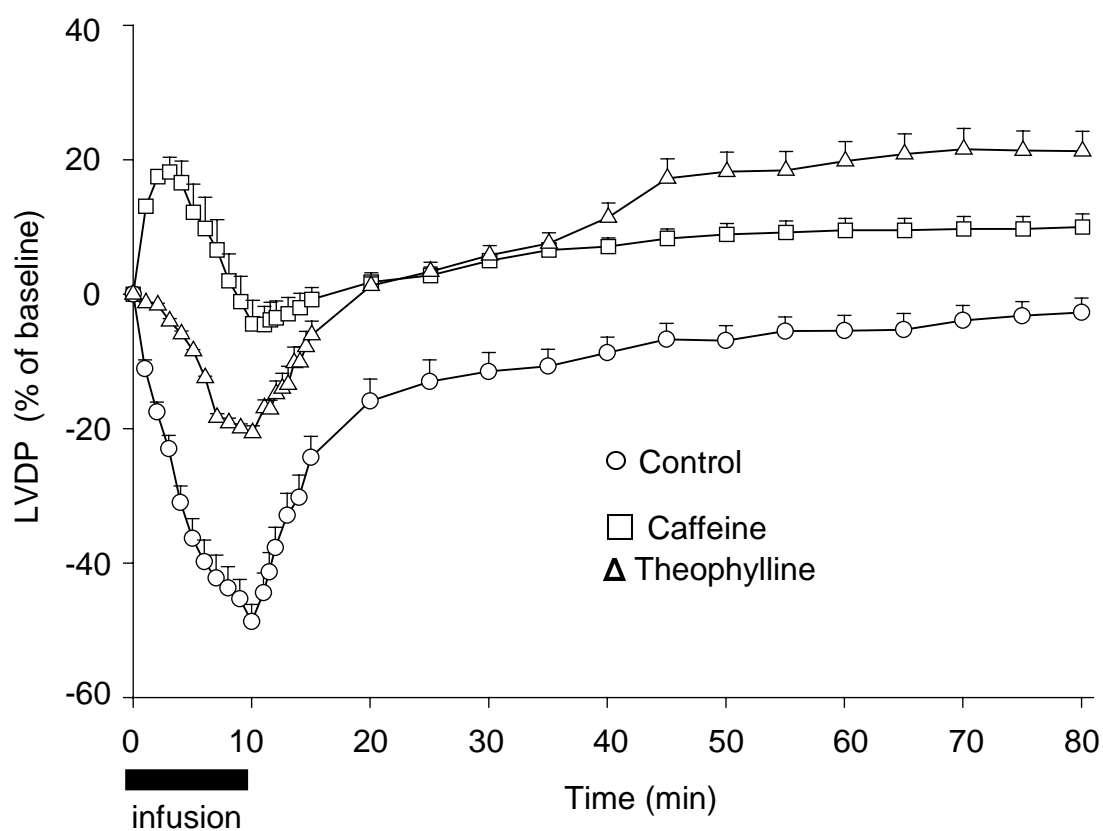**Figure 22.** Effect of IDA (0.5 mg) on left ventricular development pressure in hearts perfused with buffer (control), caffeine (1 µM), and theophylline (3 µM) (mean ± SEM; n=5 in each group).
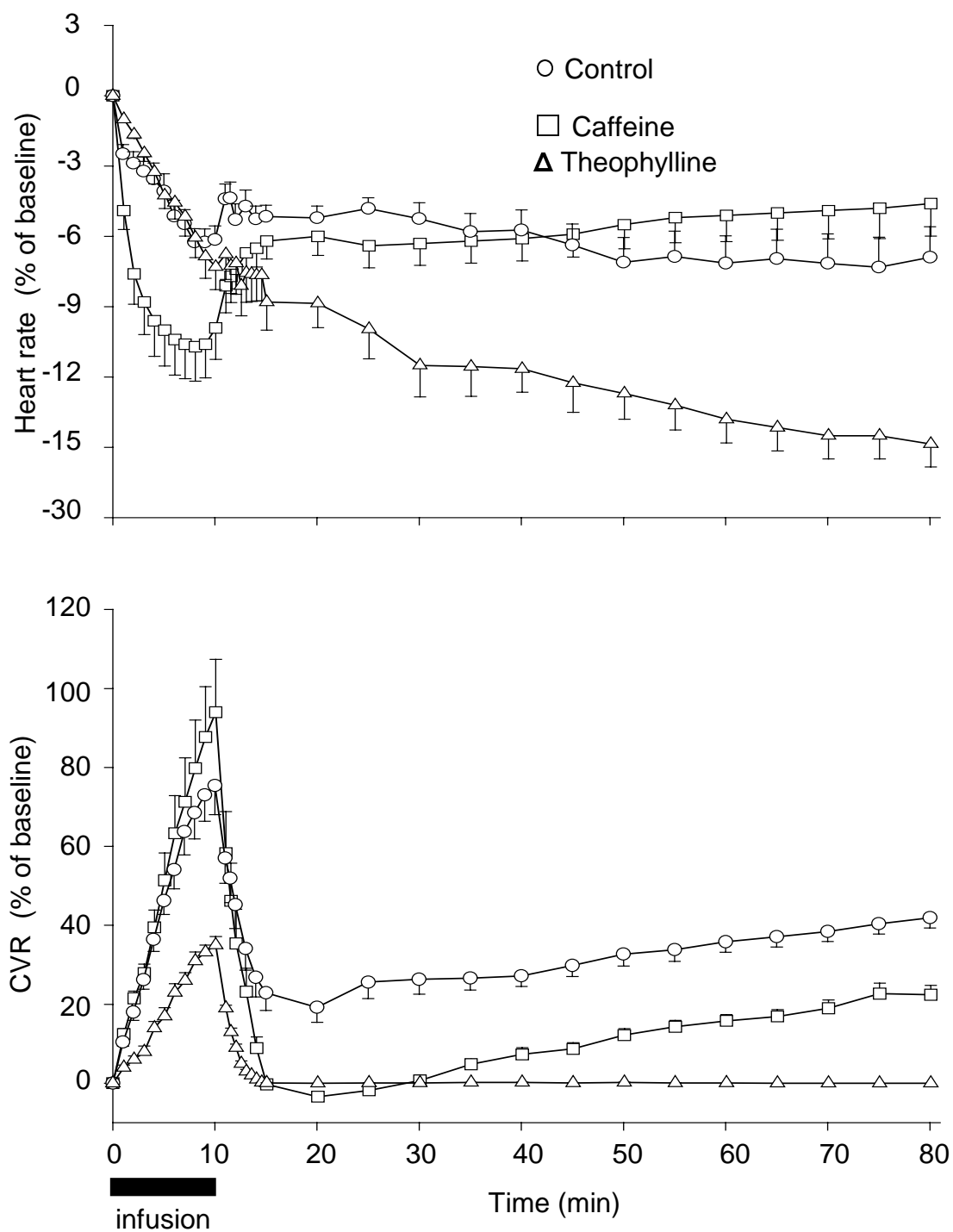
Figure 23. Effect of IDA (0.5 mg) on heart rate (A) and coronary vascular resistance (B) in hearts perfused with buffer (control), caffeine (1 μM), and theophylline (3 μM) (mean ± SEM; n=5 in each group).

9-3. Discussion

This chapter reports the influence of methylxanthines on pharmacokinetics and pharmacodynamics of IDA in rat heart after a single dose. The 2.7-fold increase in $V_{max,12}$ by caffeine underlying the enhancement of cardiac IDA uptake, exceeds the 1.8-fold increase observed for verapamil or amiodarone (Table 1, p.35). While the latter effect is suggested to be caused by an inhibition of P-glycoprotein mediated back-transport of IDA, no reasonable explanation is available for the effect of caffeine. Note that our result is in contrast to that reported by Sadzuka et al. (2000) who observed an enhancement of IDA uptake (influx) by the xanthine derivative, 1-methyl-3-propyl-7-butylxanthine (MPBX) only in leukemia cells but not in the heart or bone marrow cells. These authors suggested that MPBX might act on a nucleoside transporter, that appeared to be involved in IDA uptake in tumor but not in normal cells (Nagasawa et al., 1997). Furthermore, caffeine increased the uptake of doxorubicin in tumor cells (but not in normal tissue) by efflux inhibition (Sadzuka et al., 1995). The fact that theophylline does not influence IDA uptake in rat heart is in line with possible differences among xanthine derivatives regarding their effect on transport processes.

The reversal by caffeine of negative to positive inotropism of IDA may be due to an inhibition of IDA-induced Ca^{2+} release from sarcoplasmic reticulum (Pessah et al., 1990) that could prevent depletion of Ca^{2+}-stores (Matsushita et al., 2000) and/or intracellular Ca^{2+} overloading (Temma et al., 1996). Recently, also a concentration-dependent inhibition or stimulation of Ca^{2+} release by daunorubicin has been reported (Olson et al., 2000). This acute effect may be completely different from the situation after chronic dosing where co-administration of caffeine enhanced cardiac toxicity of doxorubicin (Hosenpud et al., 1995). Given this result, it is not unreasonable to suggest that the caffeine-induced enhancement of IDA uptake into the heart may have increased myocardial accumulation of IDA during chronic dosing. Although the lower inhibitory efficacy of theophylline (≈57 % reduction of the maximal negative inotropic IDA effect) may be consistent with the hypothesized mechanism of action, the reason for the delayed development of positive inotropy remains unclear (Figure 22). Interestingly, the enhancement of the negative chronotropic effect of IDA by caffeine or theophylline is characterized by a time course similar to that of the inotropic effect: caffeine produced

maximal effects at the end of infusion and theophylline at the end of experiment (Figure 23A). The higher effectiveness of theophylline to attenuate the IDA-induced increase in coronary vascular resistance (reduction to 37% of maximal effect) is also obvious from the complete prevention of the secondary increase in CVR (Figure 23B).

It has to be recalled that both methylxanthines are used in low concentrations which alone do not induce any changes in the measured parameters of cardiac performance. These concentrations (caffeine 1 µM and theophylline 3 µM) are below the plasma caffeine levels of 5-10 µM following a cup of coffee in humans (Daly, 1993) and the therapeutic plasma concentration of theophylline (about 50 µM), respectively. Therefore, an influence of usual dietary caffeine consumption on the cardiotoxic effects of anthracyclines cannot be excluded. The same holds for caffeine-potentiated chemotherapy (Tsuchiya et al., 2000).

Chapter 10. Pharmacokinetic modeling of Idarubicinol after infusion of IDA

The formation of pharmacologically active alcohol metabolite of IDA, idarubicinol (IDOL) in the heart tissue is of special interest since it has been speculated that the cardiac toxicity of anthracyclines could be related to its myocardial metabolism (Mushlin et al., 1993). Although plasma and tissue concentration of IDOL is greater than that of IDA following the administration of IDA in *in vivo*, (Looby et al., 1997; Eksborg et al., 1997; Schleyer et al., 1997), and IDOL has been reported to have greater cardiac toxicity than other anthracycline alcohol metabolites (Kuffel et al., 1992), little has been revealed with regard to the metabolism and disposition kinetics of IDOL in the heart.

In this chapter the myocardiac generation and disposition of IDOL are characterized after infusion of IDA in the isolated perfused rat heart. A series of experiment have been done in the absence and presence of carbonyl reductase inhibitors: phenobarbital (Kawalek and Gilbertson, 1976) and rutin (Wermuth, 1981). The influences of P-gp inhibitors (verapamil, amiodarone, PSC 833), xanthine derivatives (caffeine, theophylline), doxorubicin and hypothermia on the generation and transport of IDOL were also analysed using the IDA and IDOL outflow data obtained in the experiments described above.

10-1. Model Development for Idarubicinol

On the basis of the IDA model, additional compartments are included to describe the time profile of IDOL formed in heart tissue from IDA. As shown in Figure 24 and 25, fourteen model structures are tested to find the best minimal model with the same procedure described above for IDA. After fixing the parameter estimates of IDA (Table 1, and 2), the IDOL data sets are fitted. Compartment $IDOL_1$ and/or $IDOL_2$ are separated to clarify the generation and transport of IDOL. Compartment $IDOL_1$ and $IDOL_2$ belong to Compartment 1 and 2, respectively. $k_{m,1}$ and $k_{m,2}$ represent metabolism rate constants at Compartment 1 and 2, respectively. First order rate constants describing (passive) inter-compartmental transport of IDOL are denoted by $k_{ij,IDOL}$ and the active transport with Michaelis-Menten type kinetics is characterised by the

68

apparent maximal transport rates $V_{max,IDOL}$ and the apparent Michaelis constant $K_{M,IDOL}$. $k_{23,IDOL}$ indicates a sequestration rate constant representing an irriversible binding and metabolism to IDOL aglycone. The differential equations that describe disposition of IDA, and generation and disposition of IDOL amounts (in bold) in compartments after a 1-min infusion of IDA are

$$dIDA_1(t)/dt = -(Q/V_1 + V_{max,12}/[K_{M,12}+IDA_1(t)])IDA_1(t) + k_{21}IDA_2(t) + R_{1min}$$

$$\mathbf{-k_{m,1}IDA_1(t)} \tag{33}$$

$$dIDA_2(t)/dt = V_{max,12}/[K_{M,12}+IDA_1(t)])IDA_1(t) - (k_{21}+ k_{24}+ k_{23})IDA_2(t) + k_{32}IDA_3(t)$$

$$\mathbf{- k_{m,2}IDA_2(t)} \tag{34}$$

$$dIDA_3(t)/dt = k_{23}\,IDA_2(t) - k_{32}\,IDA_3(t) \tag{35}$$

$$\mathbf{dIDOL_1(t)/dt = -(Q/V_1 + V_{max,IDOL}/[K_{M,IDOL}+IDOL_1(t)])IDOL_1(t) + k_{21,IDOL}xIDOL_2(t)}$$

$$\mathbf{+k_{m,1}IDA_1(t)} \tag{36}$$

$$\mathbf{dIDOL_2(t)/dt = V_{max,IDOL}/[K_{M,IDOL}+IDOL_2(t)])IDOL_2(t) - (k_{21,IDOL}+ k_{23,IDOL})IDOL_2(t)}$$

$$\mathbf{+k_{m,2}IDA_2(t)} \tag{37}$$

and after a 10-min infusion of IDA are

$$dIDA_1(t)/dt = -(Q/V_1 + V_{max,12}/[K_{M,12}+IDA_1(t)])IDA_1(t) + k_{21}IDA_2(t) + R_{10min}$$

$$\mathbf{-k_{m,1}IDA_1(t)} \tag{38}$$

$$dIDA_2(t)/dt = V_{max,12}/[K_{M,12}+IDA_1(t)])IDA_1(t) - (k_{21}+ k_{2e}+ V_{max,23}/[K_{M,23}+x_2(t)])IDA_2(t)$$

$$+ k_{32}IDA_3(t)\, \mathbf{- k_{m,2}IDA_2(t)} \tag{39}$$

$$dIDA_3(t)/dt = V_{max,23}/[K_{M,23}+x_2(t)])x_2(t) - k_{32}x_3(t) \tag{40}$$

$$\mathbf{dIDOL_1(t)/dt = -(Q/V_1 + V_{max,IDOL}/[K_{M,IDOL}+IDOL_1(t)])IDOL_1(t) + k_{21,IDOL}xIDOL_2(t)}$$

$$\mathbf{+k_{m,1}IDA_1(t)} \tag{41}$$

$$\mathbf{dIDOL_2(t)/dt = V_{max,IDOL}/[K_{M,IDOL}+IDOL_2(t)])IDOL_2(t) - (k_{21,IDOL}+ k_{23,IDOL})IDOL_2(t)}$$

$$\mathbf{+k_{m,2}IDA_2(t)} \tag{42}$$

A model for the variance of the additive error of the measured data is specified as IDA. The final models of IDOL in a 1-min and a 10-min infusion of IDA are illustrated in Figure 26 and 27, respectively. The parameter estimates were listed in Table 5 and 6, respectively.
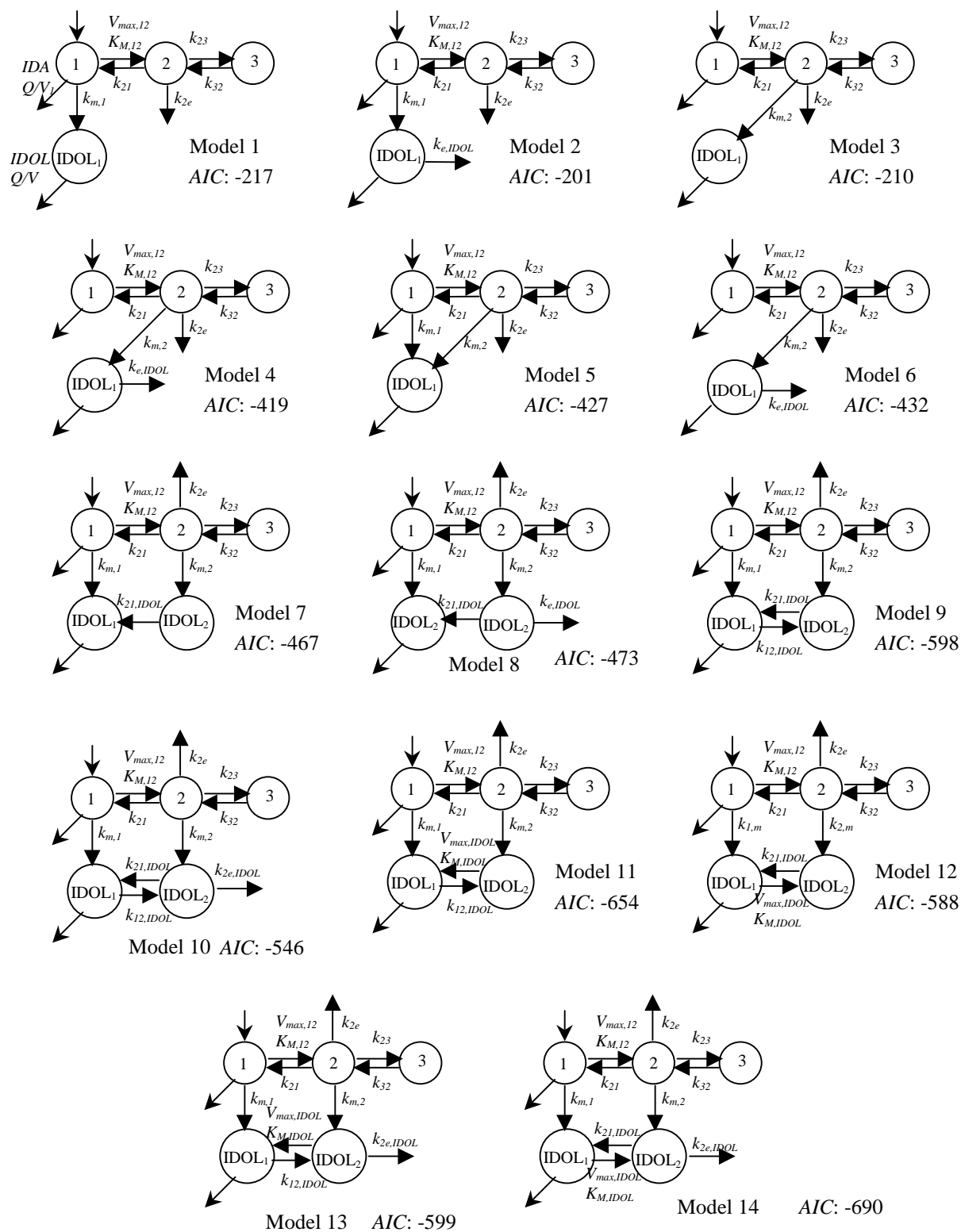
Figure 24. AIC values of tested compartment structures for IDOL after a 1-min infusion of IDA.
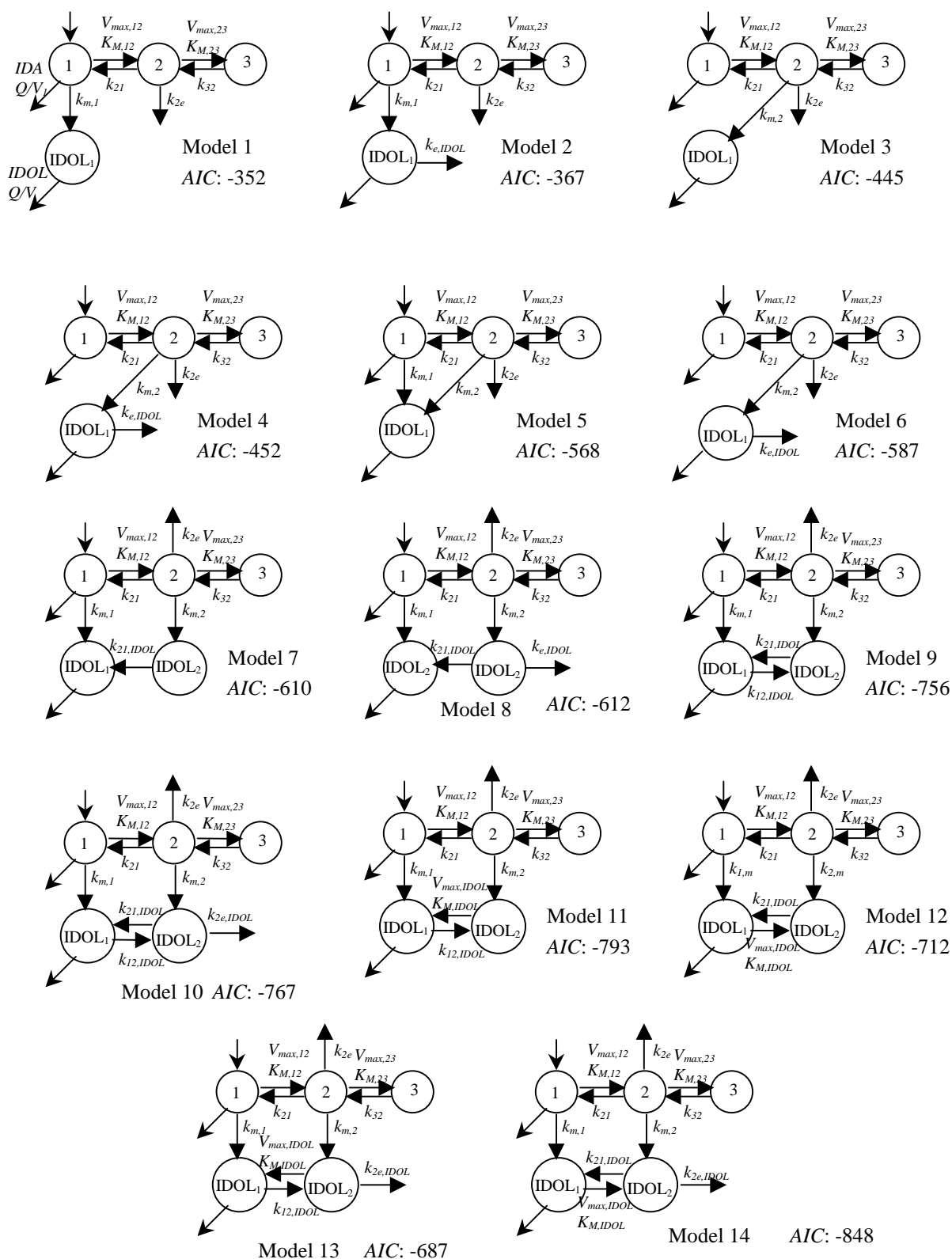
Figure 25. AIC values of tested compartment structures for IDOL after a 10-min infusion of IDA.

Nonlinear regression is performed with the average data of the control group and those of treatment groups. Thus, factor f_i of each parameter P_i describes the kinetics of control is multiplied to account for a potential change due to treatment. All possible combinations of factors are evaluated to describe treatment groups by a minimum number of factors. The factor selection is made according to the criteria previously described for IDA in Chapter 6.
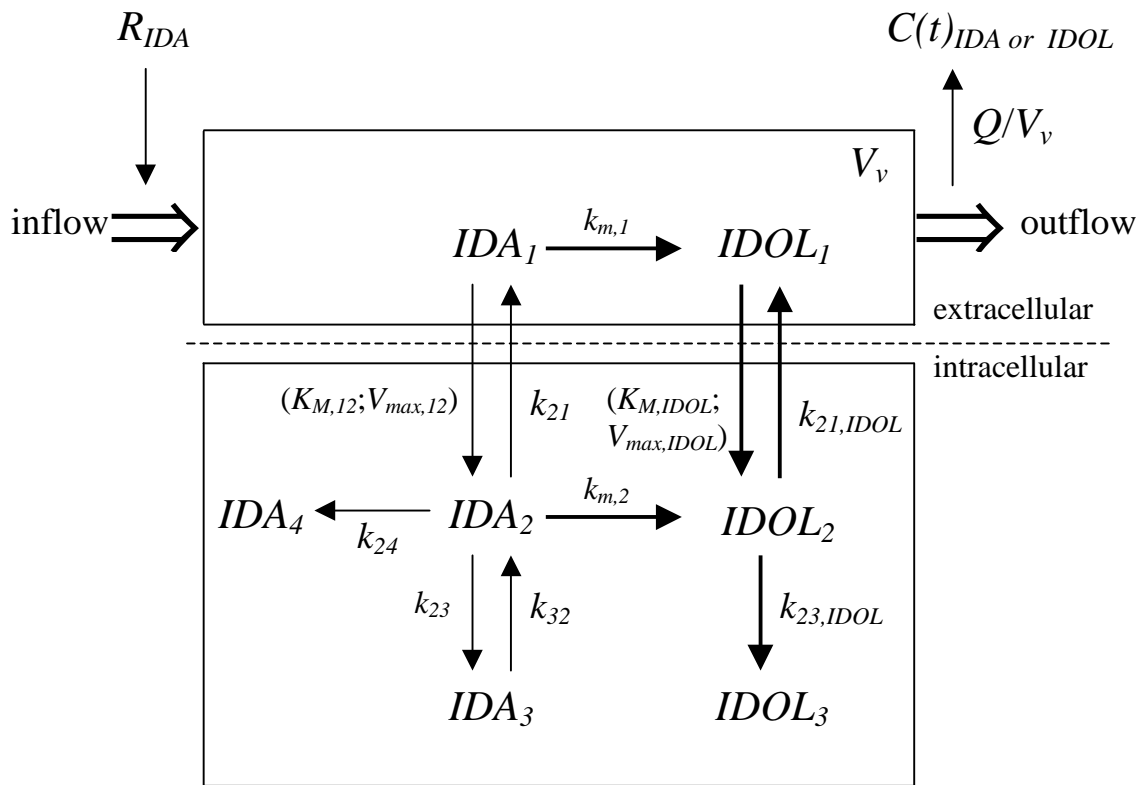
Figure 26. Compartmental model of IDOL kinetics after a 1-min infusion of IDA in the isolated perfused rat heart ($C_{out, IDOL}(t)$, outflow at time t; $k_{21,IDOL}$, first order rate constants; $k_{23,IDOL}$, sequestration rate constant; $k_{m,i}$, metabolism rate constants; $V_{max,IDOL}$ and $K_{M,IDOL}$, Michaelis-Menten parameters of the uptake transport process). Bold arrows indicate the generation or transport of IDOL.

Table 5. Model parameter estimates for metabolism and disposition of IDOL after a 1-min infusion of IDA in the isolated perfused rat heart.

Parameter	Estimate[a]	*FSD*[b]
$k_{m,1}$ (min^{-1})	0.0038	0.19
$k_{m,2}$ (min^{-1})	0.0006	0.43
V$_{max,IDOL}$ (nmol/min)	3.2	0.43
$K_{m,IDOL}$ (nmol)	0.24	0.78
$k_{21,IDOL}$ (min^{-1})	0.18	0.46
$k_{23,IDOL}$ (min^{-1})	0.08	0.34

[a] Final estimates with fixed parameters of IDA in Table 2.
[b] Fractional standard deviations.
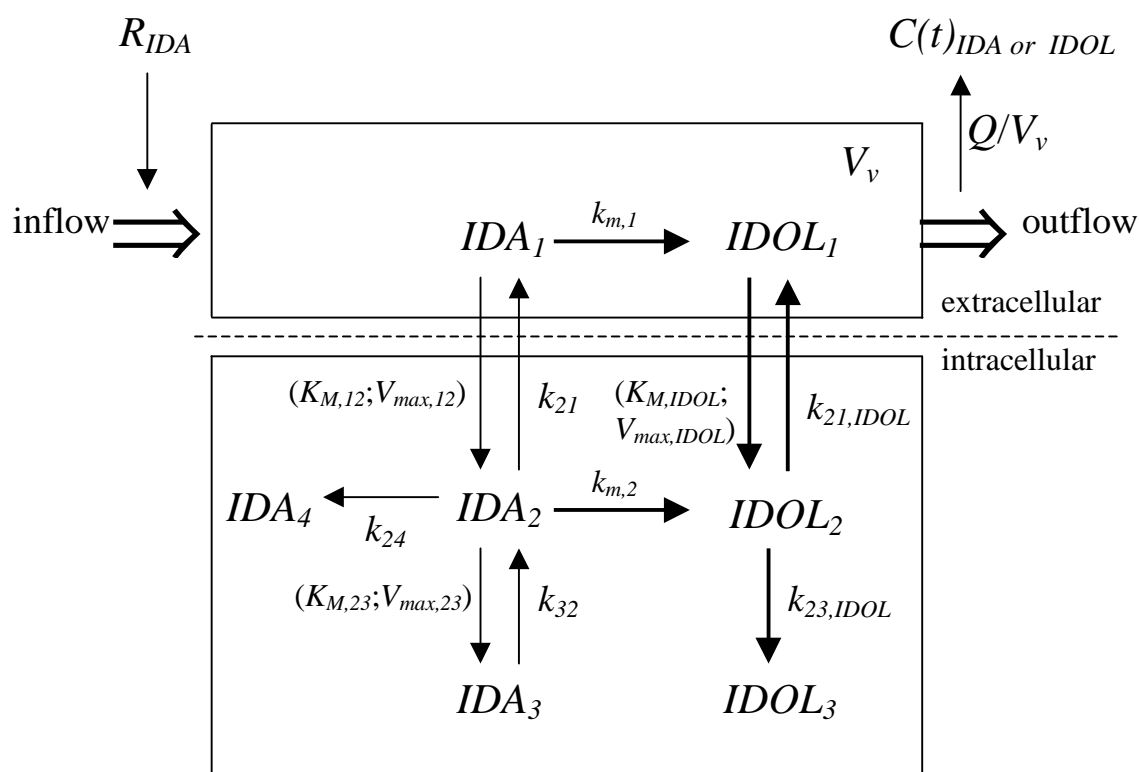
Figure 27. Compartmental model of IDOL kinetics after a 10-min infusion of IDA in the isolated perfused rat heart (k_{ij}, first order rate constants; $k_{m,i}$, metabolism rate constants; $k_{23,IDOL}$, sequestration rate constant; $V_{max,IDOL}$ and $K_{M,IDOL}$, Michaelis-Menten parameters of the uptake transport process). Bold arrows indicate the generation or transport of IDOL.

Table 6. Model parameter estimates for metabolism and disposition of IDOL after a 10-min infusion of IDA in the isolated perfused rat heart.

Parameter	Estimate [a]	FSD [b]
$k_{m,1}$ (min^{-1})	0.0023	0.08
$k_{m,2}$ (min^{-1})	0.0081	0.08
$V_{max,IDOL}$ (nmol/min)	242	0.15
$K_{M,IDOL}$ (nmol)	185	0.17
$k_{21,IDOL}$ (min^{-1})	0.047	0.14
$k_{23,IDOL}$ (min^{-1})	0.041	0.04

[a] Final estimates with fixed parameters of IDA in Table 1.
[b] Fractional standard deviations.

10-2. Generation and Transport of IDOL in Control Group

The outflow concentration of the formed IDOL after a 1-min infusion of IDA is lower than that of the parent compound by a factor of about 10^{-3}. The IDOL outflow time profile shows biphasic pattern: after reaching the peak at the end of infusion the curve decayed rapidly within 10 s, and it increases again up to 10 min and followed by a very slow decline (Figure 28A). The shape of IDOL outflow curve after a 10-min infusion of IDA is similar to that after a 1-min infusion, but there is no big drop after the first peak (Figure 28B).

In a 1-min infusion protocol the outflow recovery of IDOL generated up to 80 min is 0.28 ± 0.14 % of the IDA dose, while 1.68 ± 0.15 % remains in the heart. On the other hand, the total generation of IDOL in a 10-min infusion experiment is about 8 % of dose (outflow recovery, 0.34 ± 0.03 % of the dose; residual amount in the heart, 7.26 ± 1.74 %).

A compartment model where IDOL is generated in two different compartments, one fast equilibrating "extracellular" and one slowly equilibrating "intracellular" compartment, describes the data very well. Note that the disposition of the extracellularly generated IDOL is analogous to that of IDA. The fits of IDOL after a 1-min and a 10-min infusion of IDA are depicted in Figure 28C and D, respectively. The parameter estimates are well-determined with less than 0.5 of fractional standard deviations except the apparent Michaelis constant, $K_{M,IDOL}$ relatively poorly estimated in a 1-min infusion experiment.

77
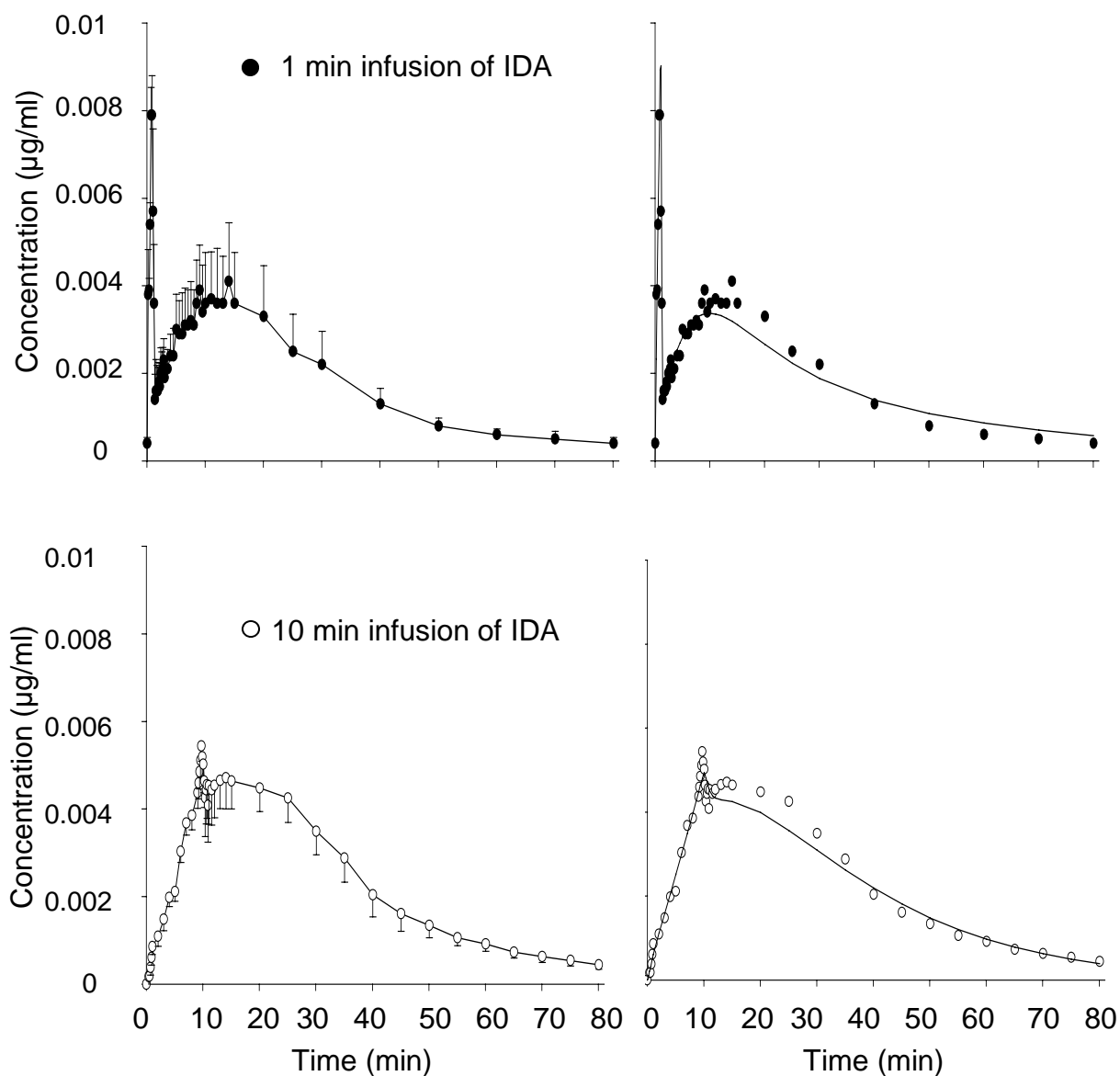
Figure 28.   Panel A, B; IDOL outflow profiles in hearts perfused with Krebs-Henseleit solution for a 1 min and 10 min infusion of 0.5 mg IDA (mean ± S.D., n = 5 in each group). Panel C, D: Fits of the mean IDOL outflow data.

10-3. Discussion

Only 2 % of the IDA-dose is converted to IDOL in heart tissue in a 1-min infusion of IDA, A myocardial concentration ratio IDOL to IDA of 11 % is observed at the end of the 80 min perfusion period following the single IDA dose of 0.5 mg, whereas a value of 4% was measured by Platel et al. (1999) in rat hearts after 70 min perfusion with 2 nM IDA. The 13-hydroxy metabolite IDOL is formed primarily via carbonyl reduction of IDA (e.g., Ferrazzi et al., 1991), mainly in the liver but to a much less extent also in the heart as indicated by the results reported by Propper and Maser (1997) for daunorubicin.

On the other hand, in a 10-min infusion of IDA experiment about 8 % of the IDA dose is metabolized to IDOL. The increase of IDOL generation may result from the uptake enhancement corresponding to the slow infusion of IDA

The metabolism in Compartment IDA_1 assumes as an extracellular space that implies an initial distribution region including vascular endothelium is mendatory to describe the biphasic pattern of IDOL concentration time profile. Interestingly, nothing has been reported with regard to the metabolism of anthracycline to its 13-hydroxy metabolite via carbonyl reductase in vascular endothelium. However, the localization of the enzyme has been profoundly observed in the endothelium of blood vessel (Wirth and Wermuth, 1992). Further investigation would be worth with regard to metabolism of anthracyclines in vascular bed. It should be noted that these results describe for the first time a possibly extracellular generation of IDOL together with a saturable uptake in the heart.

Chapter 11. Effect of metabolism inhibitors (Rutin, Phenobarbital) on myocardial kinetics and dynamics of IDA and IDOL

11-1. Model Independent Analysis

Figure 29A and 31A represent the outflow concentration-time profiles of IDA and IDOL from control, rutin- and phenobarbital-treated hearts, respectively. Time profiles of IDA concentration in metabolism inhibitor treatment groups declines rapidly compared to those of control from 30 min.

The average outflow recoveries and residual amounts at 80-min in the heart for IDA and IDOL obtained for a 1-min infusion of IDA (500 µg) in the absence and presence of rutin or phenobarbital were depicted in Figure 29D and 31D, respectively. There is no significant change in outflow recoveries of IDA due to treatment of those compounds, whereas rutin increases the residual amount by 43 % ($P<0.05$) compared with control. The generation of IDOL is significantly blocked by rutin and phenobarbital: the residual amount of IDOL is significantly decreased by 53 % ($P<0.05$) due to phenobarbital, while rutin inhibits IDOL production by 68 % ($P<0.05$) and 36 % ($P<0.01$) in the outflow recovery and the residual amount, respectively.

11-2. Effect of Rutin and Phenobarbital on Pharmacokinetics of IDA and IDOL

Figure 29B and C show the resulting simultaneous nonlinear regression of average outflow concentration time profiles of IDA for control, rutin-, and phenobarbital-treated groups. Rutin causes 2-fold increase ($P<0.01$) in the sequestration rate (k_{24}) of IDA, that reflects an increase of the residual amount of IDA in the heart. While phenobarbital increases $K_{M,12}$ by factor of 1.7, and decreased k_{32} by 25-fold. However, change of both parameters counteracts each other so that there is no change in outflow recovery and residual amount in the heart (Figure 29D).

The effect of inhibitors on metabolism of IDA to IDOL is well described by the factor of metabolism rate constant, i.e., rutin and phenobarbital decrease $k_{m,2}$ to 67 ($P<0.05$) and 80 % of the control, respectively (Figure 31B-C). As for IDA, phenobarbital also decreases the uptake of IDOL in a competitive manner (Table 7).
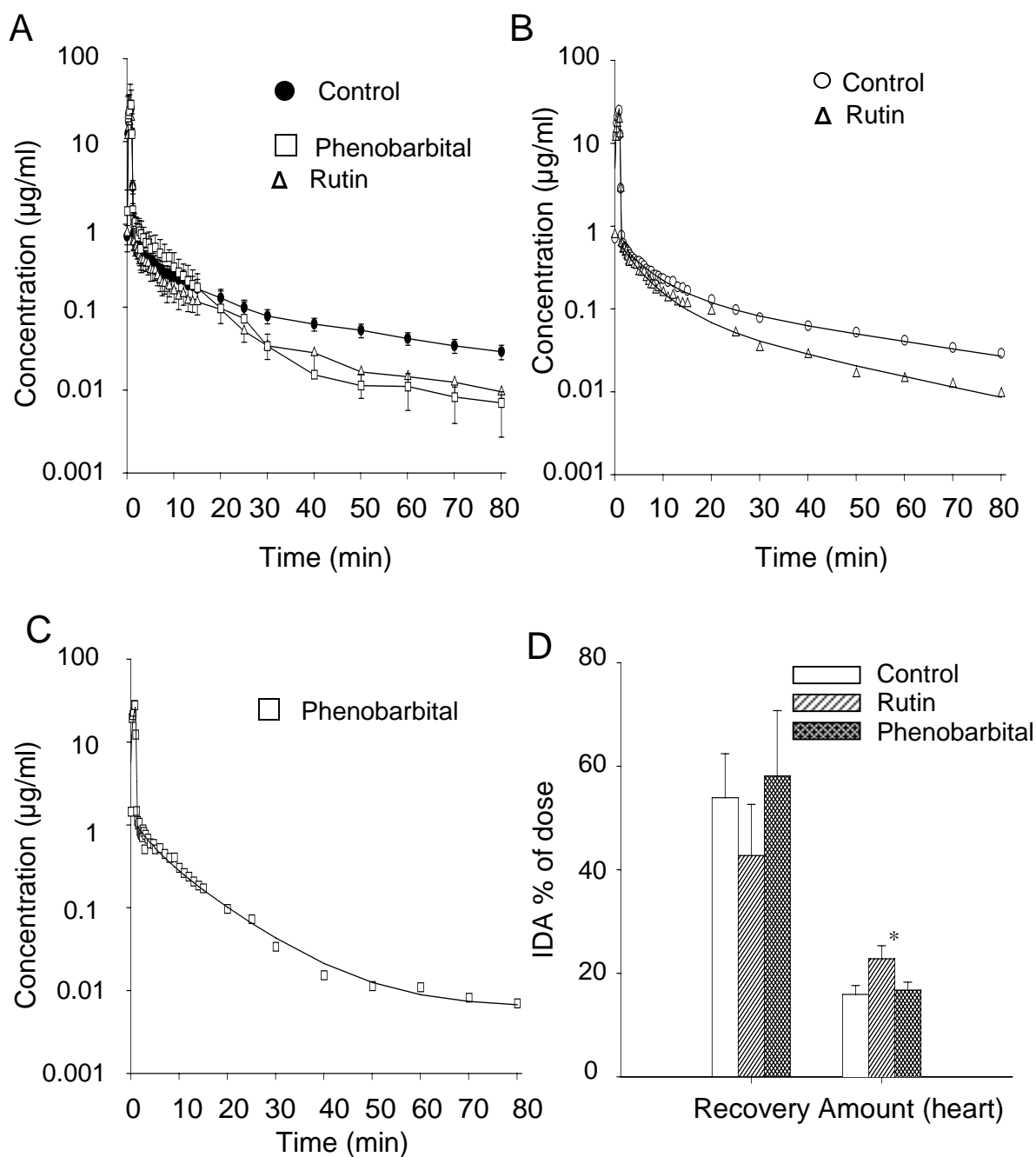
Figure 29. Panel A: IDA outflow profiles in hearts perfused with Krebs-Henseleit solution (control), rutin (10 μM), and phenobarbital (100 μM) for a 1-min infusion of 0.5 mg IDA (mean ± S.D., n = 5 in each group). Panels B-C: Simultaneous fit of the mean outflow data of the control, rutin (B) and phenobarbital experiments (C). Panel D: Outflow recovery and residual amount of IDA in the heart at the end of experiment (*, $P<0.05$ compare to control).
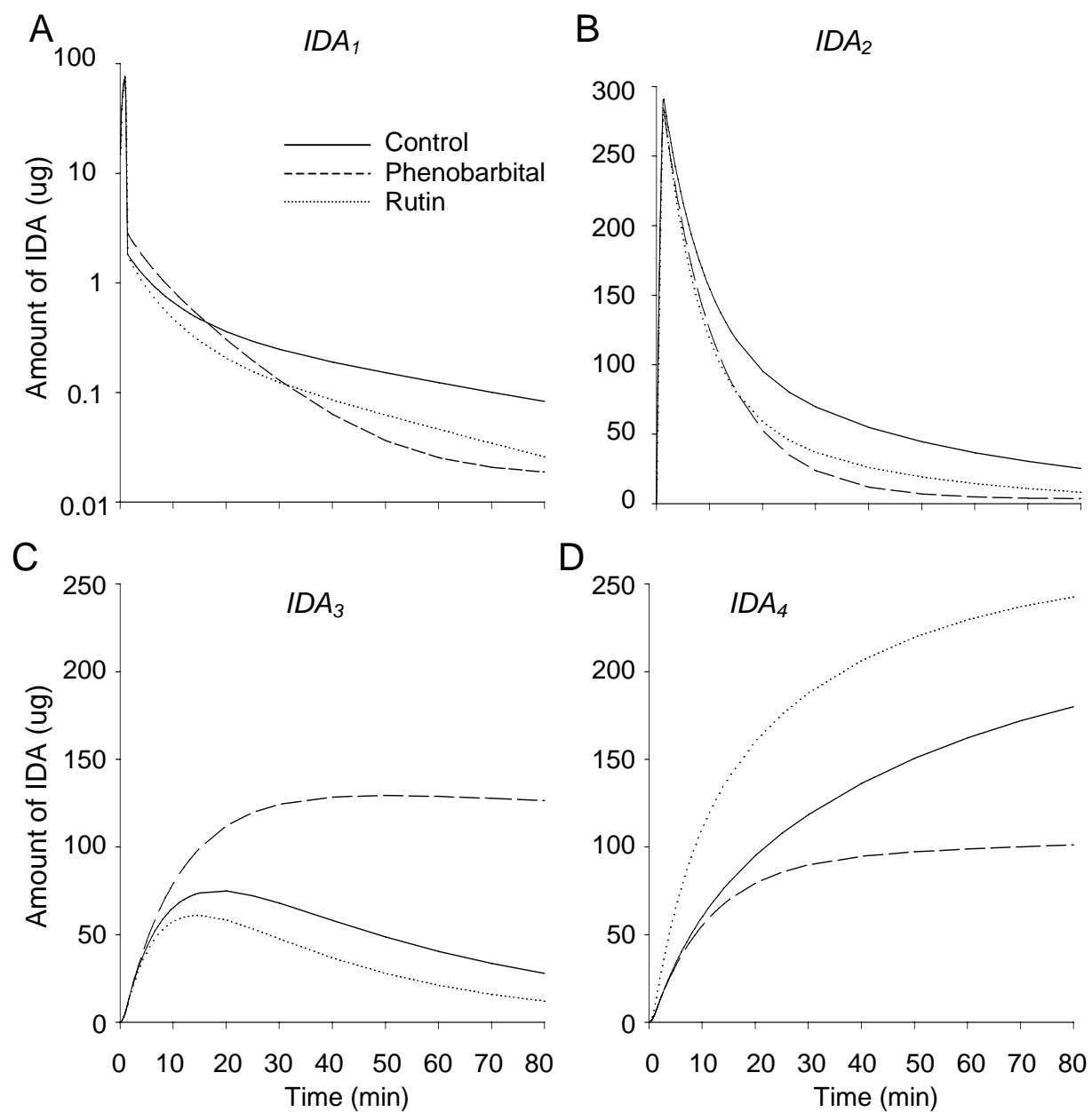
Figure 30. Predicted time course of compartmental amounts of IDA after a 1-min infusion of IDA in the heart in the absence and in the presence of metabolism inhibitors [rutin (10 uM), and phenobarbital (100uM)].
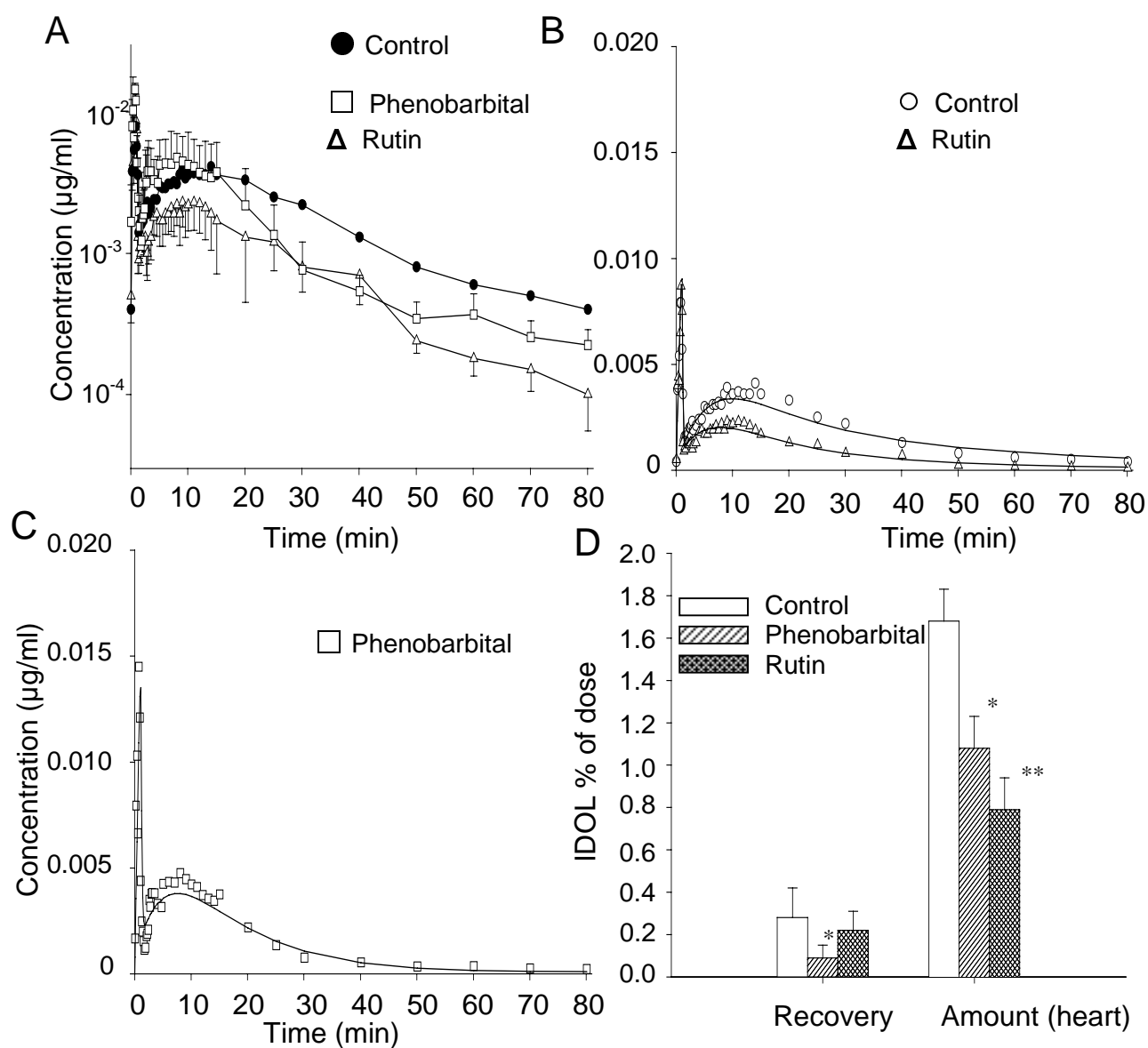
Figure 31. Panel A: IDOL outflow profiles in hearts perfused with Krebs-Henseleit solution (control), rutin (10 µM), and phenobarbital (100 µM) for a 1 min infusion of 0.5 mg IDA (mean ± S.D., n = 5 in each group). Panels B-C: Simultaneous fit of the mean outflow data of the control, rutin (B) and phenobarbital experiments (C). Panel D: Outflow recovery and residual amount of IDA in the heart at the end of experiment ([*], $P<0.05$; [**], $P<0.01$ compare to control).
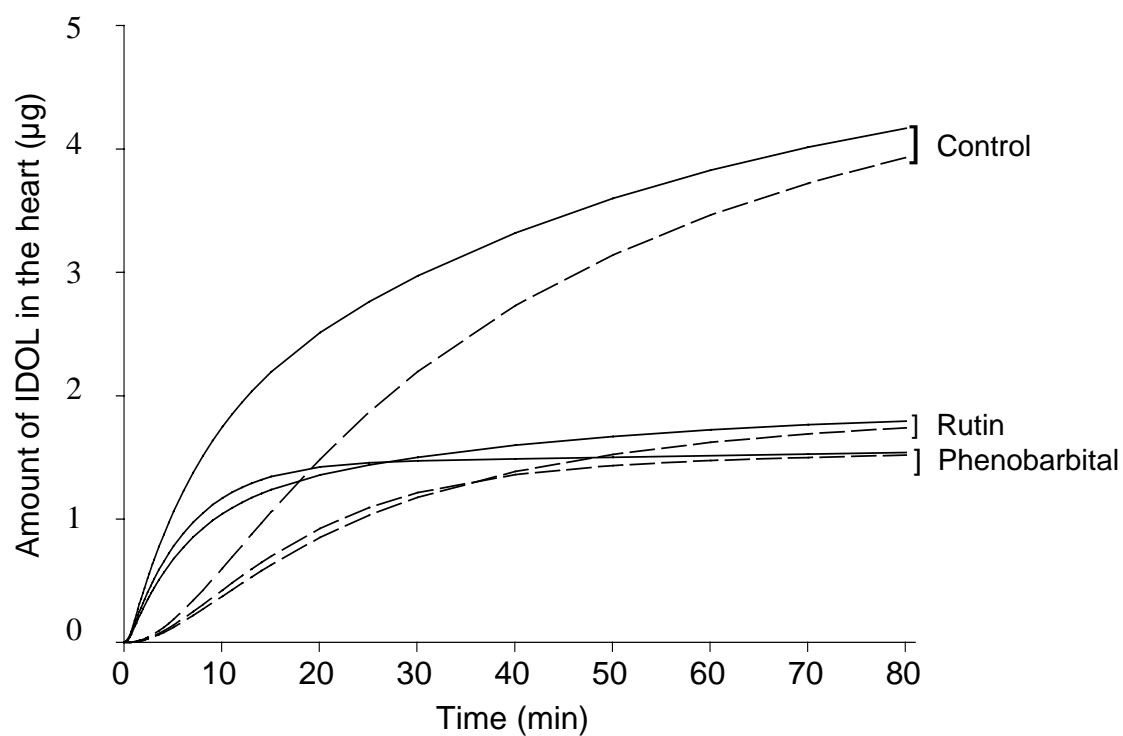
Figure 32. Model simulation of the effect of phenobarbital (100 μM) and rutin (10 μM) on the time course of total amount of IDOL in the heart (solid line) and the amount sequestered into Compartment 3 (dashed line). Not the predicted amount of IDOL also contains its metabolites formed in myocard.

Figure 30 represents the model prediction of time courses of IDA amounts in each compartment in the absence and presence of rutin and phenobarbital. The IDOL sequestrated to an intracellular compartment mostly contributes the total amount in the heart, and rutin and phenobarbital remarkably diminish the total amount of IDOL generated from IDA in the heart (Figure 32).

Table 7. Model parameter estimates for the pharmacokinetics of IDOL after infusion of IDA in hearts from treatment groups.

Idarubicin			Idarubicinol		
factors	rutin	phenobarbital	Factors	rutin	phenobarbital
$fK_{M,12}$		1.69^a (0.06^b)	$fK_{M,IDOL}$		2.26 (0.21)
fk_{32}		0.04 (0.15)	$fk_{m,2}$	0.67(0.05)	0.80 (0.14)
fk_{24}	2.07 (0.03)				

[a]Nonlinear regression of IDA and IDOL outflow concentration-time profiles where additional parameters accounted in the model equations for the effect of rutin and phenobarbital on IDA and IDOL. The parameter estimates of control for IDA and IDOL are listed Table 2 and 5, respectively.
[b] Fractional standard deviations.

11-3. Effect of Rutin and Phenobarbital on IDA Pharmacodynamics

Rutin (10 µM) and phenobarbital (100 µM) do not show any significant effect on IDA-induced cardiac performance except the change of coronary vascular resistance. The maximum vasoconstrictive effect of IDA is significantly diminished (22.3 %) by rutin, and there is no second increase (Figure 33). Phenobarbital, in contrast, potentiates IDA induced increase of vascular resistance by nearly 2-fold at 80 min despite no change at the end of infusion of IDA.

Figure 33. Effect of IDA on coronary vascular resistance in heart perfused with buffer (control), rutin (10 µM), and phenobarbital (100 µM) (mean ± SEM; n=5 in each experiment).

11-4. Discussion

Since it has been proposed that anthracycline antibiotic induced cardiac injury might be due to its 13-hydroxy metabolite by cytoplasmic NADPH dependent aldo-keto reductase (Olson and Mushlin, 1990; Gewirtz and Yanovich, 1987), the role of metabolism in cardiotoxi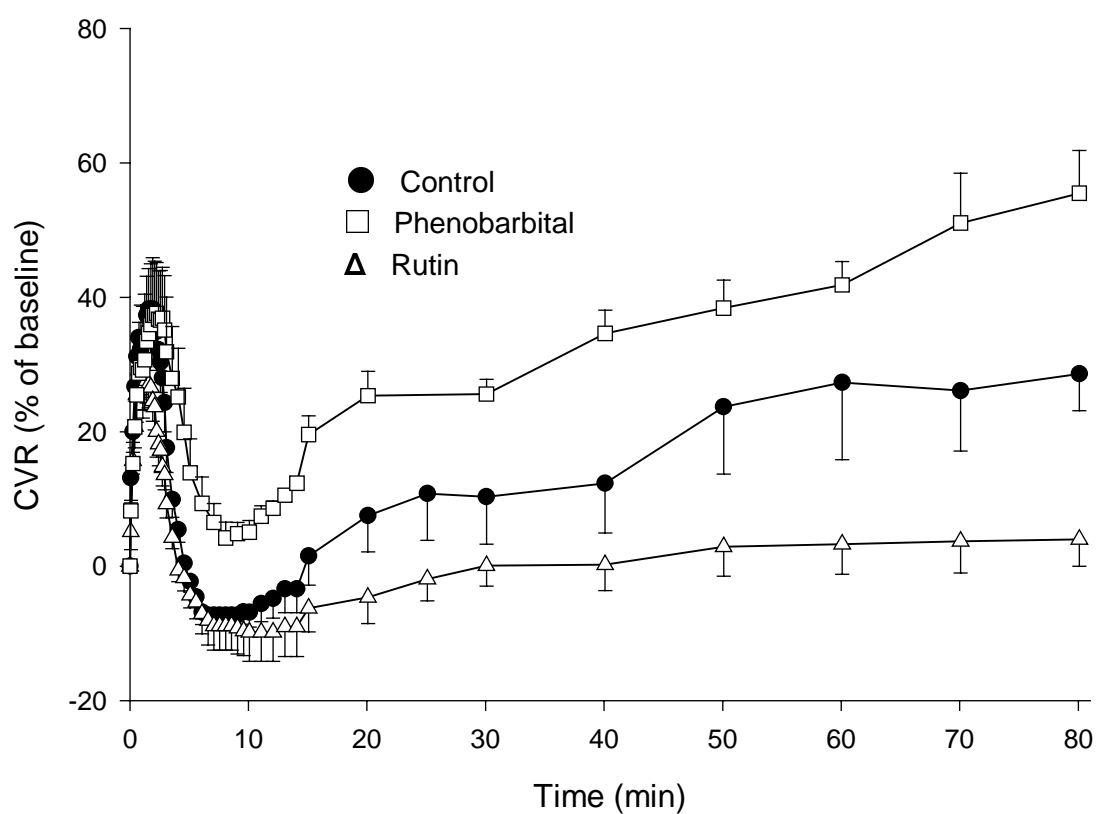city has been investigated in a variety of species and probes: human myocardium (Licata et al., 2000), rabbit papillary muscle (Cusack et al., 1993), isolated mouse atrium and transgenic mice hearts (Forrest et al., 2000). The common conclusion is that the active metabolite plays a major role in cardiotoxicity.

Many kinds of cotreatments related with regulation of anthracycline metabolism have been tested to overcome myocardial impairment of anthracycline anticancer agents. Recently phenobarbital has been reported to have an aldoketoreductase blocking effect (Behnia and Boroujerdi, 1999). Rutin, one of flavonoids which is a group of dietary compounds widely distributed in plants, has also been reported to reduce doxorubicinol by inhibition of the carbonyl reductase activity (Forrest et al., 2000). Because of its radical scavenging and iron chelating properties, rutin has been considered as potential protector against chronic cardiotoxicity caused by anthracycline antibiotics (van Acker et al., 2000)

The generation of IDOL in the isolated perfused rat heart is inhibited to 60 ($P<0.05$) and 52 % ($P<0.05$) of control in the presence of rutin (10 uM) and phenobarbital (100 uM), respectively. These results are comparable with 70 % of inhibition of daunorubicin metabolism to dauorubicinol by rutin (3 uM) in the rabbit heart (Gambliel et al., 1997). Since carbonyl reductase has a much better affinity for C-14 methyl group (Figure 1) in anthracycline molecule (Gewirtz and Yanovich, 1987) and IDA has the same structure with daunorubicin at C-14 position, the lower inhibition of metabolism in the rat heart even at higher concentration of rutin suggests an interspecies variability of metabolism.

In modeling analysis rutin and phenobarbital decrease the generation of IDOL in Compartment IDA_2. Note that the reduction of IDA amount in Compartment IDA_2 (Figure 30B) in charge of IDOL generation may also influence the decrease of IDOL formation, i.e., rutin and phenobarbital increase the amount of IDA in Compartment IDA_4 (Figure 30D) and IDA_3 (Figure 30C) due to an increase of k_{24} and a decrease of

k_{32}, respectively. While the change of the apparent Michaelis constant of IDA ($K_{M,12}$) by phenobarbital does not seem to affect the decrease of IDA in Compartment IDA_2, because there is no significant increase of IDA in Compartment IDA_1 (Figure 30A).

In this study, the inhibition of IDOL formation is not directly related to a reduction of IDA induced acute toxicity, although rutin and phenobarbital significantly inhibit metabolism, because the generation of IDOL is only less than 2 % of IDA dose. Most cardiac performances are not changed in the presence of metabolism inhibitors. However, rutin represents a beneficial influence on coronary vascular resistance. Schüssler and his colleagues (1995) reported that rutin exhibited dose-dependent vasodilation effects compared to equimolar doses of theophylline. Their results are in good agreement with this work. As previously shown in Figure 23B, theophylline (3 µM) diminished IDA induced increase of coronary vascular resistance by 53 %, and totally blocked the second increase of CVR. Furthermore, thromboxane synthesis is inhibited and prostacyclin synthesis (PGI_2) is increased by rutin (Vibes et al., 1994). The production of PGI_2 may result from a protective effect of rutin on the endothelium as suggested by the antioxidant activities of flavonoids. In contrast, Perez-Vizcaino et al. (2002) recently reported that the vasodilation effect of quercetin is not caused or modulated by endothelial factors or cyclic nucleotides and is not related to intracellular calcium concentrations. Although there is no evidence in an inhibition effect of rutin on myosin light chain kinase in vascular smooth muscle like quercetin and kaempferol (Hagiwara et al., 1988), one could also speculate that rutin may have a direct interaction with the contractile protein. The vasodilation effect of rutin needs further clarification.

The potentiation by phenobarbital of the secondary vasoconstrictor response, on the other hand, could be explained by an inhibition cGMP-mediated endothelium-dependent and independent vasorelaxations (Gerkens, 1987; Terasako *et al.,* 1994). Interestingly, the initial rapid vasoconstriction (which parallels the IDA outflow concentration profile) was not affected by phenobarbital. In view of the low fraction of IDOL generated from IDA, a significant contribution of IDOL to the pharmacodynamic effects of IDA is very unlikely in these experiments. Thus, no influence of rutin and phenobarbital on the time course of IDA-induced negative inotropism could be detected.

The increase of residual amount of IDA by rutin is not consistent with the observation that the accumulation of doxorubicin in HCT colon cells was decreased by rutin (Critchfield et al., 1994) and that there was no effect of rutin on uptake in a human breast-cancer cell line (Scambia et al., 1994). These differences may be due to the different tissues and cell lines.

Chapter 12. Effect of P-gp Inhibitors (Verapamil, Amiodarone, PSC 833) on myocardial kinetics of IDOL after infusion of IDA

Figure 34A and B show the average outflow concentration-time profiles for IDOL obtained from a 10-min infusion of IDA (0.5 mg) in the absence (n=5) and presence of verapamil (1 nM) and amiodarone (1 µM, n=5), respectively. Both verapamil and amiodarone lead to a parallel downward shift.

Nonlinear regression analysis reveals that the uptake rate of IDOL is enhanced by P-gp inhibitors, verapamil (Figure 34A) and amiodarone (Figure 34B) cause an increase by factors of 1.6 (P<0.01), and 1.2 in $V_{max,IDOL}$, and the sequestration rate ($k_{23,IDOL}$) also increased by factors of 1.3 and 1.1, respectively (Table 8).

These results confirm that the hydroxylated metabolite of IDA is involved in multidrug resistance (Roovers et al., 1999), and that P-gp mediated transport of IDOL is influenced by verapamil (Schröder et al., 2000).

On the other hand, in a 1-min infusion of IDA PSC 833, but not of verapamil, shows a different effect on the outflow curve of the formed IDOL: the prevention of the decline of the curve after the second peak (Figure 34C) increases the recovery by 203.6 % and decreases the residual amount in the heart by 53.6 % (Figure 34D).

Table 8. Parameters estimates for the disposition of IDOL generated from IDA in the heart in the presence of verapamil (1 nM), amiodarone (1 µM) and PSC 833 (1 µM).

	Parameters		
	$fV_{max,IDOL}$	$fK_{M,IDOL}$	$fk_{23,IDOL}$
Verapamil[a]	1.64 (0.03[b])		1.26 (0.04)
Amiodarone[a]	1.22 (0.05)		1.13 (0.04)
PSC 833[c]		1.29 (0.12)	6.4×10^{-7} (>0.5)

Nonlinear regression of IDOL outflow concentration-time profiles where two additional parameters accounted in the model equations for the effect of P-gp inhibitors on IDOL after a 10-min infusion[a] and a 1-min infusion[c] of IDA. The parameter estimates of control are listed Table 6 and 5, respectively.
[b] Fractional standard deviations.
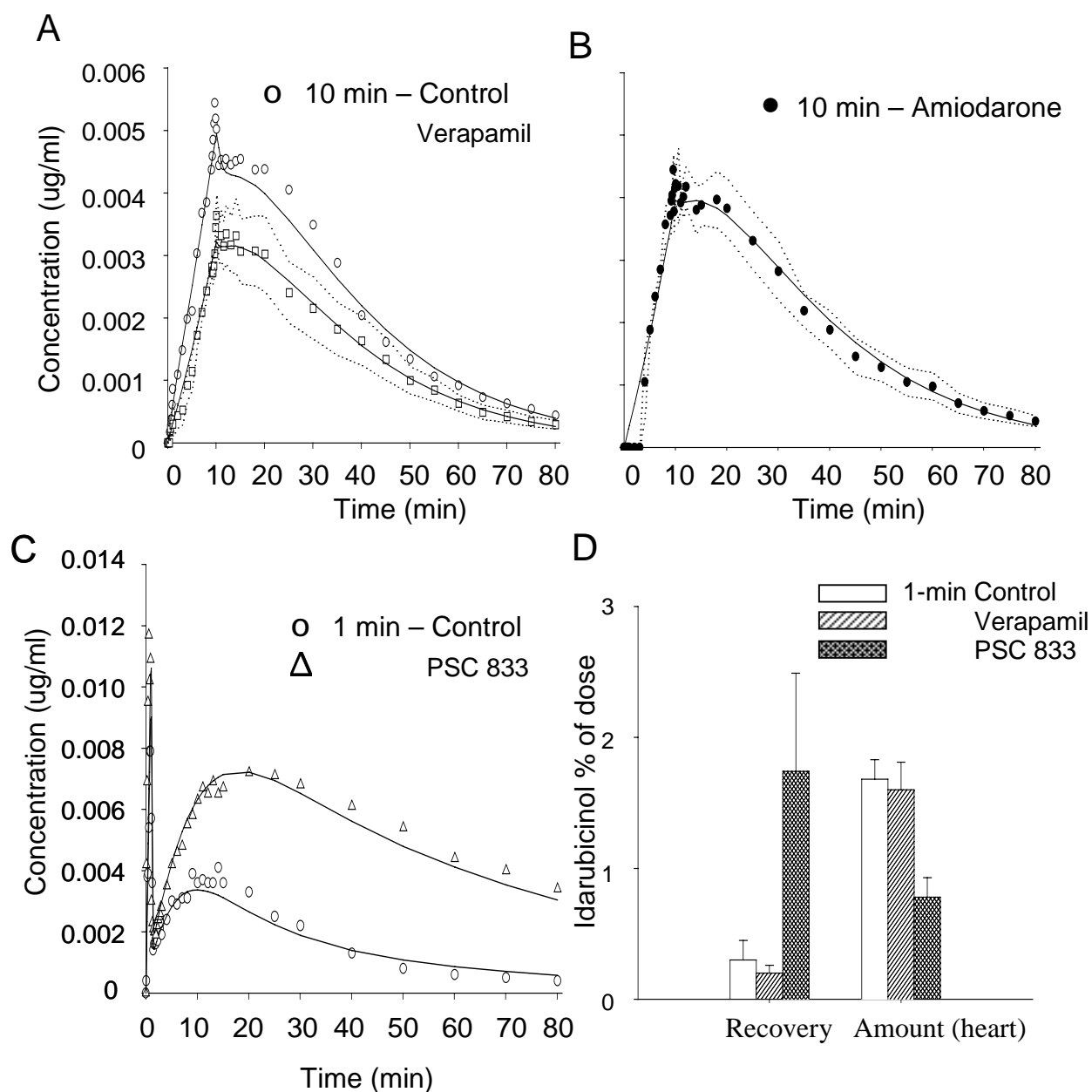
Figure 34. Panel A, B: Fits of IDOL outflow profiles in hearts perfused with Krebs-Henseleit solution (control, A), verapamil (1 nM, A), and amiodarone (1 μM, B) after a 10-min infusion of 0.5 mg IDA; average ± S.E., n = 5 in each group). Panel C: Fit of IDOL outflow profiles in hearts perfused with Krebs-Henseleit solution (control), and PSC 833 (1 μM) after a 1-min infusion of 0.5 mg IDA. Panel D: Outflow recovery and residual amount of IDOL in the heart at the end of experiment ([*], $P<0.01$; [**], $P<0.005$ compare to control).

PSC 833 hinders the uptake of IDOL in a competitive manner and decreases the sequestration rate: $K_{M,12}$ of IDOL increased by a factor of 1.3, while the sequestration rate constant, $k_{23,IDOL}$ is decreased by a factor of 6.4×10^{-7} with relatively poor estimation (Table 8), respectively.

The increase of IDOL formation is unexpected since the outflow recovery of IDA is significantly augmented by PSC 833. One may speculate that the hindrance of IDA uptake would induce a less amount of IDOL metabolized. The increase of outflow recovery of IDOL by PSC 833 is probably due to the hindrance of intracellular uptake of IDOL. This is strongly supported by the model analysis, where the sequestration rate constant quantifying metabolism and irreversible binding of IDOL is significantly decreased by the PSC 833 treatment.

Chapter 13. Effect of Xanthine derivatives (Caffeine, Theophylline), Doxorubicin and Hypothermia on myocardial kinetics of IDOL after a 10-min infusion of IDA

The IDOL outflow concentration time profile is shifted upwards by caffeine (Figure 35A). Caffeine remarkably increases the conversion of IDA to IDOL: both outflow recovery and residual amount in the heart are increased from 0.34 ± 0.03 % to 0.44 ± 0.03 % ($P<0.05$) and from 7.26 ± 1.74 % to 10.58 ± 0.76 % ($P<0.05$, Figure 35C), respectively. Theophylline also increases the generation of IDOL, namely, the residual amount is significantly increased to 11.4 ± 1.4 % ($P<0.01$, Figure 35C). The outflow concentration curve of IDOL in the treatment of theophylline is not obtained due to interference in chromatograms. The influence of caffeine on myocardial kinetics of IDOL is characterised by an increase of metabolism, i.e., the metabolic rate constant from Compartment IDA_1, $k_{m,1}$ is increased by factor of 6.2 (P<0.005) with a fractional standard deviation of 0.03 (Table 9). This parameter completely describes the outflow time profile of IDOL in the presence of caffeine (Figure 35B).

Table 9. Parameter estimate for the disposition of IDOL generated after the administration of IDA in the heart in the presence of caffeine (1 µM).

	Parameter	Estimate	*FSD*
Caffeine	$fk_{1,m}$	6.2[a]	0.03[b]

[a] Nonlinear regression of IDOL outflow concentration-time profiles where an additional parameter accounted in the model equations for the effect of caffeine on IDOL (The parameter estimates of control are listed Table 6).
[b] Fractional standard deviations.

To date, no direct evidence has been reported regarding the effect of caffeine and theophylline on the kinetics of IDOL. However, one may consider a couple of hypotheses. Firstly, the enhancement of IDA uptake due to caffeine may increase the generation of IDOL (Chapter 9). Secondly, an induction of aldoketoreductase responsible for the generation of IDOL by caffeine could be suggested by the modeling analysis. Note that an inhibition of cytochrome P-450 reductase for aglycone can be
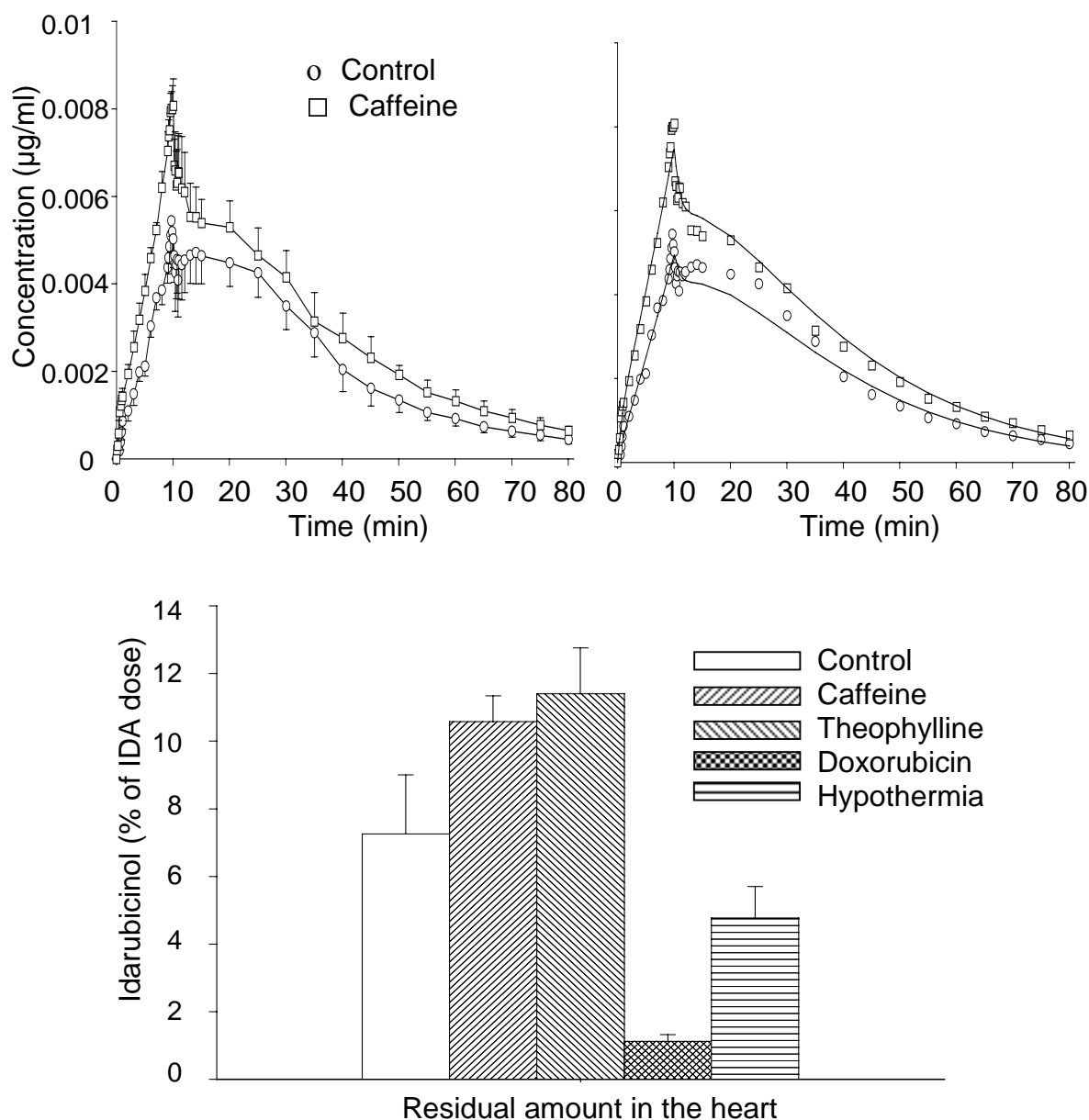
Figure 35. Panel A: IDOL outflow profiles in hearts perfused with Krebs-Henseleit solution (control) and caffeine (1 µM) for a 10 min infusion of 0.5 mg IDA (mean ± S.D., n = 5 in each group). Panels B: fits of the mean outflow data of the control and caffeine experiments. Panel C: Residual amount of IDOL in the heart at the end of experiment ([*], $P<0.05$; [**], $P<0.01$ compare to control).

excluded because Can-Eke et al. (1998) reported that caffeine is not able to alter hepatic microsomal NADPH-cytochrome P450 reductase enzyme activity.

Both doxorubicin and hypothermia significantly decreased the total generation of IDOL from IDA. The residual amount in the heart is decreased by 66 ($P<0.05$) and 75% ($P<0.01$) due to doxorubicin treatment and hypothermic condition, respectively (Figure 34C). The outflow recoveries in both experiments are not obtained because the concentrations of IDOL are under the limit of detection. The reduction of IDA conversion to IDOL seems to result from an occupation of aldoketoreductase due to doxorubicin, and from a decrease of the enzyme activity by low temperature.

Chapter 14. Potential Therapeutic Relevance

The investigation of the uptake mechanism across vessel walls and sarcolemmal membrane in the organ like the heart is very important, and it could provide a pivotal key to optimize dosage regimens and a better understanding of drug interactions concerning membrane transporters and cardiotoxicity. In general, it has been assumed that IDA diffuses passively into the cell because of its high lipophylicity. However, it has been still controversial whether cellular uptake transport of anthracyclines occurs via saturable mechanisms or passive diffusion. Recently an absorptive endocytosis in doxorubicin transport has also been suggested in cultured kidney epithelial cells (Sasaya et al., 1998), and Regev and Eytan (1997) reported that doxorubicin crosses membranes by a flip-flop mechanism. In this study, Michaelis-Menten type saturable uptake of IDA is proposed, and P-gp may act as an influx hindrance of IDA uptake into the heart. This suggestion may provide further insight into the uptake process and the role of P-gp in MDR of anthracyclines, and also probably give some pharmacokinetic information for tumor model.

Although a lot of efforts has been paid to determine optimal dosage regimens in anthracycline chemotherapy with circumvention of cardiotoxicity and multidrug resistance, rational criteria for choosing dosing schedules are still unclear (El-Kareh and Secomb, 2000). Previous pharmacokinetic studies for anthracyclines have been conducted to predict plasma concentration on the conventional assumption that the rate of cytotoxicity is linear in the free concentration in the extracellular space (e.g., Harris and Gross, 1975). However, since the drug exposure in tumor cells often does not directly relate with plasma concentrations (El-Kareh and Secomb, 1997), different schedules of delivery may give different cellular exposure. Studies at the cellular level suggested that peak levels rather than AUC are more important in determining cytotoxicity (Durand and Olive, 1981). High extracellular concentration for a short time was found to give higher cytotoxicity than low concentration for a long time for similar total exposure (Nguyen-Ngoc et al., 1984). The circumvention of MDR related to P-gp is limited by toxicity in normal tissues and organs due to an increase of accumulation of anthracyclines, because of no specificity from tumor cells to normal cells in P-gp inhibition effect. Verapamil and amiodarone show a promising effect that attenuate the IDA induced acute myocardial impairment despite an increase of cardiac uptake of

IDA. It would be worth to investigate their effect on the IDA-induced chronic cardiotoxicity.

Eksborg et al. (1997) reported that there was no significant difference in the plasma IDOL concentration time profiles in a comparison between bolus injection and 2hr infusion. However, these results show that the formation of IDOL from IDA in the heart is increased with decreasing infusion rate. Therefore one should take into account the change of IDOL formation and exposure in the heart according to the different dosing rates in toxicokinetic point of view. Note that the saturable uptake of IDOL in the heart should also be considered and further investigation for transport mechanism of IDOL would be of importance.

__Summary__

Using the isolated perfused rat heart this study investigates 1) the cardiac uptake of idarubicin (IDA), 2) the role of P-glycoprotein (P-gp) in the uptake process, 3) the formation of IDOL from IDA in the heart, and 4) the effect of P-gp inhibitors (verapamil, amiodarone, PSC 833), doxorubicin, hypothermia, xanthine derivatives (caffeine, theophylline) and metabolism inhibitors (rutin, phenobarbital) on the pharmacokinetics and pharmacodynamics of IDA using a mathematical modeling approach.

For the first time, it is shown that the cardiac uptake of IDA and IDOL is saturable and that the uptake rate is increased by P-gp inhibitors (verapamil and amiodarone), probably because of impairment of P-glycoprotein mediated influx hindrance. The evidence of a Michaelis-Menten like process is strongly supported by a noncompetitive inhibition of doxorubicin and uptake hindrance in hypothermic condition (increase of K_M). In addition, the combined kinetic-dynamic model provided further insight into the mechanism underlying the time course of the acute negative inotropic effect of anthracyclines. Verapamil and amiodarone attenuate the acute negative inotropic action of IDA despite an increase of the penetration into the heart. PSC 833, in contrast, enhanced the recovery of IDA and IDOL formed from IDA but potentiated the IDA-induced increase in coronary vascular resistance.

The enhanced myocardial uptake of IDA in the presence of caffeine can be explained by an increased maximal rate of saturable uptake process (V_{max}). The clinical significance of this interaction is not clear, however, this result suggests that caffeine intake may increase the cardiotoxicity of IDA. Further studies are needed to resolve this question.

Rutin inhibits the generation of IDOL from IDA despite the enhancement of IDA accumulation probably because it also increases the sequestration of IDA, and represents a beneficial vasodilating effect possibly due to an antioxidant property. While phenobarbital also decreases the formation of IDOL, but potentiates the IDA-induced vasoconstriction. The practical importance of a possible reduction of IDA-induced cardiotoxicity due to an inhibition of IDOL formation by rutin and phenobarbital is unclear, because only 2 % of IDA dose is transformed to IDOL in the

heart for a 1-min infusion of IDA. However, the increase of IDOL formed with increasing infusion time should be considered. The effects of all investigated drugs on the cardiac transport, metabolism and action of IDA are summarized in Table 10.

These results may provide a better understanding of the cardiac pharmacokinetics and pharmacodynamics of IDA including the influence of other drugs on these processes. Thus, these findings may contribute to predict drug interactions in anthracycline chemotherapy. They may also be useful to optimize the dosing regimens and to improve strategies to overcome multidrug resistance with respect to cardiotoxity of anthracycline.

Table 10. Effect of Drugs on the Cardiac Transport, Metabolism and Action of Idarubicin

| | Pharmacokinetics | | | | | | Pharmacodynamics | | | |
| | Idarubicin | | | Idarubicinol | | | | | | |
	uptake	Efflux	Sequestration	Generation	uptake	sequestration	Inotropy	LVEDP	Chronotropy	CVR
P-gp inhibitors										
Verapamil	↑	-	-	-	↑	↑	↓	-	-	↑
Amiodarone	↑	-	-	-	↑	↑	↓	-	-	-
PSC 833	↓	-	↓	↑	-	↓	↑	↑	-	↑
Xanthines										
Caffeine	↑	-	-	↑	-	-	↓	-	-	↓
Theophylline	-	-	-	↑	-	-	↓	-	↑	↓
Doxorubicin	↓	-	-	↓	-	-	↑	-	↑	↑
Hypothermia	↓	↓	-	↓	-	-	-	-	↑	-
Met. Inhibitors										
Rutin	-	-	↑	↓	-	-	-	-	-	↓
Phenobarbital	-	-	-	↓	↓	-	-	-	-	↑

↑, increase; ↓, decrease; LVEDP, left ventricular end-diastolic pressure; CVR, coronary vascular resistance; P-gp, P-glycoprotein;

Met., metabolism.

Zusammenfassung und Ausblick

Am isoliert perfundierten Rattenherzen werden in dieser Arbeit folgende Fragestellungen untersucht: 1) der Transportprozeß von Idarubicin (IDA) in das Herz, 2) die Rolle der P-Glykoproteintransporter (P-gp) in diesem Prozeß, 3) die Metabolisierung von IDA zu IDOL im Herzgewebe und 4) der Effekt von P-gp-Hemmern (Verapamil, Amiodaron, PSC 833), Doxorubicin Hyperthermie, Xanthinderivate (Koffein, Theophyllin) und von Hemmern der Metabolisierung (Rutin, Phenobarbital). Die Pharmakokinetik und Pharmakodynamik von IDA wurde dabei mit einem mathematischen Modell analysiert.

Es wurde zum ersten Mal gezeigt, daß der Transport von IDA und IDOL in das Herz ein Sättigungs-verhalten aufweist, und dass die Aufnahmerate durch P-gp-Hemmer (Verapamil und Amiodaron) erhöht wird. Letzteres ist wahrscheinlich auf eine Hemmung des P-Glycoprotein-vermittelten Auswärtstransports zurückzuführen. Der Hinweis auf einen Prozeß mit Michaelis-Menten Charakteristik wird dadurch unterstützt, daß der Prozeß durch Doxorubicin hemmbar ist, und die Michaelis-Menten Konstante (K_M) bei Hypothermie ansteigt. Das kombinierte kinetisch-dynamische Modell liefert zusätzlich Erkenntnisse über den Mechanismus der dem Zeitverlauf des akuten negativ inotropen Effektes der Anthrazykline zugrunde liegt. Verapamil und Amiodaron dämpften diesen akuten negativ inotropen Effekt von IDA trotz einer Erhöhung der Penetration von IDA in das Herz. Im Gegensatz dazu reduzierte PSC 833 die myokardiale Aufnahme von IDA und die Metabolisierung zu IDOL im Herz; andererseits potenzierte PSC 833 die IDA induzierte Zunahme des koronaren Widerstandes. Die erhöhte myokardiale Aufnahme von IDA in der Gegenwart von Coffein kann durch eine Erhöhung der maximalen Aufnahme-rate des sättigbaren Prozesses (V_{max}) erklärt werden. Die klinische Bedeutung dieser Wechselwirkung ist noch nicht klar, das Ergebnis weist jedoch daraufhin, daß Coffein die Kardiotoxizität voran IDA vergrößern könnte. Weitere Untersuchungen sind nötig, um diese Frage zu klären. Rutin hemmt die Bildung von IDOL aus IDA im Herzen trotz einer Erhöhung von der Aufnahme von IDA, wahrscheinlich durch einen direkten Effekt auf den Metabolismus und eine Erhöhung der Sequestrierung von IDA. Außerdem hat Rutin eine günstige vasodilatierende Wirkung (wahrscheinlich

aufgrund eines antioxidativen Effektes). Auch Phenobarbital reduziert die Bildung von IDOL im Herzen, potenziert jedoch die IDA induzierte Vasokonstriktion . Die praktische Bedeutung einer möglichen Verminderung der IDA induzierten Kardiotoxizität durch eine Hemmung der IDOL Bildung durch Rutin und Phenobarbital ist noch unklar, da unter den Bedingungen der 1-minütigen Infusion nur 2% von IDA zu IDOL metabolisiert werden. Es muß aberbeachtet werden, daß die im Herzen gebildete IDOL Menge ansteigt, wenn die Infusionszeit verlängert wird. Die Wirkungen aller untersuchten Pharmaka auf die Transportmechanismen , die Metabolisierung und die Wirkung von IDA im Rattenherzen sind in Tabelle 10 zusammengestellt.

Diese Ergebnisse tragen zu einem besseren Verständnis der kardialen Pharmakokinetik und Pharmakodynamik von IDA und der Wirkung anderer Pharmaka auf diese Prozesse bei. Sie liefern damit einen Beitrag zur Voraussage von Arzneimittelwechselwirkung in der Anthrazyklin-Chemotherapie. Die Ergebnisse können auch von Nutzen sein, die Dosierungsschemata zu optimieren und die Strategien zur Überwindung des Multiplen Drug Resistance im Hinblick auf die Kardiotoxizität der Anthrazykline zu verbessern.

References

Abernethy DR and Flockhart DA. Molecular basis of cardiovascular drug metabolism. Implications for predicting clinically important drug interactions. *Circulation* 101: 1749-1753 (2000).

Akaike H. An information criterion (AIC). *Math. Sci.* 14: 5-11 (1976).

Ames MM and Spreafico F. Selected pharmacologic characteristics of idarubicin and idarubicinol. *Leukemia* 6 Suppl 1:70-5 (1992).

Anderlini P, Benjamin RS, Wong FC, Kantarjian HM, Andreeff M, Kornblau SM, O'Brien S, Mackay B, Ewer MS, Piece SA and Estey EH. Idarubicin cardiotoxicity: a retrospective study in acute myeloid leukemia and myelodysplasia. *J. Clin. Oncol.* 13: 2827-2834 (1995).

Arcamone F Properties of antitumor anthracyclines and new developments in their application: Cain memorial award lecture. *Cancer Res.* 45: 5995-5999 (1985).

Baggetto LG. Biochemical, genetic, and metabolic adaptations of tumor cells that express the typical multidrug-resistance phenotype. Reversion by new therapies. *J. Bioenerg. Biomembr.* 29: 401-413 (1997).

Bates DA and Mackillop WJ. Hyperthermia, adriamycin transport, and cytotoxicity in drug-sensitive and -resistant Chinese hamster ovary cells. *Cancer Res.* 46: 5477-5481 (1986).

Beaulieu E, Demeule M, Ghitescu L and Beliveau R. P-glycoprotein is strongly expressed in the luminal membranes of the endothelium of blood vessels in the brain. *Biochem. J.* 326: 539-544 (1997).

Behnia K and Boroujerdi M. Inhibition of aldo-keto reductases by phenobarbital alters metabolism, pharmacokinetics and toxicity of doxorubicin in rats. *J. Pharm. Pharmacol.* 51: 1275-82 (1999).

Boucek RJ Jr, Olson RD, Brenner DE, Ogunbunmi EM, Inui M and Fleischer S. The major metabolite of doxorubicin is a potent inhibitor of membrane-associated ion pumps. A correlative study of cardiac muscle with isolated membrane fractions. *J. Biol. Chem.* 262:15851-15856 (1987).

Bristow MR, Sageman WS, Scott RH, Billingham ME, Bowden RE, Kernoff RS, Snidow GH and Daniels JR. Acute and chronic cardiovascular effects of doxorubicin in the dog: the cardiovascular pharmacology of drug-induced histamine release. *J. Cardiovasc. Pharmacol.* 2: 487-515 (1980).

Can-Eke B, Puskullu MO, Buyukbingol E and Iscan M. A study on the antioxidant capacities of some benzimidazoles in rat tissues.   *Chem. Biol. Interact.* 113: 65-77 (1998).

Caroni P, Villani F and Carafoli E. The cardiotoxic antibiotic doxorubicin inhibits the Na+/Ca2+ exchange of dog heart sarcolemmal vesicles. *FEBS Lett.*130: 184-186 (1981).

Casazza AM, Pratesi G, Giuliani F and Di Marco A. Antileukemic activity of 4-demethoxy daunorubicin in mice. *Tumori*. 66: 549-564 (1980).

Cayre A, Moins N, Finat-Duclos F, Maublant J, Albuisson E and Verrelle P. In vitro detection of the MDR phenotype in rat myocardium: use of PCR, [^{3}H]daunomycin and MDR reversing agents, *Anticancer Drugs* 7: 833-837 (1996).

Chandran K and Smets BF. Applicability of two-step models in estimating nitrification kinetics from batch respirograms under different relative dynamics of ammonia and nitrite oxidation. *Biotechnol. Bioeng.* 70: 54-64 (2000).

Colombo T, Gonzales PO and D'Incalci M. Distribution and activity of doxorubicin combined with SDZ PSC 833 in mice with P388 and P388/DOX leukaemia, *Br. J. Cancer* 73: 866–871 (1996).

Critchfield JW, Welsh CJ, Phang JM, Yeh GC. Modulation of adriamycin accumulation and efflux by flavonoids in HCT-15 colon cells. Activation of P-glycoprotein as a putative mechanism. *Biochem. Pharmacol.* 48: 1437-1445 (1994).

Cusack BJ, Mushlin PS, Voulelis LD, Li X, Boucek RJ Jr and Olson RD. Daunorubicin-induced cardiac injury in the rabbit: a role for daunorubicinol? *Toxicol. Appl. Pharmacol.* 118: 177-185 (1993).

D'Argenio DZ and Schumitzky A. *ADAPT II User's guide: Pharmacokinetic/ Pharmacodynamic Systems Analysis Software*. Biomedical Simulations Resource, Los Angeles, 1997.

Daly JW. *Mechanism of action of caffeine. In: Garattini S (ed) Caffeine, Coffee, and Health.* pp 97-150, Raven Press Ltd, New York, 1993.

Decleves X, Chappey O, Boval B, Niel E and Scherrmann JM. P-glycoprotein is more efficient at limiting uptake than inducing efflux of colchicine and vinblastine in HL-60 cells. *Pharm. Res.* 15: 712-718 (1998).

Decorti G, Peloso I, Favarin D, Klugmann FB, Candussio L, Crivellato E, Mallardi F and Baldini L. Handling of doxorubicin by the LLC-PK$_1$ kidney epithelial cell line. *J. Pharmacol. Exp. Ther.* 286: 525-530 (1998).

Duffy SJ, Castle JF, Harper RW and Meredith IT. Contribution of vasodilator prostanoids and nitric oxide to resting flow, metabolic vasodilation, and flow-mediated dilation in human coronary circulation, *Circulation* 100:1951–1957 (1999).

Durand RE and Olive PL. Flow cytometry studies of intracellular adriamycin in single cells in vitro. Earm YE, Ho WK and So I. Effects of adriamycin on ionic currents in single cardiac myocytes of the rabbit. *J. Mol. Cell. Cardiol.* 26: 163-172 (1994).

Eichholtz-Wirth H. Dependence of the cytostatic effect of adriamycin on drug concenration and exposure time in vitro. *Br. J. Cancer* 41: 886-891 (1980).

Eksborg S, Bjorkholm M, Hast R and Fagerlund E. Plasma pharmacokinetics of idarubicin and its 13-dihydro metabolite-a comparison of bolus versus 2h infusion during a 3 day course. *Anti-Cancer Drugs* 8: 42-47 (1997).

Elbaek K, Ebbehoj E, Jakobsen A, Juul P, Rasmussen SN, Bastholt L, Dalmark M and Steiness E. Pharmacokinetics of oral idarubicin in breast cancer patients with reference to antitumor activity and side effects. *Clin. Pharmacol. Ther.* 45: 627-634 (1989).

El-Kareh AW and Secomb TW. A mathematical model for comparison of bolus injection, continuous infusion, and liposomal delivery of doxorubicin to tumor cells. *Neoplasia* 2: 325-338 (2000)

Estevez MD, Wolf A and Schramm U. Effect of PSC 833, verapamil and amiodarone on adriamycin toxicity in cultured rat cardiomyocytes, *Toxicol. in Vitro* 14:17–23 (2000).

Ferrazzi E, Woynarowski JM, Arakali A, Brenner DE and Beerman TA. DNA damage and cytotoxicity induced by metabolites of anthracycline antibiotics, doxorubicin and idarubicin, *Cancer Commun.* 3: 173–180 (1991).

Ferry DR, Traunecker H and Kerr DJ. Clinical trials of P-glycoprotein reversal in solid tumours. *Eur. J. Cancer* 32: 1070-1081 (1996).

Fischer V, Rodriguez-Gascon A, Heitz F, Tynes R, Hauck C, Cohen D and Vickers AE. The multidrug resistance modulator valspodar (PSC 833) is metabolized by human cytochrome P450 3A. Implications for drug-drug interactions and pharmacological activity of the main metabolite, *Drug Metab. Disp.* 26: 802-811 (1998).

Ford JM and Hait WN. Pharmacology of drugs that alter multidrug resistance in cancer. *Pharmacol. Rev.* 42: 155-199 (1990).

Forrest GL, Gonzalez B, Tseng W, Li X and Mann J. Human carbonyl reductase overexpression in the heart advances the development of doxorubicin-induced cardiotoxicity in transgenic mice. *Cancer Res.* 60: 5158-5164 (2000).

Fromm MF, Kim RB, Stein CM, Wilkinson GR and Roden DM. Inhibition of P-glycoprotein-mediated drug transport: A unifying mechanism to explain the interaction between digoxin and quinidine. *Circulation* 99: 552-557 (1999).

Fujita K, Shinpo K, Yamada K, Sato T, Niimi H, Shamoto M, Nagatsu T, Takeuchi T and Umezawa H. Reduction of adriamycin toxicity by ascorbate in mice and guinea pigs. *Cancer Res.* 42: 309-316 (1982).

Fukushima T, Takemura H, Yamashita T, Ishisaka T, Inai K, Imamura S, Urasaki Y and Ueda T. Multidrug resistance due to impaired DNA cleavage in a VP-16-resistant human leukemia cell line. *Anticancer Res.* 19: 5111-5115 (1999).

Gambliel HA, Cusack BJ, Vestal RE, Forrest GL and Olson RD, Carbonyl reductase metabolizes daunorubicin to c-13 hydroxy metabolite daunorubicinol in heart. *Clinical Pharmacology & Therapeutics.* 61: 235, PIV-87 (1997).

Garner AP, Paine MJI, Rodriguez-Crespo I, Chinje EC, Ortiz de Montellano P, Stratford IJ, Tew DG and Wolf CR. Nitric oxide synthases catalyze the activation of redox cycling and bioreductive anticancer agents, *Cancer Res*. 59: 1929–1934 (1999).

Gerkens JF. Barbiturate inhibition of endothelium-dependent dilatation of blood- and Krebs-perfused rat tail arteries. *Eur J Pharmacol* 34: 293-301 (1987).

Gewirtz DA and Yanovich S. Metabolism of adriamycin in hepatocytes isolated from the rat and the rabbit. *Biochem. Pharmacol.* 36: 1793-1798 (1987).

Goodman J and Hochstein P. Generation of free radicals and lipid peroxidation by redox cycling of adriamycin and daunomycin. *Biochem. Biophys. Res. Commun.* 77: 797-803 (1977).

Gottesman MM and Pastan I. Biochemistry of multidrug resistance mediated by the multidrug transporter. *Annu. Rev. Biochem.* 62: 385-427 (1993).

Gros P, Fallows DA, Croop JM and Housman DE. Chromosome-mediated gene transfer of multidrug resistance. *Mol. Cell. Biol.* 6: 3785-3790 (1986).

Hagiwara M, Inoue S, Tanaka T, Nunoki K, Ito M and Hidaka H. Differential effects of flavonoids as inhibitors of tyrosine protein kinases and serine/threonine protein kinases. *Biochem. Pharmacol.* 37: 2987-2992 (1988).

Harada H, Cusack BJ, Olson RD, Stroo W, Azuma J, Hamaguchi T and Schaffer SW. Taurine deficiency and doxorubicin: interaction with the cardiac sarcolemmal calcium pump. *Biochem Pharmacol.* 39: 745-751 (1990).

Harris PA and Gross JF. Preliminary pharmacokinetic model for adriamycin (NSC-123127). *Cancer Chemother. Rep.* 59: 819-825 (1975).

Harrison LI and Gibaldi M. Physiologically based pharmacokinetic model for digoxin distrubution and elimination in the rat. *J. Pharm. Sci.* 66: 1138-1142 (1977).

Holford NHG and Sheiner LB. Kinetics of pharmacological response. *Pharmacol. Ther.* 16: 143-166 (1982).

Holford NHG and Sheiner LB. Understanding the dose-effect relationship. *Clin. Pharmacokinet.* 6: 429-453 (1981).

Holmberg SRM and Williams AJ. Patterns of interaction between anthraquinone drugs and the calcium-release channel from cardiac sarcoplasmic reticulum. *Circ. Res.* 67: 272-283 (1990).

Hosenpud JD, Wright J, Simpson L and Abramson JJ. Caffeine enhances doxorubicin cardiac toxicity in an animal model. *J. Card. Fail.* 1: 155-160 (1995).

Huet S, Bouvier A, Gruet M-A and Jolivet E. *Statistical tools for nonlinear regression*, pp 69-70, Springer, New York, 1996.

Janssen PML, Zeitz O, Keweloh B, Siegel U, Maier LS, Barckhausen P, Pieske B, Prestle J, Lehnart SE and Hasenfuss G. Influence of cyclosporine A on contractile function, calcium handling, and energetics in isolated human and rabbit myocardium, *Cardiovasc. Res.* 47: 99-107 (2000).

Kakkar T, Pak Y and Mayersohn M. Evaluation of a minimal experimental design for determination of enzyme kinetic parameters and inhibition mechanism. *J. Pharmacol. Exp. Ther.* 293: 861-869 (2000).

Kalyanaraman B and Baker JE. On the detection of paramagnetic species in the adriamycin-perfused rat heart: a reappraisal. *Biochem. Biophys. Res. Commun.* 169: 30-38 (1990).

Kawalek JC and Gilbertson JR. Partial purification of the NADPH-dependent aldehyde reductase from bovine cardiac muscle. *Arch. Biochem. Biophys.* 173: 649-657 (1976).

Kerr DJ, Kerr AM, Freshney RI and Kaye SB. Comparative intracellular uptake of adriamycin and 4'-deoxydoxorubicin by non-small cell lung tumor cells in culture and its relationship to cell survival. *Biochem. Pharmacol.* 35: 2817-2823 (1986).

Klimecki WT, Futscher BW, Grogan TM and Dalton WS. P-glycoprotein expression and function in circulating blood cells from normal volunteers. *Blood* 83: 2451-2458 (1994)

Kuffel MJ and Ames MM. Comparative resistance of idarubicin, doxorubicin and their C-13 alcohol metabolites in human MDR1 transfected NIH-3T3 Cells. *Cancer Chemother. Pharmacol.* 36: 223-226 (1995).

Kuffel MJ, Reid JM and Ames MM. Anthracyclines and their C-13 alcohol metabolites: growth inhibition and DNA damage following incubation with human tumor cells in culture. *Cancer Chemother. Pharmacol.* 30: 51-57 (1992).

Kuhlmann O, Hofmann S and Weiss M. Determination of idarubicin and idarubicinol in rat plasma using reversed-phase high-performance liquid chromatography and fluorescence detection, *J. Chromatogr. B Biomed. Sci. Appl.* 728: 279-282 (1999).

Lampidis TJ, Kolonias D, Podona T, Israel M, Safa AR, Lothstein L, Savaraj N, Tapiero H and Priebe W. Circumvention of P-GP MDR as a function of anthracycline lipophilicity and charge. *Biochemistry* 36: 2679-2685 (1997).

Larsen AK, Escargueil AE and Skladanowski A. Resistance mechanisms associated with altered intracellular distribution of anticancer agents. *Pharmacol. Ther.* 85: 217-229 (2000).

Licata S, Saponiero A, Mordente A and Minotti G. Doxorubicin metabolism and toxicity in human myocardium: role of cytoplasmic deglycosidation and carbonyl reduction. *Chem. Res. Toxicol.* 13: 414-420 (2000).

Looby M, Linke R and Weiss M. Pharmacokinetics and tissue distribution of idarubicin and its active metabolite idarubicinol in the rabbit. *Cancer Chemother. Pharmacol.* 39: 554-556 (1997).

Luo D and Vincent SR. Inhibition of nitric oxide synthase by antineoplastic anthracyclines. *Biochem. Pharmacol.* 47: 2111-2112 (1994).

Maeda A, Honda M, Kuramochi T and Takabatake T. A calcium antagonist protects against doxorubicin-induced impairment of calcium handling in neonatal rat cardiac myocytes, *Jpn. Circ. J.* 63: 123–129 (1999).

Matsushita T, Okamato M, Toyama J, Kodama I, Ito S, Fukutomi T, Suzuki S and Itoh M. Adriamycin causes dual inotropic effects through complex modulation of myocardial Ca^{2+}handling. *Jap. Circ. J.* 64: 65-71 (2000).

Mayer LD, Dougherty G, Harasym TO and Bally MB. The role of tumor-associated macrophages in the delivery of liposomal doxorubicin to solid murine fibrosarcoma tumors. *J. Pharmacol. Exp. Ther.* 280: 1406-1414 (1997).

McFalls EO, Paulson DJ, Gilbert EF and Shug AL. Carnitine protection against adriamycin-induced cardiomyopathy in rats. *Life Sci.* 38: 497-505 (1986).

McGinness JE, Grossie B Jr, Proctor PH, Benjamin RS, Gulati OP and Hokanson JA. Effect of dose schedule of vitamin E and hydroxethylruticide on intestinal toxicity induced by adriamycin. *Physiol. Chem. Phys. Med. NMR.* 18: 17-24 (1986).

Mushlin PS, Boucek RJ Jr, Parrish MD, Graham TP Jr and Olson RD. Beneficial effects of perfluorochemical artificial blood on cardiac function following coronary occlusion. *Life Sci.* 36: 2093-2102 (1985).

Mushlin PS, Cusack BJ, Boucek Jr RJ, Andrejuk T, Li X and Olson RD. Time-related increases in cardiac concentrations of doxorubicinol could interact with doxorubicin to depress myocardial contractile function, *Br. J. Pharmacol.* 110: 975-982 (1993).

Myers CE, McGuire WP, Liss RH, Ifrim I, Grotzinger K and Young RC. Adriamycin: the role of lipid peroxidation in cardiac toxicity and tumor response. *Science* 197: 165-167 (1977).

Nagaoka S, Kawasaki S, Sasaki K and Nakanishi T. Intracellular uptake, retention and cytotoxic effect of adriamycin combined with hyperthermia in vitro. *Jpn. J. Cancer Res.* 77: 205-211 (1986).

Nagasawa K, Natazuka T, Chihara K, Kitazawa F, Tsumura A, Takara K, Nomiyama M, Ohnishi N and Yokoyama T. Transport mechanism of anthracycline derivatives in huöman leukemia cell lines: uptake and efflux of pirarubicin in HL60 and pirarubicin-resistant HL60 cells. *Cancer Chemother. Pharmacol.* 37: 297-304 (1996).

Nagasawa K, Ohnishi N and Yokoyama T. Transport mechanisms of idarubicin, an anthracycline derivative, in human leukemia HL60 cells and mononuclear cells, and comparison with those of its analogs. *Jpn. J. Cancer Res.* 88: 750-759 (1997).

Nguyen-Ngoc T, Vrignaud P and Robert J. Cellular pharmacokinetics of doxorubicin in cultured mouse sarcoma cells originating from autochthonous tumors. *Oncology* 41: 55-60 (1984).

Nielsen D, Maare C and Skovsgaard T. Influx of daunorubicin in multidrug resistant Ehrlich ascites tumour cells: Correlation to expression of P-glycoprotein and efflux. Influence of verapmil. *Biochem. Pharmacol.* 50: 443-450 (1995).

Nussler V, Gieseler F, Zwierzina H, Gullis E, Pelka-Fleischer R, Diem H, Abenhardt W, Schmitt R, Langenmayer I, Wohlrab A, Kolb HJ and Wilmanns W. Idarubicin monotherapy in multiply pretreated leukemia patients: response in relation to P-glycoprotein expression. *Ann. Hematol.* 74: 57-64 (1997).

Olson RD and Mushlin PS. Doxorubicin cardiotoxicity: analysis of prevailing hypotheses. *FASEB J.* 4: 3076-3086 (1990).

Olson RD, Li X, Palade P, Shadle SE, Mushlin PS, Gambliel HA, Fill M, Boucek RJ Jr and Cusack BJ. Sarcoplasmic reticulum calcium release is stimulated and inhibited by daunorubicin and daunorubicinol. *Toxicol. Appl. Pharmacol.* 169: 168-176 (2000).

Pelikan PC, Weisfeldt ML, Jacobus WE, Miceli MV, Bulkley BH and Gerstenblith G. Acute doxorubicin cardiotoxicity: functional, metabolic, and morphologic alterations in the isolated, perfused rat heart, *J. Cardiovasc. Pharmacol.* 8: 1058–1066 (1986).

Perez-Vizcaino F, Ibarra M, Cogolludo AL, Duarte J, Zaragoza-Arnaez F, Moreno L, Lopez-Lopez G and Tamargo J. Endothelium-independent vasodilator effects of the flavonoid quercetin and its methylated metabolites in rat conductance and resistance arteries. *J. Pharmacol. Exp. Ther.* 302: 66-72 (2002).

Pessah IN, Durie EL, Schiedt MJ and Zimanyi I. Anthraquinone-sensitized $Ca2+$ release channel from rat cardiac sarcoplasmic reticulum: possible receptor-mediated mechanism of doxorubicin cardiomyopathy. *Mol. Pharmacol.* 37: 503-514 (1990).

Peterson C and Trouet A. Transport and storage of daunorubicin and doxorubicin in cultured fibroblasts. *Cancer Res.* 38: 4645-4649 (1978).

Platel D, Pouna P, Bonoron-Adele S and Robert J. Comparative cardiotoxicity of idarubicin and doxorubicin using the isolated perfused rat heart model, *Anticancer Drugs* 10:671-676 (1999).

Platel D, Pouna P, Bonoron-Adele S and Robert J. Preclinical evaluation of the cardiotoxicity of taxane-anthracycline combinations using the model of isolated perfused rat heart. *Toxicol. Appl. Pharmacol.* 163: 135-140 (2000).

Pomposiello S, Yang XP, Liu YH, Surakanti M, Rhaleb NE, Sevilla M and Carretero OA. Autacoids mediate coronary vasoconstriction induced by nitric oxide synthesis inhibition, *J. Cardiovasc. Pharmacol.* 30: 599–606 (1997).

Propper D and Maser E. Carbonyl reduction of daunorubicin in rabbit liver and heart, *Pharmacol. Toxicol.* 80:240–245 (1997).

Regev R and Eytan GD. Flip-flop of doxorubicin across erythrocyte and lipid membranes. *Biochem. Pharmacol.* 54: 1151-1158 (1997).

Reid JM, Pendergrass TW, Krailo MD, Hammond GD and Ames MM. Plasma pharmacokinetics and cerebrospinal fluid concentrations of idarubicin and idarubicinol in pediatric leukemia patients: a Childrens Cancer Study Group report. *Cancer Res.* 50: 6525-6528 (1990).

Robert J, Rigal-Huguet F, Harousseau JL, Pris J, Huet S, Reiffers J, Hurteloup P and Tamassia V. Pharmacokinetics of idarubicin after daily intravenous administration in leukemic patients. *Leuk. Res.* 11: 961-964 (1987).

Robert J. Multidrug resistance in oncology: diagnostic and therapeutic approaches, *Eur. J. Clin. Invest.* 29:536-545 (1999).

Rodriguez I, Abernethy DR and Woosley RL. P-glycoprotein in clinical cardiology. *Circulation* 99: 472–474 (1999).

Roovers DJ, van Vliet M, Bloem AC, and Lokhorst HM. Idarubicin overcomes P-glycoprotein-related multidrug resistance: comparison with doxorubicin and daunorubicin in human multiple myeloma cell lines, *Leukemia Res.* 23: 539-548 (1999).

Ross DD, Doyle LA, Yang W, Tong Y and Cornblatt B. Susceptibility of idarubicin, daunorubicin, and their C-13 alcohol metabolites to transport-mediated multidrug resistance. *Biochem. Pharmacol.* 50: 1673-1683 (1995).

Russo AL, Passaquin AC, Andre P, Skutella M and Ruegg UT. Effect of cyclosporin A and analogues on cytosolic calcium and vasoconstriction: possible lack of relationship to immunosuppressive activity, *Br. J. Pharmacol.* 118: 885–892 (1996).

Sadzuka Y, Egawa Y, Sugiyama T, Sawanishi H, Miyamoto K and Sonobe T. Effects of 1-methyl-3-propyl-7-butylxanthine (MPBX) on idarubicin-induced antitumor activity and bone marrow suppression. *Jpn. J. Cancer Res.* 91: 651-657 (2000).

Sadzuka Y, Mochizuki E and Takino Y. Mechanism of caffeine modulation of the antitumor activity of adriamycin. *Toxicol. Lett.* 75: 39-49 (1995).

Sasaya M, Wada I, Shida M, Sato M, Hatakeyama Y, Saitoh H and Takada M. Uptake of doxorubicin by cultured kidney epithelial cells LLC-PK1. *Biol. Pharm. Bull.* 21: 527-529 (1998).

Scambia G, Ranelletti FO, Panici PB, De Vincenzo R, Bonanno G, Ferrandina G, Piantelli M, Bussa S, Rumi C and Cianfriglia M. Quercetin potentiates the effect of adriamycin in a multidrug-resistant MCF-7 human breast-cancer cell line: P-glycoprotein as a possible target. *Cancer Chemother. Pharmacol.* 34: 459-464 (1994).

Schleyer E, Kuhn S, Ruhrs H, Unterhalt M, Kaufmann CC, Kern W, Braess J, Straubel G and Hiddemann W. Oral idarubicin pharmacokinetics-correlation of trough level with idarubicin area under curve. *Leukemia* 11: S15-S21 (1997).

Schott B and Robert J. Comparative activity of anthracycline 13-dihydrometabolites against rat glioblastoma cells in culture. *Biochem. Pharmacol.* 38: 4069-4074 (1989).

Schröder JK, Kasimir-Bauer S, Seeber S and Scheulen ME. In vitro effect of multidrug resistance modifiers on idarubicinol efflux in blasts of acute myeloid leukemia. *J. Cancer Res. Clin. Oncol.* 126:111-116 (2000).

Schüssler M, Holzl J and Fricke U. Myocardial effects of flavonoids from Crataegus species. *Arzneimittelforschung.* 45: 842-845 (1995).

Seber GAF and Wild CJ. *Nonlinear regression*, pp 21-42, John Wiley & Sons, New York, 1989.

Sharom FJ. The P-glycoprotein multidrug transporter: interactions with membrane lipids, and their modulation of activity. *Biochem. Soc. Trans.* 25: 1088-1096 (1997).

Skovsgaard T. Carrier-mediated transport of daunorubicin, adriamycin and rubidazone in Ehrlich ascites tumour cells. *Biochem. Pharmacol.* 27: 1221-1227 (1978).

Speelmans G, Staffhorst RW, Steenbergen HG and de Kruijff B. Transport of the anti-cancer drug doxorubicin across cytoplasmic membranes and membranes composed of phospholipids derived from Escherichia coli occurs via a similar mechanism. *Biochim. Biophys. Acta* 1284: 240-246 (1996).

Stein WD. Kinetics of the multidrug transporter (P-glycoprotein) and its reversal. *Physiol. Reviews* 77: 545–590 (1997).

Sudhir K, MacGregor JS, DeMarco T, de Groot CJM, Taylor RN, Chou TM, Yock PG and Chatterjee K. Cyclosporine impairs release of endothelium-derived relaxing factors in epicardial and resistance coronary arteries, *Circulation* 90: 3018–3023 (1994).

Temma K, Akera T, Akihito C, Ozawa S and Kondo H. Cellular Ca^{2+} loading and inotropic effects of doxorubicin in atrial muscle preparations isolated from rat or guinea-pig hearts. *Eur. J. Pharmacol.* 252: 173-181 (1994).

Temma K, Chugun A, Akera T, Kondo H and Kurebayashi N. Doxorubicin alters Ca^{2+} transient but fails to change Ca^{2+} sensitivity of contractile proteins. *Environ. Toxicol. Pharmacol.* 1: 131-139 (1996).

Terasako K, Nakamura K, Toda H, Kakuyama M, Hatano Y and Mori K. Barbiturates inhibit endothelium-dependent and independent relaxations mediated by cyclic GMP. *Anesth Analg* 78:823-830 (1994).

Thiebaut F, Tsuruo T, Hamada H, Gottesman MM, Pastan I, Willingham MC. Cellular localization of the multidrug-resistance gene product P-glycoprotein in normal human tissues. *Proc. Natl. Acad. Sci. USA*. 84: 7735-7738 (1987).

Thornalley PJ, Bannister WH and Bannister JV. Reduction of oxygen by NADH/NADH dehydrogenase in the presence of adriamycin. *Free Radic. Res. Commun.* 2: 163-171 (1986).

Tsuchiya H, Yamamoto N, Asada N, Terasaki T, Kanazawa Y, Takanaka T, Nishijima H and Tomita K. Caffeine-potentiated radiochemotherapy and function-saving surgery for high-grade soft tissue sarcoma. *Anticancer Res.* 20: 2137-2143 (2000).

Usansky JI, Liebert M, Wedemeyer G, Grossman HB and Wagner JG. The uptake and efflux of doxorubicin by a sensitive human bladder cancer cell line and ist doxorubicin-resistant subline. *Sel. Cancer. Ther.* 7: 139-150 (1991).

van Acker FA, van Acker SA, Kramer K, Haenen GR, Bast A and van der Vijgh WJ. 7-monohydroxyethyl-rutoside protects against chronic doxorubicin-induced cardiotoxicity when administered only once per week. *Clin. Cancer Res.* 6: 1337-1341 (2000).

van Asperen J, Mayer U, van Tellingen O and Beijnen JH. The functional role of P-glycoprotein in the blood-brain barrier. *J. Pharm. Sci.* 86: 881-884 (1997).

van Asperen J, Van Tellingen O and Beijnen JH. The pharmacological role of P-glycoprotein in the intestinal epithelium. *Pharmacol. Res.* 37: 429-435 (1998).

van Asperen J, van Tellingen O, Tijssen F, Schinkel AH and Beijnen JH. Increased accumulation of doxorubicin and doxorubicinol in cardiac tissue of mice lacking mdr1a P-glycoprotein, *Br. J. Cancer* 79:108–113 (1999).

van der Valk P, Van Kalken CK, Ketelaars H, Broxterman HJ, Scheffer G, Kuiper CM, Tsuruo T, Lankelma J, Meijer CJLM, Pinedo HM and Scheper RJ. Distribution of multi-drug resistance-associated P-glycoprotein in normal and neoplastic human tissues. *Ann. Oncol.* 1: 56–64 (1990).

Vásquez-Vivar J, Martasek P, Hogg N, Masters BS, Prichard Jr KA and Kalyanaraman B. Endothelial nitric oxide synthase-dependent superoxide generation from adriamycin, *Biochemistry* 36: 11293–11297 (1997).

Vibes J, Lasserre B, Gleye J and Declume C. Inhibition of thromboxane A2 biosynthesis in vitro by the main components of Crataegus oxyacantha (Hawthorn) flower heads. *Prostaglandins Leukot. Essent. Fatty Acids.* 50: 173-175 (1994).

Wakabayashi I, Mayer B and Groschner K. Inhibitory effects of aclarubicin on nitric oxide production in aortic smooth muscle cells and macrophages. *Biochem. Pharmacol.* 59: 719-726 (2000).

Wakabayashi I, Sakamoto K and Hatake K Inhibitory effect of aclarubicin on endothelium-dependent relaxation of rat aorta. *Pharmacol. Toxicol.* 68: 187-191 (1991).

Watanabe T, Nakayama Y, Naito M, Oh-hara T, Itoh Y and Tsuruo T. Cremophor EL reversed multidrug resistance in vitro but not in tumor-bearing mouse models. *Anticancer Drugs*. 7: 825-32 (1996).

Watanabe Y and Kimura J. Inhibitory effect of amiodarone on Na(+)/Ca(2+) exchange current in guinea-pig cardiac myocytes. *Br. J. Pharmacol.* 131: 80-84 (2000).

Weiss M. Pharmacokinetics in organs and the intact body: model validation and reduction. *Eur. J. Pharm. Sci.* 7: 119-127 (1998).

Weiss M. The relavance of residence time theory to pharmacokinetics. *Eur. J. Clin. Pharmacol.* 43: 571-579 (1992).

.

Weisser J, Martin J, Bisping E, Maier LS, Beyersdorf F, Hasenfuss G and Pieske B. Influence of mild hypothermia on myocardial contractility and circulatory function. *Basic Res. Cardiol.* 96: 198-205 (2001).

Welling PG, Tse FLS and Dighe SV. *Pharmaceutical bioequivalence.* pp 303-312, Marcel Dekker, New York, 1991.

Wermuth B. Purification and properties of an NADPH-dependent carbonyl reductase from human brain. Relationship to prostaglandin 9-ketoreductase and xenobiotic ketone reductase. *J. Biol. Chem.* 256: 1206-1213 (1981).

Wielinga PR, Westerhoff HV and Lankelma J. The relative importance of passive and P-glycoprotein mediated anthracycline efflux from multidrug-resistant cells. *Eur. J. Biochem.* 267: 649-657 (2000).

Wirth H and Wermuth B. Immunohistochemical localization of carbonyl reductase in human tissues. *J. Histochem. Cytochem.* 40: 1857-1863 (1992).

Woo S, Kang W and Kwon Ki. Pharmacokinetic and pharmacodynamic modeling of the antiplatelet and cardiovascular effects of cilostazol in healthy humans. *Clin. Pharmacol. Ther.* 71: 246-252 (2002).

Publications

Kang W and Weiss M. Influence of P-glycoprotein modulators on cardiac uptake, metabolism, and effects of idarubicin. *Pharmaceutical Research* 18: 1535-1541 (2001).

Weiss M and Kang W. P-glycoprotein inhibitors enhance saturable uptake of idarubicin in rat heart: Pharmacokinetic/pharmacodynamic modeling. *Journal of Pharmacology and Experimental Therapeutics* 300: 688-694 (2002).

Kang W and Weiss M. Digoxin uptake, receptor heterogeneity and inotropic response in the isolated rat heart: A comprehensive kinetic model. *Journal of Pharmacology and Experimental Therapeutics* 302: 557-583 (2002).

Woo S, Kang W and Kwon Ki. Pharmacokinetic and pharmacodynamic modeling of the antiplatelet and cardiovascular effects of cilostazol in healthy humans. *Clinical Pharmacology and Therapeutics* 71: 246-252 (2002).

Conference abstracts

Kang W, Kuhlmann O, Weiss M. Effect of rutin on pharmacokinetics and pharmacodynamics of idarubicin in the isolated perfused rat heart. *European. J. Pharmaceutical Science* 11(Suppl. 1): S92 (2000).
Conference of the European Federation for Pharmaceutical Sciences, Budapest, Hungary. Sep. 16-19, 2000.

Kang W, Weiss M. Digoxin uptake, receptor interaction and inotropic response in the isolated intact rat heart. *Naunyn-Schmiedeberg's Archives of Pharmacology* 365(Suppl. 1): R92 (2002).
Annual meeting of Deutsche Gesellschaft für Experimentelle und Klinische Pharmacologie und Toxikologie, Mainz, Germany, Mar. 12-14, 2002.

Weiss M, Kang W. Modelling, parameter estimation, and sensitivity analysis of transport and receptor binding kinetics of cardiac glycoside in the intact heart.
Conference, "Topics in biomathematics and related computational problems at the bedinning of the third millennium" Vietri sul Mare, Italy, Jun. 3-9, 2002.

Acknowledgements

When someone asks me "What did you learn during your Ph.D. course?", I should say that I learned not only knowledge and skill, but also generosity and patience from my supervisor. I sincerely appreciate consideration and encouragement of my mentor, Professor Michael Weiss throughout my study towards this degree.

I acknowledge to Mrs. Dagmar Günther and Mrs.Barbara Wiele for their assistance.

The financial support provided by Deutsche Forschungs Gemeinschaft is gratefully acknowledged.

I also sincerely thank Professor Kwang-il Kwon, at College of Pharmacy, Chungnam National University, South Korea for providing my background of this work and for his encouragement.

I would like to express a special note of thanks to my wife, Chun-sung Kim and my two kids, Ju-hyung and Je-na in Germany for their love and patience, and to my mother in Korea for her sacrificial pray and anxiety.

Finally, I deeply thank God for guidance and preservation of my family and for coming true the present work.

Curriculum Vitae

Name　　　　　:　Kang, Wonku

Date of birth　　:　Nov. 3, 1969

Nationality　　　: South Korea

Current address : Fliederweg 36, 06130 Halle, Germany

Education

Mar. 1989 – Feb. 1993　Bachelor of Pharmacy at College of Pharmacy,
　　　　　　　　　　　Chungnam National University, South Korea.

Mar. 1997 – Feb. 1999　Master of Science, Clinical Pharmacy at College of
　　　　　　　　　　　Pharmacy, Chungnam National University, South Korea.

Aug. 1999 – May 2002　Ph.D. course at Section of Pharmacokinetics, Department of
　　　　　　　　　　　Pharmacology, Martin-Luther University Halle-Wittenberg.

Achievement

　Pharmacist's license in April 1993.

Employment

Aug. 1992 – Sep. 1992　Internship account at Dong A pharmaceutical company.

Sep.　1994 – Aug. 1996　Manager of Pharmacy.

Sep.　1997 – Aug. 1998　Tutorial fellow at College of Pharmacy,
　　　　　　　　　　　Chungnam National University, South Korea.

Jun.　2002 –　　　　　Postdoctoral Fellow at Section of Pharmacokinetics,
　　　　　　　　　　　Department of Pharmacology, Martin-Luther University
　　　　　　　　　　　Halle-Wittenberg.

Hiermit erkläre ich, daß ich die vorliegende Arbeit selbständig angefertigt, die benutzten Quellen und Hilfsmittel vollständig angegeben und die wissenschaftlichen Werken entnommenen Stellen als solche gekennzeichnet habe.

Die Arbeit wurde bisher weder im In- noch im Ausland in gleicher oder ähnlicher Weise einer anderen Prüfungsbehörde vorgelegt.

Ich habe mich bisher an keiner Stelle um den Doktorgrad beworben.

im Juni 2002

Kang, Wonku